LPV/Gain-Scheduled lateral control architectures for autonomous vehicles

Dimitrios Kapsalis

Université Grenoble Alpes

THÈSE

pour obtenir le grade de

DOCTEUR DE LA COMMUNAUTE UNIVERSITE GRENOBLE ALPES

Spécialité : **Automatique-Productique**

Arrêté ministériel : 7 août 2006

Présentée par
Dimitrios KAPSALIS

Thèse dirigée par **Olivier SENAME**,
codirigée par **John J. MOLINA** et **Vicente MILANÉS**

préparée au sein du **GIPSA-Lab**
dans **Electronique, Electrotechnique, Automatique, Traitement du Signal (EEATS)**

LPV/Gain-Scheduled Lateral Control Architectures for Autonomous Vehicles

Thèse soutenue publiquement le **5 Avril 2022**,
devant le jury composé de:

M. Christophe BERENGUER
Professeur, Grenoble INP, Président
M. Jimmy LAUBER
Professeur, Université Polytechnique Hauts-de-France, Rapporteur
M. Peter GÁSPÁR
Directeur de Recherche, Académie des Sciences, Hongrie, Rapporteur
M. Vicenç PUIG
Professeur, Institut de Robòtica (IRI), Espagne, Examinateur
M. Olivier SENAME
Professeur, Grenoble INP, Directeur de thèse
M. Vicente MILANÉS
Innovation Project Manager, Renault Espagne, Co-Directeur de thèse
M. John J. MOLINA
Professeur, Grenoble INP, Invité

To my parents *Margarita* & *Konstantinos*,

to my brothers *Panagiotis* & *Giannis*.

Acknowledgements

This manuscript couldn't be completed without giving the props to the people that helped me so far, in this exciting but tough journey.

First of all, I would like to express my appreciation to my main supervisor Prof. Olivier SENAME, who believed in me and offered me this opportunity to learn and work in such a unique topic. I have to thank him for his trust and for letting me be independent enough to work on my ideas while he was available to discuss and provide me with theoretical and practical aide. I have to mention that his attitude and advices towards the problems that I faced throughout this thesis were a significant motivation and inspiration for me.

I'm also extremely grateful to my co-supervisors Dr. Vicente MILANÉS and Prof. John J. MOLINA. Vicente's passion for autonomous vehicles and persistence to push the limits, set the example for me and helped me evolve as an engineer. I will certainly miss our "Mediterranean" talks and his comments to my writings. Finally, I also would like to thank John for his nice ideas and interventions to broaden the aspect of the problems we tackled. His suggestions helped me think the control problems from different aspects.

I feel the need to express my gratitude to my past Prof. George BITSORIS and my deal uncle Dr. Spilios THEODOULIS. I owe them my passion to follow a control engineering career and pursue a PhD on that topic. I have to thank them also for urging me to come to France for advanced studies and especially Spilios for his support and help throughout my staying in France.

I would like to extend my sincere thanks to the researchers who comprise my thesis defense and CSI committee Prof. Peter GÁSPÁR, Prof. Jimmy Lauber, Prof. Vicenç Puig, Prof. Christophe Berenguer and Prof. Maria Laura Delle Monache. The reviewers of the dissertation had a significant contribution in the improvement of the manuscript through their insightful comments.

I have to express my gratitude to my Renault colleagues David, Fran, Hussam, Fabio, Nievsabel, Mathieu, Alexandre, my manager Eric and the rest of the group. Their help in the organization and overall practical experience on the autonomous vehicles made the experimental validation of my thesis feasible.

Also, a few words for my friends in GIPSA-Lab: Chhay, Mohammad, Mariana and Patrick, Phong, Karthik, and Mukhtar. I am grateful to all of you for our discussions, your help, the food and beers we had together, the skiing and all the nice moments we shared in Grenoble.

I cannot forget my "parisian-greek" friends Dasoulas, Psilos, Liakos, Kyriakos, Giannis, Manou, Zak, Sofia, Sissy and Manolis. The moments we had will be a pleasant memory. I have to express my gratitude to my greek friends and especially to Theofilos for being close to me all this time. I thank also Mayia for her companionship for the most of this period. Her

presence and thoughts meant a lot..

Last but not least, I have to thank my family. My parents, Margarita and Konstantinos that supported me in every decision I made and gave me strength even by distance. My brothers, Panagiotis and Giannis that were always in my mind and there for me in case I needed them. Without you, I wouldn't made it that far..

Contents

Résumé des contributions (in French)

Introduction

Cette thèse est le résultat d'un travail de trois ans commencé d'avril 2019 à mars 2022. Dans le cadre de la CIFRE (Convention Industrielle de Formation par la Recherche) un financement est accordé pour un programme de recherche conjoint entre le **Groupe Renault** et notamment au sein de l'équipe R&D responsable des véhicules autonomes située dans les installations du Technocentre de Renault à Paris, et l'équipe SAFE du **GIPSA-lab** (Grenoble Image Parole Signal Automatique) de l'Université de Grenoble Alpes, sur la conception d' **architectures de contrôle latéral LPV/Gain programmé pour les véhicules autonomes**. Le travail réalisé sur travaux menés ont été supervisés par **Olivier Sename**, **John-Jairo Martinez-Molina** (tous deux professeurs à Grenoble INP) et **Vicente Milanes**, chef de projet innovant chez Renault.

Ce doctorat est axé sur deux sujets principaux :

- Le contrôle latéral automatique des véhicules autonomes, c'est-à-dire le processus de contrôle du volant d'un véhicule pour gérer les scénarios de suivi de voie et les manœuvres de changement de voie.
- Configuration et synthèse de la commande LPV (Linear Parameter Varying) pour gérer un système de contrôle latéral.

Les 36 mois de cette thèse ont été répartis en une année au GIPSA-lab, où l'accent a été mis sur l'étude de la théorie de commande LPV et de ses approches, principalement la Polytopique et le Gridding (voir le chapitre deux pour plus de détails) pour synthétiser un contrôleur LPV et la manière d'implémenter un tel système de commande. Les deux dernières années de la thèse ont été menées dans les installations du Technocentre de Renault à Paris. Là, dans un premier temps, une collaboration plus étroite avec le reste des ingénieurs de contrôle du R&D a eu lieu afin d'avoir un aperçu de l'architecture de contrôle et du logiciel de la plate-forme de test. De plus, les ingénieurs qui ont travaillé dans les autres modules de la voiture automatisée, par exemple la localisation ou la perception, ont contribué en partageant leurs connaissances sur les limites et les avantages des différents composants de la voiture et comment la partie contrôle est affectée. Enfin, au cours de cette période, dans l'environnement industriel de Renault, il a été possible de procéder à des essais expérimentaux en utilisant une véritable plate-forme de banc d'essai en mode autonome sur une piste d'essai privée près de Paris, afin de tester et de valider les architectures de contrôle latéral proposées.

Motivation et objectifs

L'objectif de ce travail de thèse est directement lié à la stratégie de conduite autonome selon le projet ADCC (Autonomous Driving Commuter Car) chez Renault. Ainsi, l'objectif principal

de cette thèse est de laisser le véhicule conduire de manière autonome dans des sections spécifiques de la route. Les spécifications de conduite sont basées sur l'ODD (Operational Design Domain) du projet, qui est une description des conditions dans lesquelles un véhicule autonome est conçu pour fonctionner en toute sécurité. Par la suite, les objectifs de ce travail sont concernés par les points ci-dessous :

- Développer un système de contrôle latéral capable de gérer complètement la direction autonome du véhicule.
- Le système de contrôle latéral doit être capable de gérer différents scénarios de direction, c'est-à-dire le maintien et le changement de voie, tout en maintenant la sécurité et le confort de conduite du passager.
- Concevoir une architecture de direction capable d'adapter ses performances au profil de vitesse longitudinale variable en fonction des différentes courbes qui seront suivies par le véhicule autonome.
- Proposer une stratégie de configuration du contrôle qui est accordable et qui peut donc être modifiée en fonction des préférences des passagers, du domaine de fonctionnement de la vitesse ou de l'architecture du véhicule.
- Formuler un système de contrôle qui puisse prendre en compte les capacités de direction du véhicule automatisé et ainsi respecter les limitations physiques lors de la conduite en mode autonome.
- Mettre en œuvre l'architecture de pilotage proposée dans la plateforme de banc d'essai afin d'évaluer expérimentalement, en plus des simulations, la validité et les capacités selon les ODD des projets.

Contributions

Cette thèse vise à fournir des méthodologies implémentables de conception de contrôle pour les systèmes de contrôle latéral des véhicules de passagers autonomes. Les principales contributions par chapitre concernent les :

- **Formulation du modèle latéral LPV**, en particulier, le chapitre 2 présente un nouveau modèle LPV augmenté qui inclut la dynamique linéaire de la voiture, la dynamique de l'erreur d'anticipation dont la minimisation permet de suivre une trajectoire de référence et le modèle d'actionneur de direction identifié. Le principal avantage de ce modèle est qu'il décrit la dynamique réaliste de la direction du véhicule et que, par conséquent, un système de contrôle latéral peut être traité dans le cadre du LPV.
- **LPV Contrôle du suivi de la voie**, où la conception d'un contrôleur dynamique à rétroaction de sortie LPV est détaillée dans le chapitre quatre. Deux conceptions différentes sont présentées, basées sur 1) l'approche polytopique et 2) l'approche par

grille garantissant H_∞ performance. L'intérêt de ces approches réside dans les différentes méthodologies qui doivent être suivies afin d'assurer un maintien performant de la voie à basse et haute vitesse tout en maintenant le confort du passager et les capacités de direction de l'actionneur.

- **Fusionner le suivi des voies et le contrôle des changements de voie**, où un système complet de contrôle latéral est présenté, capable de gérer à la fois le suivi de la voie, le changement de voie et la transition d'un scénario à l'autre (voir chapitre cinq). Deux approches différentes sont détaillées, 1) la première est basée sur l'approche LPV présentée dans la dernière section du chapitre quatre qui est généralisée et 2) la seconde est basée sur le traitement de la fusion comme une génération en temps réel d'une référence virtuelle (appelée Gouverneur de référence) qui permet au système de suivi de voie en boucle fermée d'effectuer des manœuvres de maintien et de changement de voie. Cette référence virtuelle est la solution d'un problème d'optimisation convexe en temps réel qui satisfait à des critères de performance et de contraintes.

Organisation du manuscrit

Ce manuscrit de thèse est organisé en six chapitres différents. Un bref résumé des autres chapitres est donné ci-dessous :

- Le chapitre deux fournit les outils mathématiques nécessaires pour que le lecteur soit capable de suivre la procédure de conception d'un contrôleur à rétroaction dynamique LPV. Par la suite, les LMI et les systèmes LPV sont introduits ainsi que les théorèmes nécessaires à la synthèse des contrôleurs LPV selon les approches correspondantes. De plus, à la fin de ce chapitre, un bref résumé de la bibliographie existante sur la conception de systèmes de contrôle latéral est donné.

- Le troisième chapitre détaille l'architecture du véhicule pour permettre à un véhicule de tourisme automatisé (Renault Zoe) utilisé dans cette thèse de rouler en mode autonome. De plus, nous construisons progressivement le modèle de la dynamique latérale du véhicule, qui comprend les états du châssis du véhicule, la dynamique de l'erreur d'anticipation et le modèle identifié LTI du système EPS. Ainsi, le modèle générique LPV est formulé et ce modèle est utilisé dans les chapitres quatre et cinq pour la conception de la commande LPV.

- Le quatrième chapitre présente l'analyse et la conception de contrôleurs dynamiques de suivi de voie LPV, selon les deux approches du chapitre 2, à savoir l'approche polytopique et l'approche par grille. Les contrôleurs LPV prennent en compte la vitesse longitudinale, qui est un paramètre variable inhérent au modèle, et la distance d'anticipation devant le véhicule, qui est un paramètre de réglage. Ainsi, ce chapitre propose de nouvelles architectures de contrôle latéral LPV. Les systèmes de contrôle suggérés sont validés dans divers résultats de simulation et sur une piste d'essai réelle où la plate-forme de banc d'essai automatisé est utilisée pour suivre des courbes à faible vitesse et des lignes droites à grande vitesse ou des courbes plus lisses.

- Le cinquième chapitre est divisé en deux sections principales, l'objectif principal étant de traiter la fusion des scénarios de suivi de voie et de changement de voie. La première section propose une formulation basée sur un paramètre de haut niveau qui est introduit pour modéliser la transition linéaire entre le suivi de voie et le changement de voie. Par la suite, un contrôleur LPV est synthétisé pour la fusion des deux scénarios. Les résultats prometteurs sont validés par plusieurs simulations et expériences sur une piste d'essai où le code de contrôle est intégré à la Renault Zoe automatisée. La deuxième approche est basée sur la résolution d'une optimisation convexe en temps réel, appelée Gouverneur de référence. La solution de ce problème est une référence virtuelle qui alimente un contrôleur de suivi de voie à vitesse de lacet pour lequel les contraintes de direction en boucle fermée sont satisfaites et permettant ainsi la manœuvre de changement de voie par un contrôleur de suivi de voie. Les performances sont validées et illustrées par des résultats de simulation.
- Le chapitre six résume les chapitres suivants de cette thèse, les contributions présentées et enfin, il propose des extensions et des travaux futurs possibles.

Perspectives

Quelques idées pour des travaux futurs et des extensions aux contributions actuelles détaillées dans les chapitres de cette thèse. En fonction de chaque chapitre et d'autres domaines d'applications, on peut faire ce qui suit :

Au sujet du chapitre deux, ci-dessous, il est proposé de :

- Construire un nouveau modèle LTI identifié pour l'ESP du véhicule. Appliquer différentes approximations de Padé du terme de retard et comparer les performances globales du véhicule contrôleur.
- Construire un nouveau modèle LPV latéral en incluant un modèle d'actionneur LPV qui est dérivé d'un algorithme d'identification LPV pour une vitesse longitudinale variable du véhicule.
- Étudier le cas où les forces latérales appliquées dans le modèle de bicyclette ne sont pas linéarisées. Ainsi, les forces latérales peuvent être exprimées en fonction de paramètres mesurés et variables dans le temps. Ces paramètres sont les angles de glissement latéral et peuvent être estimés en temps réel et alimenter un contrôleur LPV. En outre, ces paramètres variables peuvent être utilisés dans les fonctions de pondération H_∞ afin de régler un contrôleur LPV capable de traiter le cas non linéaire de la dynamique du véhicule.

D'autres extensions sont proposées pour les contributions présentées dans le chapitre quatre.

- Proposer un nouvel algorithme pour la réduction de la taille d'un polytope qui décrit l'espace des paramètres, lorsque la taille du vecteur des paramètres est supérieure à trois.

- Élaboration d'un problème LS contraint en temps réel pondéré pour améliorer les performances du contrôleur LPV/Polytopic en limitant la contribution des contrôleurs de sommets conservateurs.
- Concevoir un planificateur de haut niveau basé sur le processus LS contraint. Cela peut être réalisé en introduisant certains critères de performance, exprimés sous forme de fonctions quadratiques pour le suivi des performances et du confort du passager.
- Formuler la distance d'anticipation comme la solution d'un problème d'optimisation convexe en temps réel en fonction du scénario (suivi de voie/changement) ou des agents de la circulation à proximité du véhicule afin de réguler en temps réel la vitesse du véhicule.

Selon le chapitre cinq, les suggestions suivantes sont données :

- Introduire un nouveau paramètre de haut niveau qui vise à améliorer les performances de suivi des voies dans le cas où des courbes plus élevées doivent être suivies ou lorsque l'erreur latérale est accrue.
- Validation expérimentale du schéma de gouverneur de référence proposé pour une vitesse fixe et pour le cas où la vitesse longitudinale varie.
- Développer un schéma de gouverneur de référence qui permet à un contrôleur rapide (encore une fois de suivi de voie) d'effectuer une manœuvre d'évitement d'obstacle. L'évitement de l'obstacle peut être formulé comme une contrainte de vitesse de lacet en temps réel via des calculs géométriques simples.
- Proposer un schéma de gouverneur de référence non linéaire qui, dans le problème d'optimisation, permet également de modifier en temps réel la vitesse longitudinale. Ainsi, la vitesse peut être régulée en fonction de la dynamique du contrôle latéral en boucle fermée. De cette façon, le suivi et la régulation de la vitesse peuvent être évalués en même temps.

Outre l'extension du travail présenté aux applications de contrôle latéral, nous suggérons de :

- Intégrer le contrôle longitudinal & latéral dans le cadre du LPV. Ainsi, la vitesse longitudinale est un état et devra être considérée comme un paramètre quasi-LPV. Ce paramètre en temps réel alimentera un contrôleur LPV pour adapter la régulation de la vitesse et les performances de suivi en fonction du scénario.
- Développer un schéma de commande LPV pour les cas de régulateur de vitesse adaptatif ou même de régulateur de vitesse coopératif. Ces applications sont fortement dépendantes de la perception et donc des capteurs. Ainsi, nous proposons qu'un travail futur soit de concevoir un système de contrôle qui adapte ses performances en fonction de la qualité des capteurs.

List of Figures

Table of Acronyms

LTI	Linear Time Invariant
LTV	Linear Time Varying
LPV	Linear Parameter Varying
NLPV	NonLinear Parameter Varying
MPC	Model Predictive Control
LMI	Linear Matrix Inequality
BMI	Bilinear Matrix Inequality
SDP	Semi-Definite Programming
DOF	degree of freedom
COG	center of gravity
FD	Fault Diagnosis
FTC	Fault Tolerant Control
ODE	Ordinary Differential Equation
PDLF	Parameter Dependent Lyapunov Function
CIFRE	Conventions Industrielles de Formation par la Recherche
LS	Least-Squares
ODD	Operational Design Domain
RTK-DGPS	Real-Time Kinematic Differential Global Positional System
IMU	Inertial Measurement Unit
MABx	MicroAutoBox
EPS	Electric Power Steering
w.r.t	with respect to

$\mathbb{R}$	Real values set
$\mathbb{C}$	Complex values set
A^*	Conjugate of $A \in \mathbb{C}$
A^T	Transpose of $A \in \mathbb{R}$
$A \prec (\preceq) 0$	Matrix A is symmetric and negative (semi)definite
$A \succ (\succeq) 0$	Matrix A is symmetric and positive (semi)definite
$Co(X)$	Convex hull of set X
$A = A^T$	Matrix A is real symmetric
$He(A) = A^T + A$	

Chapter 1

Introduction

Contents

1.1 Thesis Framework

This thesis is the result of three years work started from April 2019 till the March 2022. Under the CIFRE (from french: Convention Industrielle de Formation par la Recherche) framework, a funding is given for a joint research program between the **Renault Group** and especially within the R&D team responsible for autonomous vehicles located in the Technocentre facilities of Renault in Paris, and the team SAFE of **GIPSA-lab** (from french: Grenoble Image Parole Signal Automatique) from the University of Grenoble Alpes, on the design of **LPV/Gain-scheduled lateral control architectures for autonomous vehicles**. The conducted work was supervised from **Olivier Sename**, **John-Jairo Martinez-Molina** (both Professors of Grenoble INP) and **Vicente Milanes**, Innovative Project Manager of Renault.

This PhD is focused on two main topics:

- Autonomous vehicles automatic lateral control, i.e the process of controlling the steering wheel of a vehicle to handle the scenarios of lane-tracking and the lane-change maneuvers.
- The LPV (Linear Parameter Varying) control configuration and synthesis to handle a lateral control system.

The 36 months of this thesis were split to one year at GIPSA-lab, where an emphasis was given on the study of LPV control theory and its approaches, mainly the Polytopic and Gridding (see Chapter two for more details) to synthesize an LPV controller and the way to implement such a control system. The two last years of the thesis were conducted in the Technocentre facilities of Renault in Paris. There, at first a closer collaboration with the rest of the R&D control engineers took place to have a hands-on of the control architecture and the SW/HW of the test-bed platform. Moreover, engineers that worked in the other modules of the automated car, e.g Localization or Perception, contributed by sharing their knowledge on the limitations and advantages of the several components of the car and how the control part is affected. Finally, during that period in the industrial environment of Renault, the experimental testing was possible where a real test-bed platform was utilized in autonomous mode in a private test track close to Paris in order to test and validate the proposed lateral control architectures.

The underlying objectives, the achieved contributions, the manuscript organization and the associated publications are presented below.

1.2 Objectives

The aim of this PhD work is directly linked to the autonomous driving strategy according to the ADCC (Autonomous Driving Commuter Car) project at Renault. Thus, the main objective if this thesis, is to let the vehicle drive autonomously in specific sections on the road. The driving specifications are based-on the project's ODD (Operational Design Domain), which is a description of the conditions in where an autonomous vehicle is designed to operate safely. Subsequently, the objectives of this work are concerned with points below:

- Develop a lateral control system that is capable to handle completely the autonomous steering of the passenger vehicle.
- The lateral control system must be able to handle different steering scenarios, i.e lane-keeping and lane-change, while the driving of the passenger is sustained safe and comfort.
- Design a steering architecture that can adapt its performance for the varying longitudinal speed profile according to the different curves that will be tracked from the autonomous vehicle.
- Propose a control configuration strategy that is tunable and thus it can be altered w.r.t the preferences of the passengers, the speed operating domain or the vehicle's architecture.
- Formulate a control system that can take into account the steering capabilities of the automated vehicle and in that way respect the physical limitations while driving in autonomous mode.

- Implement the proposed steering architecture in the test-bed platform in order to assess experimentally, apart from simulations, the validity and the capabilities according to the projects ODD.

1.3 Contributions

This thesis aims at providing control design implementable methodologies for lateral control systems of autonomous passenger vehicles. The main contributions per chapter are concerned with the:

- **LPV lateral model formulation**, especially in chapter two a novel augmented LPV model is presented that includes the linear dynamics of the car, the look-ahead error dynamics whose minimization enables the tracking of a reference trajectory and the identified steering actuator model. The main advantage of that model is that describes the realistic steering dynamics of the vehicle and thus, a lateral control system can be treated in the LPV framework.
- **LPV lane-tracking control** where the design of an LPV dynamic output feedback controller is detailed in chapter four. Two different designs are presented based-on 1) the Polytopic and 2) the Gridding approaches guaranteeing H_∞ performance. The interest of these approaches lies on the different methodologies that have to be followed so that a performant lane-keeping can be performed for low and high speeds while the comfort is sustained for the passenger and the steering capabilities of the actuator.
- **Merging lane-tracking and lane-change control** where a complete lateral control system is presented that can handle both the lane-tracking, lane-change and the transition to one scenario to another (see chapter five). Two different approaches are detailed, 1) the first is based-on the LPV approach presented in the last section of chapter four which is generalized and 2) the second is based on treating the merging as a real-time generation of a virtual reference (called Reference Governor) that enables the closed-loop lane-tracking system to perform lane-keeping and lane-change maneuvers. That virtual reference is the solution of a real-time convex optimization problem that satisfies performance and constraints criteria.

1.4 Manuscript Structure

This PhD typescript is organized in six different chapters. A brief summary of the rest of the chapters is given below:

- Chapter two provides the necessary mathematical tools so that the reader is capable to follow the procedure to design an LPV dynamic feedback controller. Subsequently, LMIs

and LPV systems are introduced and the necessary theorems for the synthesis of LPV controllers according to the corresponding approaches. In addition, at the end of this chapter is given a brief summary of the existing bibliography about the lateral control system design.

- The third chapter details the vehicle's architecture to enable an automated passenger vehicle (Renault Zoe) used in this thesis to drive in autonomous mode. Moreover, we gradually construct the model of the lateral dynamics of the vehicle, that includes the states in the vehicle's frame, the look-ahead error dynamics and the LTI identified model of the EPS system. Thus, the generic LPV model is formulated and that model is used in the chapters four and five for the LPV control design.

- The fourth chapter presents the analysis and the design of LPV dynamic output feedback lane-tracking controllers, according to the two approaches from chapter two, i.e the Polytopic and the Gridding ones. The LPV controllers take into account the longitudinal speed which is an inherent varying parameter of the model, and the look-ahead distance in front of the vehicle that is a tuning parameter. Thus, this chapter proposes novel LPV lateral control architectures. The suggested control systems are validated in various simulation results and in a real test track where the automated test-bed platform is utilized to track low speed curves and high speed straight stretches or smoother curves.

- The fifth chapter mainly is split between two main sections while the main goal is to handle the merging of the lane-tracking and lane-change scenarios. The first section proposes the formulation based-on a high-level parameter that is introduced to model the linear transition between the lane-tracking and lane-change. Subsequently, an LPV controller is synthesized for the the merging of both scenarios. The promising results are validated in several simulations and experiments in a test track where the control code is embedded to the automated Renault Zoe. The second approach is based-on solving a real-time convex optimization, called Reference Governor. The solution of that problem is a virtual reference that feeds a yaw-rate lane-tracking controller for which closed-loop steering constraints are satisfied and enabling thus, the lane-change maneuver by a lane-tracking controller. The performance is validated and illustrated in simulation results.

- Chapter six sums up the following chapters of this thesis, the contributions presented and finally, it proposes extensions and possible future works.

1.5 Publications

The present PhD thesis is conducted under the industrial CIFRE framework, giving thus the opportunity to test and recover experimental results. This gave the advantage to pursue the publication of journal articles, among conferences, and the opportunity to submit a patent including an engineering-based method. The results of this thesis are listed below per category:

1.5.1 Journal articles

J1
Title: Gain-scheduled steering control for autonomous vehicles
Authors: D. Kapsalis, O. Sename, V. Milanes, J. J. Martinez
Journal: IET Control Theory & Applications
Status: Published, **Year:** 2020 **Volume:** 14, **Number:** 20 **Pages:** 3451-3460.

J2
Title: A 3D Reduced LPV Polytopic Look-Ahead Steering Controller for Autonomous Vehicles
Authors: D. Kapsalis, O. Sename, V. Milanes, J. J. Martinez
Journal: Control Engineering Practice (selected from the committee of IFAC CTS 2021)
Status: Submitted, **Year:** 2021, **Month:** December

J3
Title: Merging Lane-Tracking and Lane-Change for Autonomous Vehicles: A LPV Gain-Scheduling approach
Authors: D. Kapsalis, O. Sename, V. Milanes, J. J. Martinez
Journal: IEEE Transactions on Intelligent Transportation Systems
Status: Submitted, **Year:** 2021, **Month:** December

1.5.2 International conference papers with proceedings

C1
Title: Design and Experimental Validation of an LPV Pure Pursuit Automatic Steering Controller
Authors: D. Kapsalis, O. Sename, V. Milanes, J. J. Martinez
Conference: 16th IFAC Symposium on Control in Transportation Systems
Location: Lille, France, **Date:** 8-10 June 2021.

C2
Title: LPV/LFT Control Design Equipped with a Command Governor for Different Steering Scenarios
Authors: D. Kapsalis, O. Sename, V. Milanes, J. J. Martinez
Conference: 4th IFAC Workshop Linear-Parameter Varying Systems
Location: Milan, Italy, **Date:** 19-22 July 2021.

C3

Title: A Reference Governor approach for Lane-Change Maneuvers of Autonomous Vehicles
Authors: D. Kapsalis, O. Sename, V. Milanes, J. J. Martinez
Conference: 24th IEEE International Conference on Intelligent Transportation
Location: Indiana, USA, **Date:** 19-22 September 2021.

1.5.3 Patent

P1
Title: PJ-21-0311: Apparatus and method for fast and safe reference generator for lane-change maneuvers for ADAS and AD vehicle applications
Authors: D. Kapsalis, O. Sename, V. Milanes, J. J. Martinez
Status: Submitted to the patent office.

Chapter 2

Vehicle Model & System Architecture

Contents

2.1 Introduction

This section presents the description of the in-vehicle architecture that enables the safe and performant autonomous driving mode. Figure 2.1 illustrates an automated electric Renault Zoe which is considered the test bed platform throughout this thesis, equipped with all the necessary software/hardware.

Figure 2.1: Automated Electric Renault Zoe

This PhD CIFRE benefits from Renault resources, having a fully robotized platform for the experimental validation. Apart from several simulations, the proposed lateral control architectures presented in the next chapters, they have been tested and stressed for different speed profiles in a private test track for straight stretches and curves.

That test track is located at Satory, approximately 30 km away from Paris. The test track, depicted by an image taken from Google Earth in Figure 2.2, that consists of curves of different curvatures. The turns of total distance 600-700 m in red colour have been used for low speed tracking purposes, whereas the orange area of around 1.5 km illustrates smoother curves compensated for faster velocities. The same segment in orange is used for lane-change purposes since it makes easy the deviation of the car from the reference trajectory and subsequently, perform a lane-change maneuver.

Moreover, this chapter introduces the gradual extension of the augmented model that describes the yaw dynamics of the vehicle. The final overall model represents the states of the car at the vehicle frame, the actuator's identified transfer function and, the error dynamics at a selected look-ahead distance in front of the vehicle.

This chapter is structured as follows: Section 2.2 introduces the main components that cooperate in the vehicle's architecture to drive in autonomous mode. Then, section 2.3 explains the linearized vehicle's dynamics at the vehicle frame, leading to a model that enables the design of a steering controller. In addition, the look-ahead errors at the target point expand the dynamics of the bicycle model (section 2.4). As a final step, the identified actuator model is added to the previous model, to give a more realistic description of the steering process (see section 2.5). Section 2.6 presents the final augmented LPV model that is going to be used in the next chapters. The final section 2.7 sums up this chapter.

Figure 2.2: Private test track at Satory

2.2 Test-bed Platform Architecture

Intelligent vehicles' architecture is at the intersection of multiple research fields such as localization, perception, navigation and decision making, and dynamic vehicle control. Their functional cooperation of different modules play the main role to achieve the needed performance for the prescribed ODD.

The in-vehicle architecture of the automated Renault Zoe, utilized in this thesis, is the product of a project launched to provide a robotaxi service. That prototype was used in the TORNADO project whose objective was the autonomous functioning in rural and peri-urban environments of Paris in France [Milanés et al. 2021].

The following section briefly explain each of these components, as their interaction is depicted in Fig.2.3:

- *Map and Localization:* The vehicle is equipped with a Real-Time Kinematic Differential Global Positional System (RTK-DGPS) and an Inertial Measurement Unit (IMU) that serves as precise positioning system. This component is responsible for gathering and centralizing all map related information, aiding to localize the vehicle within the available map of the operational area. The localization provides as an output at every instant the velocity, timing information, position and the heading of the vehicle in the global axis frame, together with an index associated with the quality of the data.
- *Cloud Support & Communications:* This module provides a platform where the vehicle is able to communicate with a cloud server. That system provides three features: 1)

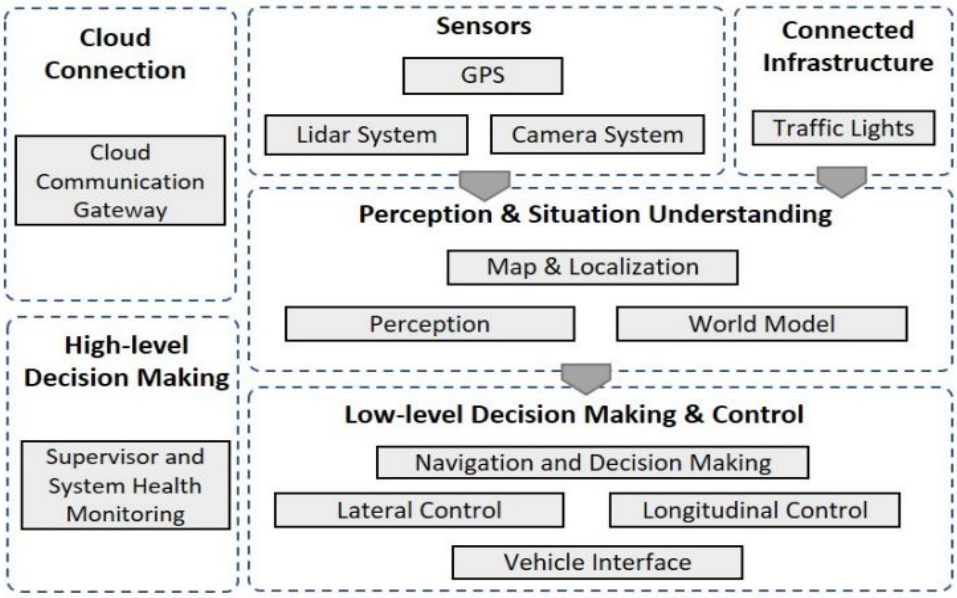

Figure 2.3: Functional Components of Tornado Vehicle

Remote vehicle tracking and map visualization of all connected vehicles, thus enabling safety warnings such as, bad road conditions or unusable road segments; 2) Distant control during urgent cases as priority vehicle nearby and, 3) Connectivity between vehicles and cloud via cellular communication.

- *Supervisory System:* This is the main component that checks and controls all the components to ensure the overall good behavior of the operational modules. It determines the functionality that every component must switch-on at every instant. Subsequently, it selects the appropriate module, according to the operational modes (manual, autonomous or standby).

- *Perception:* This module denotes the sensor configuration/fusion and the algorithms designed to provide reliable detection of the obstacles in the surrounding environment of the Tornado vehicle. As depicted in Fig. 2.4, the system configuration is based on five evenly distributed cameras (side, rear and a front) and a 32-layer LiDAR located in the center of the roof rack, providing a full 360° view. For more information of the algorithmic part of that component, readers may refer to [Beltrán et al. 2020].

- *World Model:* The output of the perception module provides data for the recognized vehicles or obstacles. Then, the World Model component combines the output of the perception with additional information already stored in the digital map, as speed limits, driving directions or marking types. In that way, the World Model module is able to perceive and understand the scene and the surrounding environment of the vehicle at every instant.

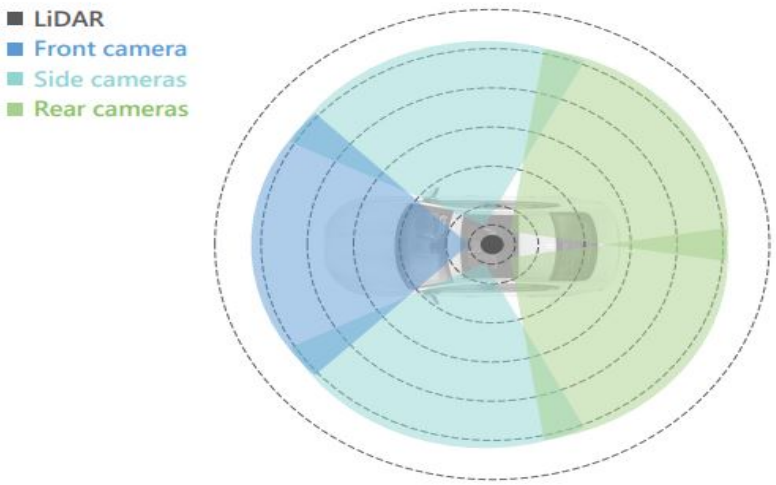

Figure 2.4: Sensors configuration for the Perception

- *Navigation & Decision Making:* The Navigation process takes into account a set of high level requirements w.r.t comfort and mission destination. It aims at transmitting a safe and comfortable short-term trajectory in real-time to the control system module. The computed route is planned as the solution of a short-term horizon optimization problem that takes into account indices about the geometric description of the desired path, maximum lateral error limitations and the associated speed profile. Another general functionality of the Navigation process consists of evaluating the consequence of each obstacle perceived at a given process time and then, an appropriate maneuver is chosen. This selected driving plan is then modified according to the expected interaction between the ego vehicle and the detected obstacle to sustain a safe and comfortable behavior at the same time. The expected interaction is formulated based on the relative obstacle position, its direction w.r.t the ego vehicle. Consequently, the selected maneuver adds constraints both on the longitudinal and lateral motions that must be handled next by the control system module.

- *Vehicle Dynamic Control:* This component describes both lateral and longitudinal controllers. They use as main inputs the localization and navigation systems' information. A MicroAutoBox (MABx) is installed in the trunk. It is a real-time system for performing fast function stand-alone prototyping. It receives both the current vehicle positioning and reference trajectory via Ethernet connection from an industrial control PC. The real-time supervision and deployment is achieved by using dSPACE to upload the built control code.

    1. *Longitudinal Control:* The experimental test-bed platform is already equipped with a low-level longitudinal controller. This controller receives the speed reference as the output from the navigation system, thus regulating the automated throttle and brake pedals.
    2. *Lateral Control:* The path-following control is based on the minimization of control

errors computed at a varying look-ahead distance L in front of the vehicle. The steering command is computed in rad and is converted in degrees that leads as input to the Electric Power Steering (EPS) system that is running at 100 H_z. The EPS controls and assists with the support of an intelligent electric motor the vehicle steering. The desired steering wheel angle δ is fed to EPS to follow the trajectory and it is computed according to the 1) lateral error at the target point, 2) the longitudinal speed of the vehicle and 3) the associated maneuver i.e Lane-tracking or Lane-change. It is emphasized that the component of Lateral Control is the component where the contributions of this thesis are based on.

2.3 Two-Wheeled Linear Vehicle Model

This part presents the gradual construction of the model that gives a realistic representation of the yaw dynamics of the vehicle.

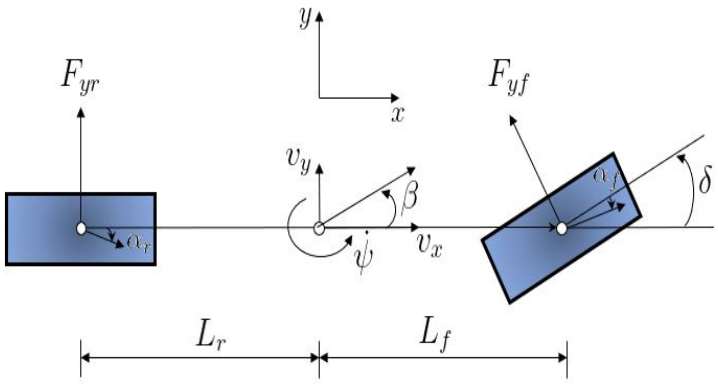

Figure 2.5: Two-wheeled bicycle model representing the vehicle lateral dynamics.

The lateral vehicle dynamics can be modeled as a two-wheeled bicycle model [Rajamani 2011]. Using this model and by parameterizing the longitudinal speed of the vehicle, the yaw dynamics can be decoupled and a steering controller can be designed regardless of the longitudinal dynamics of the vehicle.

Fig. 2.5 shows the resulting vehicle model which is expressed by the parameters where v_x and v_y are the longitudinal and lateral velocity accordingly. $\dot{\psi}$ is the yaw rate of the car. α_f, α_r are the tire side-slip angles of the front and rear wheels respectively. β is the side slip angle of the vehicle body. δ is the steering wheel angle. L_f, L_r are the distances of the front and rear wheel from the center of the gravity of the car and C_f, C_r the front and rear cornering stiffness.

The lateral tire forces are approximated as linear functions:

$$\begin{aligned} F_{yf} &= C_f \alpha_f \\ F_{yr} &= C_r \alpha_r \end{aligned} \tag{2.1}$$

The following relations can be used to calculate a_f and a_r:

$$\begin{aligned} tan(\alpha_f) &= \delta - \frac{v_y + L_f \dot{\psi}}{v_x} \\ tan(\alpha_r) &= \frac{-v_y + L_r \dot{\psi}}{v_x} \end{aligned} \tag{2.2}$$

Using small angles approximations i.e

$$\begin{aligned} a_f &\simeq tan(a_f) \\ a_r &\simeq tan(a_r) \end{aligned} \tag{2.3}$$

Thus, the side slip angles can be written as:

$$\begin{aligned} \alpha_f &= \delta - \frac{v_y + L_f \dot{\psi}}{v_x} \\ \alpha_r &= \frac{-v_y + L_r \dot{\psi}}{v_x} \end{aligned} \tag{2.4}$$

Using Newton's second law and the moment balance at the z axis, the next equations are derived:

$$\begin{aligned} m a_y = m(\dot{v}_y + v_x \dot{\psi}) &= F_{yf} + F_{yr} \\ I_z \ddot{\psi} &= L_f F_{yf} - L_r F_{yr} \end{aligned} \tag{2.5}$$

where a_y is the lateral acceleration, m the mass and I_z the car inertia.

Considering v_y and $\dot{\psi}$ as state variables and combining the equations (2.1), (2.4), (2.5) the linear vehicle model in state space form is derived:

$$\begin{bmatrix} \dot{v}_y \\ \ddot{\psi} \end{bmatrix} = \begin{bmatrix} -\frac{C_f + C_r}{m v_x} & -v_x + \frac{C_r L_r - C_f L_f}{m v_x} \\ \frac{-L_f C_f + L_r C_r}{I_z v_x} & -\frac{L_f^2 C_f + L_r^2 C_r}{I_z v_x} \end{bmatrix} \begin{bmatrix} v_y \\ \dot{\psi} \end{bmatrix} + \begin{bmatrix} \frac{C_f}{m} \\ \frac{L_f C_f}{I_z} \end{bmatrix} \delta \tag{2.6}$$

2.4 Look-Ahead Errors Dynamics & Augmented Vehicle Model

Fig. 2.6 presents the look-ahead system [Taylor et al. 1999], where y_L is the lateral offset from the reference trajectory at a target point in a distance L away from the vehicle. ε_L is the angular error between the reference heading at the target point and the vehicle's orientation.

Considering y_L and ε_L as state variables, the equations that describe their evolution are:

$$\begin{aligned} \dot{y}_L &= -v_y - L\dot{\psi} + v_x\varepsilon_L \\ \dot{\varepsilon}_L &= \dot{\psi}_{ref} - \dot{\psi} \end{aligned} \tag{2.7}$$

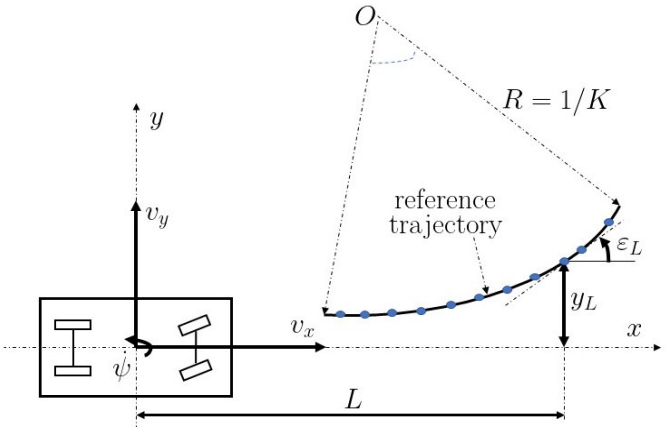

Figure 2.6: Look-ahead errors according to the reference trajectory.

The equations 2.7 denote that the rate of the lateral error at the target point y_L is proportional to (i) the velocity v_x at the vehicle's center of gravity and the angle between the vehicle's heading and the tangent of the curve ε_L, (ii) to the lateral velocity v_y and (iii) the yaw-rate of the car $\dot{\psi}$ at the look-ahead distance L. Moreover, the rate of the angular error at the target point is simple expressed as the difference between the reference yaw-rate $\dot{\psi}_{ref} = v_x K$, for a curvature K, and the vehicle's current yaw-rate $\dot{\psi}$.

Combining the state space equations (2.6), (2.7), and considering that only the lateral error y_L is measured, the augmented vehicle model is derived as follows:

$$\begin{aligned} \dot{x}_v(t) &= A_v x_v(t) + B_{v_1} r(t) + B_{v_2} u(t) \\ y(t) &= C_v x_v(t) \end{aligned} \tag{2.8}$$

$$x_v(t) = \begin{bmatrix} v_y \\ \dot{\psi} \\ y_L \\ \varepsilon_L \end{bmatrix}, \quad A_v = \begin{bmatrix} -\dfrac{C_f + C_r}{m v_x} & -v_x + \dfrac{C_r L_r - C_f L_f}{m v_x} & 0 & 0 \\ \dfrac{-L_f C_f + L_r C_r}{I_z v_x} & -\dfrac{L_f^2 C_f + L_r^2 C_r}{I_z v_x} & 0 & 0 \\ -1 & -L & 0 & v_x \\ 0 & -1 & 0 & 0 \end{bmatrix},$$

$$B_{v_1} = \begin{bmatrix} 0 \\ 0 \\ 0 \\ 1 \end{bmatrix}, \quad B_{v_2} = \begin{bmatrix} \frac{C_f}{m} \\ \frac{L_f C_f}{I_z} \\ 0 \\ 0 \end{bmatrix} \quad C = \begin{bmatrix} 0 & 0 & 1 & 0 \end{bmatrix}.$$

where $x_v(t)$ is the combined state vector, $r(t) = \dot{\psi}_{ref}$ is the exogenous input, $u(t) = \delta$ the control input and $y(t) = y_L$ is the measurement used for feedback.

2.5 Identified Actuator Model & Extended Lateral Dynamics

Steering actuator dynamic plays a key role when it comes to design a lateral control system. A second order transfer function of the actuator model has been identified in the form below:

$$G_{act} = \frac{k}{s^2 + 2\zeta w_n s + w_n^2} e^{-T_d s} \tag{2.9}$$

where k, ζ, w_n and T_d are the static gain, the damping, the natural frequency and the time delays respectively. In state space the actuator model can be written as follows:

$$\begin{aligned} \dot{x}_{act}(t) &= A_{act} x_{act}(t) + B_{act} u(t) \\ u_{act}(t) &= C_{act} x_{act}(t) + D_{act} u(t) \end{aligned} \tag{2.10}$$

We remark that the identification of the steering actuator is not in the scope of this thesis. The model identification is presented in [Mahtout 2020].

For control design purpose, a second order Padé approximation of the time delay has been chosen [Dugard and Verriest 1998]. Below it is explained how the second order transfer function is obtained that models the time-delay term.

$$e^{-T_d s} = \frac{\sum_{j=0}^{M} \frac{[M]^j}{[2M]^j} (-T_d s)^j}{\sum_{j=0}^{M} \frac{[M]^j}{[2M]^j} (T_d s)^j} \tag{2.11}$$

where $[M]^j = M(M-1),\ldots,(M-j+1)$, i.e. the j leading terms of M! When M=1 :

$$\begin{aligned} M=1:\ e^{-T_d s} &= \frac{1-\frac{T_d s}{2}}{1+\frac{T_d s}{2}} \\ M=2:\ e^{-T_d s} &= \frac{1-\frac{T_d s}{2}+\frac{(T_d s)^2}{12}}{1+\frac{T_d s}{2}+\frac{(T_d s)^2}{12}} \end{aligned} \tag{2.12}$$

Therefore, M is selected as $M=2$, $x_{act} \in \mathbb{R}^4$ is the vector expressing the states of the actuator, $A_{act} \in \mathbb{R}^{4\times4}$, $B_{act} \in \mathbb{R}^{4\times1}$, $C_{act} \in \mathbb{R}^{1\times4}$, $D_{act} \in \mathbb{R}^{1\times4}$ are the systems matrices and $u_{act} \in \mathbb{R}$ is the output.

Considering the output of the actuator as the input of the vehicle model leads to the extended equation:

$$\dot{x}_v(t) = A_v x_v(t) + B_{v_1} r(t) + B_{v_2}(C_{act} x_{act}(t) + D_{act} u(t))$$

Consequently, the extended model can be given as:

$$\begin{aligned} \dot{x} &= Ax(t) + B_1 r(t) + B_2 u(t) \\ y &= Cx \end{aligned} \tag{2.13}$$

where $x(t) = \left[\frac{x_v(t)}{x_{act}(t)}\right] \in \mathbb{R}^8$ is the extended state vector, $A = \left[\begin{array}{c|c} A_v & B_{v_2}C_{act} \\ \hline 0 & A_{act} \end{array}\right] \in \mathbb{R}^{8\times8}$, $B_1 = \left[\frac{B_{v_1}}{0}\right] \in \mathbb{R}^8$, $B_2 = \left[\frac{B_{v_2}D_{act}}{B_{act}}\right] \in \mathbb{R}^8$ and $C = [C_v\ 0] \in \mathbb{R}^{1\times8}$ are the extended system matrices.

2.6 LPV Extended Lateral Dynamics Formulation

This section presents how the state space model, described in (2.13), can be formulated in a generic LPV model.

The vehicle model that has been utilized is the linearized bicycle model that includes the errors dynamics at the target point and the second-order delayed actuator transfer function. The state space representation (2.13) can be written in an LPV form by expressing the parameter-dependent matrix $A(v_x, L)$ in an LPV form, with v_x and L as parameters, known at each instant and bounded, and vary with respect to time.

The varying parameters in this case, are the speed v_x and the look-ahead distance L. These parameters are explicitly included in the system through the system matrix $A(v_x, L)$.

Therefore, defining the vector of varying parameters $\rho^T = [v_x \; L]^T$ we obtain the resulted LPV model of the form

$$\begin{aligned} \dot{x}(t) &= A(\rho(t))x(t) + B_1 r(t) + B_2 u(t) \\ y(t) &= Cx(t) \end{aligned} \tag{2.14}$$

According to the Pure-Pursuit algorithm [Coulter 1992], the control of the vehicle is achieved by minimizing the lateral error at the target point. At the same time, look-ahead time T is a design parameter since target points depends on it—i.e the look-ahead distance is affected ($L = v_x T$). For small look-ahead distance, the target points are located close to the vehicle and since the main goal is to reach these points, the vehicle will react quickly. On the contrary, when the target points are chosen to be far from the vehicle's position, then the vehicle will respond slower. Hence, it is clear that the look-ahead time T is a parameter that affects the bandwidth of the closed-loop system.

We will see later that (i) following different approaches for the synthesis of a dynamic output feedback LPV controller (Polytopic or Gridding approach) and (ii) selecting differently the look-ahead time T (constant or varying), the LPV model will change. This will be detailed in chapter four about the LPV path-following control.

2.7 Concluding Remarks

In this chapter we presented the in-vehicle architecture including the hardware and the software of the vehicle. We also emphasized on how a realistic model of the overall yaw dynamics of the vehicle can be constructed. That model includes the vehicle's dynamics, the errors through which the tracking of a trajectory can be achieved and, the steering's system identified model so that to include information about the steering capabilities in the extended model.

The final generic LPV model is the one that combined with the LPV control theory, presented in the next chapter, will be used for the design of dynamic output feedback steering controllers.

The next chapter will present (i) the LPV control methodlogies utilized in this thesis and (ii) a brief lateral control review.

Chapter 3

Theoretical & Methodological Control Background

Contents

3.1 Introduction

This chapter presents some basic definitions of Linear Matrix Inequalities (LMI), dynamical systems as a) Non-linear, b) Linear Time Invariant (LTI), c) Linear Time Varying (LTV) and

d) Linear Parameter Varying (LPV) so as to introduce gradually the needed LPV methodology utilized in this study to design a dynamic output feedback LPV controller for lateral control applications.

Apart from the mathematical tools for LPV controller synthesis, in this chapter we provide as well a brief lateral control review. Thus, we present some studies to achieve the tracking of a reference trajectory and how these approaches have been combined with different control techniques.

Let us recall that three approaches are mostly used for the representation of an LPV model and then for LPV control synthesis: 1) Polytopic Set of Parameters; 2) Linear Fractional Transformation; and 3) Set of Gridded Parameter Points.

Throughout this thesis, LPV dynamic output feedback controllers are designed, using the:

- Polytopic Set of the Parameter Space
- Set of Gridded Parameter Points approach

The mathematical definitions presented below are derived from the lectures in ["Linear matrix inequalities in control"], the books of [Boyd et al. 1994], [Boyd and Vandenberghe 2004] and from the articles [Apkarian, Gahinet, and Becker 1995], [Wu et al. 1996], [Scherer, Gahinet, and Chilali 1997]. Such key studies were used and implemented successfully other PhD thesis from GIPSA-lab as is documented in [Poussot-Vassal 2008], [Dubuc 2018], [Yamamoto 2017], [Robert 2007].

The rest of the chapter is organized as follows. Section 3.2 define the LMIs and it's combined with section 3.3 to present the LMI programming. Section 3.4 presents the different dynamical systems description in state space formulation. The previous sections lead to section 3.5 where the LPV control problem is defined. Sections 3.6 and 3.7 present the Polytopic and Gridding approaches for the design of an LPV dynamical output feedback controller. Finally, sections 3.8 and 3.9 give a lateral control review and sums up this chapter, respectively.

3.2 Linear Matrix Inequalities

We need to define first the LMIs, since they will be presented in the following sections as a tool for the synthesis of the LPV controllers.

A linear matrix inequality is an expression of the form

$$F(x) = F_0 + x_1F_1 + \cdots + x_nF_n = F_0 + \sum_{i=1}^{n} F_i x_i \prec 0 \tag{3.1}$$

where

- $x = (x_1, \ldots, x_n)$ is a vector of n real numbers called the decision variables.
- $F_0, \ldots, F_n$ are Hermitian matrices, i.e $F_j = F_j^T \in \mathbb{H}\ \forall j = 0, \ldots, n$
- The equation (3.1) means 'negative definite'. that is $u^T F(x) u < 0\ \forall\ u$ vector $\neq 0$. Since all eigenvalues of Hermitian matrices are real, (3.1) is equivalent to saying that all eigenvalues $\lambda(F(x)) < 0$.

Definition 1. *A LMI is an inequality*

$$F(x) \prec 0 \tag{3.2}$$

where F is an affine function mapping a finite dimensional vector space $\mathbb{X}$ to $\mathbb{H}$ or to the set $\mathbb{S}$.

The interest of LMIs lies on the fact that (3.2) defines a convex constraint on x. Then, the set $\mathbb{P}$ such that :

$$\mathbb{P} = \{x | F(x) \prec 0\} \tag{3.3}$$

defines the set of solutions of the LMI $F(x) \prec 0$ is convex.

Definition 2. *A system of LMI is a finite set of linear matrix inequalities*

$$F_1(x) \prec 0, \ldots, F_K(x) \prec 0 \tag{3.4}$$

The set of all x that satisfy (3.4) is convex. This set can be represented as the feasibility set of another LMI. Indeed, eq. (3.4) stands if and only if

$$F(x) = \begin{pmatrix} F_1(x) & 0 & \cdots & 0 \\ 0 & F_2(x) & \cdots & 0 \\ \vdots & \vdots & \ddots & \vdots \\ 0 & 0 & \cdots & F_K(x) \end{pmatrix} \tag{3.5}$$

where the last inequality makes sense as $F(x)$ is symmetric (or Hermitian) $\forall x$. Moreover, since the set of euigenvalues of $F(x)$ is simply the union of the eigenvalues of $F_1(x), \ldots, F_K(x)$, any x that satisfies $F(x) \prec 0$ also satisfies the system of LMIs 3.2 and vice versa. This concludes that multiple LMI constraints can always be converted into one single LMI constraint.

The LMIs find application in control, identification and signal processing where many optimization problems can be formulated using LMIs. Since $F(x) \prec 0$ defines a convex constraint on the cariable x, optimization problems involving the minimization/maximization of an objective function $f : \mathbb{P} \to \mathbb{R}$ with $\mathbb{P} = \{x | F(x) \prec 0\}$ belong to the class of convex optimization problems.

3.3 Semi-Definite Programming Problem

The optimization problem involved in this thesis is called LMI optimization. In terms of mathematical programming, this means semi-definite programming (SDP). In optimization, LMI programming is a generalization of the Linear Programming (LP) to cone positive semi-definite matrices, which is defined as the set of all symmetric positive semi-definite matrices of particular dimension.

Definition 3.3.1. *SDP problem*
A SDP problem is defined as:

$$\begin{aligned} &\textit{minimize} \quad c^T x \\ &\textit{subject to} \quad F(x) \preceq 0 \end{aligned} \tag{3.6}$$

From the control engineer point of view, if we can end to this problem formulation, then we can consider that the control problem is solved.

3.4 Dynamical Systems

This sections presents the basic notions of the state-space representation of dynamical systems. We provide the basic definitions of dynamical systems that they are mathematically formulated as a set of first-order Ordinary Differential Equations (ODEs).

3.4.1 Non-Linear Dynamical Systems

For given non-linear functions, $f : \mathbb{R}^n \times \mathbb{R}^u \to \mathbb{R}^n$ and $g : \mathbb{R}^n \times \mathbb{R}^u \to \mathbb{R}^p$, the ODE that represents the dynamics of a system is describes as follows:

$$\Sigma_{NL} : \begin{aligned} \dot{x}(t) &= f(x(t), u(t)) \\ y(t) &= g(x(t), u(t)) \end{aligned} \tag{3.7}$$

where $x(t) \in \mathbb{R}^n$ is the state space vector and $u(t) \in \mathbb{R}^m$ is the input vector and $y(t) \in \mathbb{R}^p$ is the output vector.

3.4.2 LTI Dynamical Systems

For the case where the non-linear dynamics are linearized or by definition the model is

linear then, the state-space representation is expressed below:

$$\Sigma_{LTI}: \begin{array}{l} \dot{x}(t) = Ax(t) + Bu(t) \\ y(t) = Cx(t) + Du(t) \end{array} \tag{3.8}$$

where $A \in \mathbb{R}^{n\times n}$, $B \in \mathbb{R}^{n\times m}$, $C \in \mathbb{R}^{p\times n}$ and $D \in \mathbb{R}^{p\times m}$ are the LTI state space matrices. $x(t) \in \mathbb{R}^n$ is the state space vector and $u(t) \in \mathbb{R}^m$ is the input vector and $y(t) \in \mathbb{R}^p$ is the output vector.

3.4.3 LTV Dynamical Systems

For the case where the linear expression of the dynamical systems includes explicitly the time t in the state space matrices, then a LTV system arises.

$$\Sigma_{LTV}: \begin{array}{l} \dot{x}(t) = A(t)x(t) + B(t)u(t) \\ y(t) = C(t)x(t) + D(t)u(t) \end{array} \tag{3.9}$$

where $A(t) \in \mathbb{R}^{n\times n}$, $B(t) \in \mathbb{R}^{n\times m}$, $C(t) \in \mathbb{R}^{p\times n}$ and $D(t) \in \mathbb{R}^{p\times m}$ are the LTV state space matrices. $x(t) \in \mathbb{R}^n$ is the state space vector and $u(t) \in \mathbb{R}^m$ is the input vector and $y(t) \in \mathbb{R}^p$ is the output vector.

3.4.4 LPV Dynamical Systems

An extension of the linear case rises in the LPV model formulation which is an overset inclusion of the linear model and a subset of the non-linear. As a result, an LPV system may arrive by interpreting the nonlinear model into an LPV one as a linear differential inclusion [Boyd et al. 1994]. This procedure is much more complex than simply linearizing the nonlinear system at many working points. The general idea consists in finding a transformation that turns the nonlinear model into a linear parameterized one. This parameterized (LPV) model should match the whole nonlinear system state space range. A nonlinear system can be described, in a non unique way, as an LPV system. Briefly, the general aim is to find $\rho \in P$ such that the LPV model is equivalent to the nonlinear one, i.e:

$$\begin{array}{l} A(\rho)x + B(\rho)u = f(x(t), u(t)) \\ C(\rho)x + D(\rho)u = g(x(t), u(t)) \end{array} \tag{3.10}$$

where $f(x, u)$ and $g(x, u)$ describe the nonlinear dynamical system and ρ is the known parameter vector that depends on a measured signal.

$$\Sigma_{LPV}(\rho): \begin{array}{l} \dot{x}(t) = A(\rho(t))x(t) + B(\rho(t))u(t) \\ y(t) = C(\rho(t))x(t) + D(\rho(t))u(t) \end{array} \tag{3.11}$$

where $A(\rho(t)) \in \mathbb{R}^{n\times n}$, $B(\rho(t)) \in \mathbb{R}^{n\times m}$, $C(\rho(t)) \in \mathbb{R}^{p\times n}$ and $D(\rho(t)) \in \mathbb{R}^{p\times m}$ are the LPV state space matrices. $x(t) \in \mathbb{R}^n$ is the state space vector and $u(t) \in U^m$ is the input vector and $y(t) \in Y\mathbb{R}^p$ is the output vector. $\rho = [\rho_1(t)\ \rho_2(t)\ ..\ \rho_s(t)] \in \Omega$ (convex set $\in \mathbb{R}^s$) is the vector of time varying parameters, assumed to be known and bounded $\forall t$. s denotes the number of varying parameters.

We stress that from a perspective of the form of varying parameter, different expressions appear.

- $\rho(t) = \rho$ is constant $\forall t$, then is a LTI dynamical system.
- $\rho(t) = l(t)$, where $l \in \mathbb{R} \rightarrow \mathbb{R}^s$ is merely a known function of time, then is a LTV dynamical system.
- $\rho(t)$ is a known external parameter, then is an LPV system.
- $\rho(t) = \rho(x(t))$, then is a quasi-LPV system.

3.5 LPV Control

The next step, which we focus on in this thesis, is, for a given LPV system, the synthesis of an LPV controller. Finding a Lyapunov function that ensures the stability of the parameter dependent closed-loop system results in an infinite set of LMIs (due to the infinite values of the ρ parameter vector), as it will be explained below. To relax this problem, different approaches to reduce this problem into a finite number of LMIs are commonly used:

1. Gridding parameter space ([Apkarian and Adams 2000]).
2. Transforming the system into a Polytopic system ([Apkarian, Gahinet, and Becker 1995]).

3.5.1 Generalized LPV system

In order to introduce the LMI based solution for controller synthesis, first the definition of the generalized system is recalled. It is worth noting that the generalized plant does include the plant model as well as some weighting functions representing the control objectives (as well known in H_∞ control) and illustrated later in the thesis.

Now, let us consider the following description of the generalized LPV system $\Sigma(\rho)$ as,

Definition 3.5.1. *Generalized LPV System*
A dynamical LPV system can be expressed by the following state space equations:

$$\Sigma(\rho): \begin{bmatrix} \dot{x}(t) \\ \hline z(t) \\ y(t) \end{bmatrix} = \left[\begin{array}{c|cc} A(\rho) & B_1(\rho) & B_2(\rho) \\ \hline C_1(\rho) & D_{11}(\rho) & D_{12}(\rho) \\ C_2(\rho) & D_{21}(\rho) & D_{22}(\rho) \end{array}\right] \begin{bmatrix} x(t) \\ \hline w(t) \\ u(t) \end{bmatrix} \tag{3.12}$$

where $x(t) \in \mathbb{R}^n$ express the states of the system, $w(t) \in \mathbb{R}^{n_w}$ are the exogenous inputs, $u(t) \in \mathbb{R}^{n_w}$ the control input, $z(t) \in \mathbb{R}^{n_z}$ controlled outputs, $y(t) \in \mathbb{R}^{n_y}$ hold for the system's measurements. $A(\rho) \in \mathbb{R}^{n \times n}$, $B_1(\rho) \in \mathbb{R}^{n \times n_w}$, $B_2(\rho) \in \mathbb{R}^{n \times n_u}$, $C_1(\rho) \in \mathbb{R}^{n_z \times n}$, $C_2(\rho) \in \mathbb{R}^{n_y \times n}$, $D_{11}(\rho) \in \mathbb{R}^{n_z \times n_w}$, $D_{12}(\rho) \in \mathbb{R}^{n_z \times n_u}$, $D_{21}(\rho) \in \mathbb{R}^{n_y \times n_w}$ and $D_{22}(\rho) \in \mathbb{R}^{n_y \times n_u}$. $\rho = [\rho_1(t)\ \rho_2(t)\ ..\ \rho_s(t)] \in \Omega$ (convex set) and $|\dot{\rho}(t)| \leq v_i$ $(i = 1, 2, .., s)$ is a vector of time varying parameters, assumed to be known and bounded $\forall t$.

3.5.2 LPV Controller

Then according to the general formulation, the LPV controller that is the solution of the LPV control problem, presented in the next subsection, is defined below:

Definition 3.5.2. *LPV Controller*
An LPV Controller can be described in the following form:

$$K(\rho): \begin{bmatrix} \dot{x}_c(t) \\ u(t) \end{bmatrix} = \begin{bmatrix} A_c(\rho) & B_c(\rho) \\ C_c(\rho) & D_c(\rho) \end{bmatrix} \begin{bmatrix} x_c(t) \\ y(t) \end{bmatrix} \tag{3.13}$$

where $x_c(t) \in \mathbb{R}^{n_c}$ define the states of the LPV controller. $A_c(\rho) \in \mathbb{R}^{n_c \times n_c}$, $B_c(\rho) \in \mathbb{R}^{n_c \times n_y}$, $C_c(\rho) \in \mathbb{R}^{n_u \times n_c}$ and $D_c(\rho) \in \mathbb{R}^{n_u \times n_y}$.

3.5.3 LPV Control Problem

For any system, the H_∞ control synthesis is a disturbance attenuation problem. It consists in finding a stabilizing controller $K(\rho)$ that minimizes the impact of the input disturbances $w(t)$ on the controlled output $z(t)$. In the case of the H_∞ control, this impact is measured thanks to the induced L_2 norm [Becker and Packard 1994].

Remark: It is known that the H_∞ norm is defined for LTI systems only. For LPV systems, we should here refer to as the L_2-induced norm. However, for simplicity we keep the usual term.

A more formal way to formulate this problem can be written as: minimize the H_∞ norm of the interconnection of $\Sigma(\rho)$ and $K(\rho)$ on the set of internally stabilizing controllers so that the H_∞ norm of the transfer functions G, from input w to output z satisfies

$$\|G\|_\infty = \sup_{\rho\in\Omega} \sup_{\|w\|\neq 0} \frac{\|z\|_2}{\|w\|_2} < \gamma_\infty \tag{3.14}$$

Now, when we refer to the H_∞ control problem, we mean: Find a controller $K(\rho)$ for system $\Sigma(\rho)$ such that, given γ_∞

$$\gamma_\infty = \min_{A_c(\rho),B_c(\rho),C_c(\rho),D_c(\rho)} \|G\|_\infty \tag{3.15}$$

In this way, we can utilize the LMIs, that will be introduced in the next sections according to the two approaches, to solve a SDP and compute an LPV controller.

3.6 LPV Polytopic Approach

Now, we provide the several steps to follow and achieve the design of a dynamical output feedback controller according to the polytopic approach. These steps consider the polytopic model formulation and the considtions that must be sastisfied and the associated LMIs to be solved for the control synthesis.

3.6.1 LPV/Polytopic Modeling

The generic LPV representation (3.11), can be written in an LPV/Polytopic form, by considering the varying parameters in the plant matrices as bounded and real-time measured. In that sense, the system matrices are fixed functions of the parameter vector $\rho(t)$.

More specifically, it is assumed that the vector ρ varies in a polytope Θ of vertices θ_i.

$$\begin{gathered} \rho(t) \in \Theta \\ \Theta = Co\{\theta_1, \theta_2, .., \theta_N\} \end{gathered} \tag{3.16}$$

where Co denotes the convex hull of the finite N vertices θ_i.

The vertices θ_i correspond to the combinations of the extremum values of the parameters ρ_i, i.e $\underline{\rho_i} \leq \rho_i \leq \overline{\rho_i}$. Respectively, the LPV Polytopic model is constructed by assuming that the LPV plant matrices, which contain the parameters ρ_i, vary in a matrix polytope. That polytope is defined as the convex hull of a number of vertex matrices of the same dimention. These vertex matrices are computed for frozen values of parameters equal to the vertices θ_i.

Another assumption, it is the *Affine* dependance of the LPV matrices on the parameter vector ρ [Mohammadpour and Scherer 2012], i.e for the LPV matrix should stand that:

$$A(\rho) = A_{\rho_0} + \sum_{i=1}^{s} \rho_i A_{\rho_i} \tag{3.17}$$

where A_{ρ_0}, A_{ρ_i} are LTI state matrices and n is the number of parameters.

Then, the LPV matrix $A(\rho)$ can be expressed, according to the vertex property [Apkarian, Gahinet, and Becker 1995], as a convex hull of the vertex matrices created by all the possible combinations of the parameter bounds, as shown below:

$$\begin{aligned} A(\rho) &= \sum_{i=1}^{N} a_{\theta_i}(t) A_i \\ \sum_{i=1}^{N} a_{\theta_i}(t) &= 1,\ a_{\theta_i}(t) \geq 0 \end{aligned} \tag{3.18}$$

where $a_\theta^T(t) = (a_{\theta_1}(t), .., a_{\theta_N}(t))^T$, N are the scaling variables and the number of vertices accordingly. The variables $a_\theta(t)$ are computed according to the real-time position of $\rho(t)$ in the polytope Θ and, subsequently w.r.t the vertices $\theta_i \in \mathbb{R}^n$, formulated as such:

$$\rho(t) = \sum_{i=1}^{N} a_{\theta_i}(t) \theta_i \tag{3.19}$$

By replacing the Polytopic matrices formed as in (4.12) to the (3.11), we provide the resulting LPV Polytopic model, expressed below:

$$\begin{aligned} \dot{x}(t) &= A(\rho(t))x(t) + B(\rho(t))u(t) \\ y(t) &= C(\rho(t))x(t) + D(\rho(t)u(t) \\ \begin{pmatrix} A(\rho) & B(\rho) \\ C(\rho) & D(\rho) \end{pmatrix} &= \sum_{i=1}^{N} a_{\theta_i} \begin{pmatrix} A_i & B_i \\ C_i & D_i \end{pmatrix},\ a_{\theta_i} \geq 0,\ \sum_{i=1}^{N} a_{\theta_i} = 1 \end{aligned} \tag{3.20}$$

3.6.2 LPV Polytopic Controller Synthesis

This part of the LPV/Polytopic approach overview presents how an LPV dynamical output feedback controller according to the polytopic approach. In this subsection, we recall the necessary LMIs (see [Scherer, Gahinet, and Chilali 1997]) to be solved at every vertex of the parameters polytope as it is proven from [Apkarian, Gahinet, and Becker 1995] for the LPV/H_∞ polytopic controller synthesis.

We remark that the polytopic system under consideration is the same defined in (3.20).

Definition 3.6.1. *LPV Control Problem:*
The LPV control synthesis problem consists in finding an LPV controller $K(\rho)$, so that the closed-loop system is stable and equation (3.14) *stands.*

Theorem 3.6.1. *If there exists $\hat{A}$, $\hat{B}$, $\hat{C}$, $\hat{D}$ and positive definite matrices $X \succ 0$, $Y \succ 0$ satisfying the following LMIs* (3.21)*, then the LPV Polytopic Controller which stabilizes the LPV system is given by* (3.23)*.*

$$\begin{bmatrix} M_{11}(\rho_i) & M_{12}(\rho) \\ M_{12}^T(\rho_i) & M_{22}(\rho_i) \end{bmatrix} \prec 0 \qquad i = 1, 2, .., N \tag{3.21}$$

where

$$\begin{aligned} M_{11}(\rho_i) &= A(\rho_i)X + XA^T(\rho_i) + B_2\hat{C}(\rho_i) + \hat{C}^T(\rho_i)B_2^T \\ M_{12}(\rho_i) &= \hat{A}(\rho_i) + A^T(\rho_i) + C_2^T\hat{D}^T(\rho_i)B_2^T \\ M_{22}(\rho_i) &= YA(\rho_i) + A^T(\rho_i)Y + \hat{B}(\rho_i)C_2 + C_2^T\hat{B}^T(\rho_i) \end{aligned} \tag{3.22}$$

Here it is presented the LPV polytopic controller as the convex hull of the LTI vertex controllers.

$$K(\rho) = Co\begin{pmatrix} A_c(\rho_i) & B_c(\rho) \\ C_c(\rho_i) & D_c(\rho_i) \end{pmatrix} \tag{3.23}$$

where

$$\begin{aligned} D_c(\rho_i) &= \hat{D}(\rho_i) \\ C_c(\rho_i) &= (\hat{C}(\rho_i) - D_c(\rho_i)C_2X)M^{-T} \\ B_c(\rho_i) &= N^{-1}(\hat{B}(\rho_i) - YB_2D_c(\rho_i)) \\ A_c(\rho_i) &= N^{-1}(\hat{A}(\rho_i) - YA(\rho_i) - YA(\rho_i)X - YB_2D_c(\rho_i)C_2X)M^{-T} \\ &\quad -B_c(\rho_i)C_2XM^{-T} - N^{-1}YB_2C_c(\rho)_i) \end{aligned} \tag{3.24}$$

where M, N are defined such that

$$MN^T = I_n - XY \tag{3.25}$$

which can be solved through a singular value decomposition and a Cholesky factorization.

3.7 Gridded Parameter Points Approach

Let us recall the basics of the LPV Gain scheduled Gridded Controller for a simplified case of the generalized system (3.12) in order to present the explicit solution. The interested reader may find more details in [Wu 1995], [Wu et al. 1996].

For the purpose of simplification, the following assumptions (Δ_{1-4}) are considered on the LPV Generalized state space system.

$\Delta_1 : D_{11}(\rho) = 0_{n_z \times n_w}$
$\Delta_2 : D_{22}(\rho) = 0_{n_y \times n_u}$
$\Delta_3 : D_{12}(\rho)$ is of full column rank for all $\rho \in \Omega$
$\Delta_4 : D_{21}(\rho)$ is of full row rank for all $\rho \in \Omega$

Definition 3.7.1. *Simplified Generalized LPV System*
Taking into account the previous assumptions, a dynamical LPV system can be expressed by the following state space equations:

$$S(\rho) : \begin{bmatrix} \dot{x}(t) \\ \hline z_1(t) \\ z_2(t) \\ y(t) \end{bmatrix} = \left[\begin{array}{c|ccc} A(\rho) & B_{11}(\rho) & B_{12}(\rho) & B_2(\rho) \\ \hline C_{11}(\rho) & 0 & 0 & 0 \\ C_{12}(\rho) & 0 & 0 & I_{n_{w_2}} \\ C_2(\rho) & 0 & I_{n_{z_2}} & 0 \end{array}\right] \begin{bmatrix} x(t) \\ \hline w_1(t) \\ w_2(t) \\ u(t) \end{bmatrix} \tag{3.26}$$

where $B_1(\rho) = [B_{11}(\rho) \;\; B_{12}(\rho)]$, $C_1(\rho) = [C_{11}(\rho) \;\; C_{12}(\rho)]$.

The control objective considered for the closed-loop LPV system is to minimize the L_2-norm from the disturbance to error signal, i.e. to provide disturbance/error attenuation.

Below, is presented the theorem from [Wu et al. 1996] as the solution of the control synthesis problem for the minimization of (3.14).

Theorem 3.7.1. *Given a compact set $\Omega \subset \mathbb{R}^s$, non-negative $\{v_i\}_{i=1}^s$ numbers, performance level $\gamma > 0$, and the open-loop LPV system in* (3.26)*, the LPV synthesis γ-performance/ v-variation problem is solvable if and only if there exist continuously differentiable matrix functions $X : \mathbb{R}^s \to \mathbb{R}^{n \times n}$ and $Y : \mathbb{R}^s \to \mathbb{R}^{n \times n}$, such that for all $\rho \in \Omega$, $X(\rho) \succ 0$, $Y(\rho) \succ 0$ and the set of Linear Matrix Inequalities (LMIs) expressed by* (3.28) *is satisfied.*

where:

$$\begin{aligned} \hat{A}(\rho) &= A(\rho) - B_2(\rho)C_{12}(\rho) \\ \tilde{A}(\rho) &= A(\rho) - B_{12}(\rho)C_2(\rho) \end{aligned} \tag{3.27}$$

Using this control synthesis procedure, the existence of such a parameter-dependent controller $K(\rho)$ is determined. That controller will stabilize the closed-loop LPV system and guarantee the induced L_2-norm performance of the closed-loop system less or equal than $\gamma > 0$.

Solving the set of LMIs (3.28), an n-dimensional strictly proper controller (3.13) is defined

$$\begin{bmatrix} Y(\rho)\hat{A}^T(\rho) + \hat{A}(\rho)Y(\rho) - \sum_{i=1}^{s} \pm \left(v_i \frac{\partial Y(\rho)}{\partial \rho_i} \right) - \gamma B_2(\rho) B_2^T(\rho) & Y(\rho)C_{11}^T(\rho) & B_1(\rho) \\ C_{11}(\rho)Y(\rho) & -\gamma I_{n_{z_1}} & 0 \\ B_1^T(\rho) & 0 & -\gamma I_{n_w} \end{bmatrix} \prec 0$$

$$\begin{bmatrix} \tilde{A}^T(\rho)X(\rho) + X(\rho)\tilde{A}(\rho) + \sum_{i=1}^{s} \pm \left(v_i \frac{\partial X(\rho)}{\partial \rho_i} \right) - \gamma C_2^T(\rho) C_2(\rho) & X(\rho)B_{11}^T & C_1(\rho) \\ B_{11}^T(\rho)X(\rho) & -\gamma I_{n_{w_1}} & 0 \\ C_1^T(\rho) & 0 & -\gamma I_{n_z} \end{bmatrix} \prec 0$$

$$\begin{bmatrix} X(\rho) & I_n \\ I_n & Y(\rho) \end{bmatrix} \succeq 0 \tag{3.28}$$

in state space form, which aims at minimizing (3.14), where:

$$\begin{aligned} A_c(\rho) &= \left[A(\rho) + \gamma^{-1}[Q^{-1}(\rho)X(\rho)L(\rho)B_{12}^T + B_1(\rho)B_1^T(\rho)]Y^{-1}(\rho) + B_2(\rho)F(\rho) + \right. \\ &\quad \left. Q^{-1}(\rho)X(\rho)L(\rho)C_2(\rho) - Q^{-1}(\rho)H(\rho,\dot{\rho}) \right], \\ B_c(\rho) &= -\left[Q^{-1}(\rho)X(\rho)L(\rho) \right], \\ C_c(\rho) &= F(\rho) \end{aligned} \tag{3.29}$$

with

$$\begin{aligned} Q(\rho) &= \left[X(\rho) - Y(\rho)^{-1} \right], \\ F(\rho) &= -\left[\gamma B_2^T(\rho)Y^{-1}(\rho) + C_{12}(\rho) \right], \\ L(\rho) &= -\left[\gamma X^{-1} C_2^T(\rho) + B_{12}(\rho) \right], \\ H(\rho,\dot{\rho}) &= -\left[A_F^T(\rho)Y^{-1} + Y^{-1}A_F(\rho) + \sum_i \left(\dot{\rho} \frac{\partial Y^{-1}}{\partial \rho} \right) + \right. \\ &\quad \left. \gamma^{-1} C_F^T(\rho) C_F(\rho) + \gamma^{-1} Y^{-1}(\rho) B_1(\rho) B_1^T(\rho) Y^{-1}(\rho) \right] \end{aligned} \tag{3.30}$$

In this way, the LPV control problem is tackled directly avoiding the need of design a LTI controller for each value of the parameter.

3.7.1 Computational Aspects

An ad hoc approach to solve the LMIs presented above in eq. (3.28), is to select scalar

differentiable basis functions $\{f_i : \mathbb{R}^s \to \mathbb{R}\}_{i=1}^N$ and $\{g_i : \mathbb{R}^s \to \mathbb{R}\}_{i=1}^N$ to express $X(\rho)$, $Y(\rho)$ accordingly and optimize (3.28) over $\{X_i\}_{i=1}^N$, $X_i \in \mathbb{R}^{n\times n}$ and $\{Y_i\}_{i=1}^N$, $Y_i \in \mathbb{R}^{n\times n}$.

$$\begin{aligned} X(\rho) &= \sum_{i=1}^{N} f_i(\rho) X_i \\ Y(\rho) &= \sum_{i=1}^{N} g_i(\rho) Y_i \end{aligned} \tag{3.31}$$

Subsequently, selecting a grid of the parameter space Ω by M points $\{\rho_k\}_{k=1}^M$, a finite dimensional convex optimization problem is obtained. Finally, a grid of LTI state-space controllers is obtained where a linear interpolation between the grid points is performed for the implementation of the LPV gain-scheduled controller. We remark that the LPVTools toolbox [Hjartarson, Seiler, and Packard 2015] is utilized for the gridding of the LPV model and for the synthesis of the LPV/Gridded controller.

The implementation of the LPV gridded controller is presented and explained in chapter four where the case of the embedded platform is concerned and thus, a off-line discretization for a sampling time T_s takes place as well.

3.8 Brief Lateral Control Review

Intelligent vehicles' architecture is at the intersection of multiple research fields ranging from location or perception to path planning and control [González et al. 2015]. Among them the control architecture can be classified into different categories according to the considered dynamics (and degrees of freedom) such as: Lateral control, Longitudinal control, Integrated Lateral/Longitudinal control and higher control issues [Shladover 1995].

Lateral control refers to as the ability of automatically steer a vehicle, and perform maneuver such as lane changes. If lateral control can be tackled using several actuators, as active front steering with an additional yaw moment (see [Guo et al. 2017] for a nonlinear MPC method and [Doumiati et al. 2013] for an H_∞/LPV one) it is still of high interest to deal with the steering control only.

3.8.1 Some Lateral Control Approaches

Major contributions have been achieved the previous decades on the steering control for autonomous vehicles. Ackermann [Ackermann, Bünte, and Odenthal 1999] was one of the first that made a breakthrough on lateral control by applying active steering with yaw rate error compensation to decouple the yaw and lateral dynamics. In 1995, Carnegie Mellon

University demonstrated the Navlab car [Jochem and Pomerleau 1996] completing a cross-country journey, whose steering control minimized the lateral deviation of the vehicle and its heading error. In 1998, Broggi [Broggi et al. 1999] leading the ARGO project, performed a journey through Italy in autonomous mode and its control implementation was based on a variable gain proportional controller minimizing a lateral offset at a look-ahead distance according to the reference trajectory. In 2005, Stanley vehicle [Thrun et al. 2006] won the second DARPA Grand Challenge whose steering action was a non-linear function of the cross-track error and the vehicle's orientation error, measured relatively to the nearest path segment. In 2013, [Ziegler et al. 2014] demonstrated the Bertha Benz experimental vehicle that completed around 103 km in an historical route in Germany. The lateral control algorithm consists of a feed-forward term aiming at disturbance compensation of the road curvature at a close look-ahead point and of a feedback term to minimize the lateral displacement of the car to the desired trajectory. Summing these two terms, a yaw-rate reference is computed that is used to an inverse single-kinematic in order to calculate the desired steering command that is fed to the steering actuation system. In [Xu et al. 2018], the authors demonstrated in the Grand Cooperative Driving Challenge of 2016 a driverless electric vehicle whose control system was a state feedback with pole placement using the kinematic bicycle model of the vehicle, minimizing the cross-track and heading errors of the vehicle.

More recently, various control techniques have been successfully applied for lateral control. To cite a few, in [Falcone et al. 2007], Model Predictive Control (MPC) approaches were formulated using a non-linear model in the first case and in the second an on-line linearization vehicle model, solving a finite horizon optimal control problem respecting the state constraints for the stabilization of the car. [Xu, Peng, and Tang 2020] proposes a preview steering control design that tackles communication delay, steering lag and is implemented as a state feedback controller that uses as a feedforward term the future road curvature information. In AUTOPIA program different steering systems were implemented in mass-produced cars focused on fuzzy logic: A cascade control architecture [Pérez, Milanés, and Onieva 2011] was implemented mimicking a human driver's behaviour and in [Onieva et al. 2011] genetic algorithms were used to adjust automatically a fuzzy steering controller. Moreover, fuzzy logic was used in [Guechi et al. 2009] where a fuzzy Takagi-Sugeno representation is utilized to find a stabilizing controller for the mobile robot tracking problem. Moreover, [Guechi et al. 2012] used flatness properties to design an output feedback controller of a unicycle-type vehicle while sliding mode theory is applied for the estimation of the delay of the measurements. The same theory is applied in [Nguyen, Sentouh, and Popieul 2018], where they demonstrated a constrained Takagi-Sugeno control method using fuzzy Lyapunov control framework for automatic lane keeping. The lab of Stanford, under the lead of Prof. Gerdes, presents the MPC approach for vehicle stabilization at the limits of handling. They utilize a model predictive envelope controller to bound the vehicle within the stable region and for the case of obstacle avoidance [Beal and Gerdes 2012], [Funke et al. 2016]. In [Tan and Huang 2014], a PID controller was proposed as a model of how drivers steer based on observations and was validated on a bus revenue service. The output of the controller is the rate of the steering angle with a single gain that minimizes desired and current yaw rate values. More recently, in 2020 the TORNADO project was presented in a two-week robot-taxi demonstration in peri-urban and rural areas of France [Milanés et al. 2021]. The lateral control module consists of two yaw-rate tracking

controllers, where the yaw-rate reference is computed with respect to a target point (set at a look-ahead distance) onto the reference trajectory. These two controllers were designed independently off-line to handle the case of lane-tracking (high-bandwidth) and lane-change (low-bandwidth). The proper switching between these two controllers were achieved by a switching supervisor scheme based-on the Youla-Kucera parameterization.

3.8.2 LPV-based Lateral Control Approaches

On the other hand, to deal with complex non-linear systems, gain-scheduling control is a key design procedure which arises in many applications. Indeed LPV control theory emerged to handle robustness and performance guarantees for the whole operating domain of the varying parameters of dynamical system [Mohammadpour and Scherer 2012]. Let us mention that LPV gain-scheduling control has been successfully applied to the control synthesis for many aerospace applications as in the problem of active flutter suppression [Barker and Balas 2000] but also in the automotive sector. Thus this approach has shown its value for various complex intelligent vehicle applications [Sename, Gaspar, and Bokor 2013], such as global chassis control, semi-active suspension control [Gáspár et al. 2016], or active anti-roll bar system of heavy vehicles [Sename, Dugard, and Gáspár 2019]. See [Hoffmann and Werner 2014] for an interesting survey of LPV applications.

However, as far as our knowledge is concerned, its potential with regard to autonomous vehicles has so far been very little explored. As illustration, LPV theory has been used for automatic lane keeping in [Hingwe et al. 2002], where a grid-based approach is used to synthesize LPV controller which is implemented and tested on a tractor-trailer. The velocity-dependent controller is designed imposing performance constraints via H_∞ weighting functions. Another interesting approach to treat the longitudinal speed, which is an inherent parameter in the lateral control problem, is the polytopic approach. According to that method, the parameter set is represented by a polytope which is defined by the combinations for the maximal values of the parameters. Due to that fact, the polytope may be over-bounded, meaning that the volume of the geometrical representation is far larger than the "true" parameter trajectory, and the associated LPV controller cannot satisfy the closed-loop performance adequately. For that reason, several attempts have been made to reduce the size of the polytope and provide a less conservative vehicle model [Corno et al. 2020; Li et al. 2021], where the performance is likely improved. In [Kang, Lee, and Chung 2018] a kinematic vehicle model is used and an LPV state feedback steering control has been designed using the polytopic approach, with varying parameters the longitudinal speed and the look-ahead distance. [Fényes et al. 2021] presents the learning-based observer and an LPV one in a joint observer to tackle the path-following control. Moreover, [Fényes, Németh, and Gáspár 2020] provides a data-driven LPV-based modeling and control for the lateral control problem of an autonomous vehicle. Furthermore, LPV control theory has been used to tackle an online planning application for race autonomous vehicles [Alcalá, Puig, and Quevedo 2020], where LPV was used to reformulate a non-linear vehicle model into a pseudo-linear expressing it in an LPV form and consequently convexify an objective function to be included in a MPC formulation. In [Alcalá et al. 2020], another

LPV-MPC formulation is also developed to design a high-level planner and control for the case of autonomous racing. More recently, in [Atoui et al. 2021] a comparison of the LPV approaches is conducted for path-following purposes, while a single yaw-rate tracking controller is designed for the case of the bicycle model while the only parameter is considered the longitudinal speed of the vehicle.

3.9 Concluding Remarks

In this chapter we presented the main the definitions required for the reader to understand the LPV control theory. The LPV controller synthesis problem is solved by following the approaches a) Polytopic and b) the Gridding.

Finally, we presented some significant contributions and the different control methods that combined for the design of an automatic steering system.

These two approaches will be followed in the next chapters, combined with the complete steering model presented in the previous chapter, in order to design LPV controllers for the lateral system of an autonomous vehicle.

Chapter 4

LPV Path-Following Control

Contents

4.1 Introduction & Contributions

This chapter presents the gradual exploration and design of a dynamic output feedback LPV Lateral control system for autonomous vehicles. Thus, it presents the main contributions of this thesis on the different LPV-based steering controllers.

The main emphasis is given for the scenario of path-following of a reference trajectory for a varying speed. As already mentioned in the previous chapter three, the problem of designing a performant lateral control system is crucial and, it is considered a problem of control synthesis [Tan and Huang 2014], [Li et al. 2021], [Falcone et al. 2007], [Rajamani 2011].

This chapter considers as input the LPV model from chapter 2 that describes fully the yaw & steering mechanism of the vehicle. As it is already mentioned, the (i) Polytopic and the (ii) Gridding set of parameter space are utilized to design an LPV controller. That theory is combined with different selections of the look-ahead time T per speed.

Thus, the approaches presented in this chapter are the following:

1. LPV/Polytopic Control Design with constant look-ahead time T.

   It details the investigation of the LPV control design according to the Polytopic approach and its 2D Polytope reduction for varying longitudinal speeds while the look-ahead time is selected constant. This contribution has been:

   - Accepted and published in the *16th IFAC Symposium on control in Transportation Systems*, held in Lille, France (see [Kapsalis et al. 2021b]). Selected to extended submission for a Special Issue of *Control Engineering Practice Journal*.

2. LPV/Polytopic Control Design with varying look-ahead time T.

   details the novel proposed LPV Polytopic approach where the look-ahead time is considered then varying. Subsequently, a 3D polytope, associated to the parameter vector, is treated and reduced. In that way, the inherent conservatism of the method is avoided, as it can be seen by the encouraging results. The journal article associated to that contribution has been:

   - Submitted as an extended version of [Kapsalis et al. 2021b] (as explained above) for the Special Issue on *Innovative Control Approaches for Smart transportation Systems* in *Control Engineering Practice*.

3. LPV/Gridding Control Design with varying look-ahead time T.

   It presents a different approach for the case where the look-ahead time T is considered varying. In contrast with the polytopic approach, the gridding approach treats every speed point and its selected look-ahead time. Then, simulations and experimental results illustrate the good performance of the proposed control scheme. The related journal article with that contribution has been:

   - Accepted and published in the *IET Control Theory & Applications* (see [Kapsalis et al. 2020]).

This chapter is structured as follows: Section 4.2 presents the 1*st* approach and the associated simulation and experimental results. Section 4.3 presents the 2*nd* approach and the

results proving that the improvement and how the limitations of the $1st$ are avoided. Finally, section 4.4 explains the LPV/Gridding approach, the controller synthesis and the tracking assessment based on the results.

4.2 LPV/Polytopic Controller with constant Look-ahead time T

This part of the current chapter presents the primal work that has been conducted, and details how a proper lateral control system should be designed that depends on the minimization of look-ahead errors.

These errors are computed at a target point w.r.t a selected look-ahead distance L per speed v_x in front of the vehicle. The simplest way to define the look-ahead distance profile per speed is to select the look-ahead time T constant.

This section presents the simulation and experimental results of the designed LPV/Polytopic controller for constant look-ahead time T.

4.2.1 LPV/Polytopic Model Formulation

The state space representation in (2.14) (see chapter 2) is expressed as an LPV system, with v_x and L as parameters, by expressing subsequently the parameter-dependent matrix $A(v_x, L)$ in an LPV form.

Therefore, defining the vector of varying parameters $\rho^T = [v_x \ L]^T$ we obtained that the state matrix is of the form

$$A(\rho) = \rho_1 A_{\rho_1} + \frac{1}{\rho_1} A_{\frac{1}{\rho_1}} + \rho_2 A_{\rho_2} \tag{4.1}$$

To be able to express the model system in a proper LPV form for the chosen design method (here the polytopic one); see [Mohammadpour and Scherer 2012], the matrices that depend on time-varying parameters must be affine with respect to the the vector of varying parameters. From (4.1), $A(\rho)$ is not affine with respect to the parameter vector ρ. To get such an affine form, it is necessary to define $1/v_x$ as a new additional parameter, which leads to a vector of 3 varying parameters.

Such a choice may increase the conservatism due to the overbounding of the parameter space. That leads to a larger convex set to be considered during the optimization process. However, as seen later, some reduction of the polytopic set might be considered.

On the other hand, the look-ahead time $T = 1.5\ s$ is chosen constant to further reduce the size of polytope, by considering $L = 1.5v_x$ which is a coherent choice for the path tracking control. Therefore the vector of varying parameters is considered as:

$$\rho^T = [v_x\ 1/v_x]^T \tag{4.2}$$

Considering as bounds of the parameters $\underline{\rho_i} \leq \rho_i \leq \overline{\rho_i}$, the LPV matrix $A(\rho)$ can be written as:

$$A(\rho) = \sum_{i=1}^{4} a_i(\rho) A_i \tag{4.3}$$

where $i = 1, \ldots, 4$ are the number of vertices θ_i of the polytope i.e all the possible combinations of the lower and upper bounds $\underline{\rho_i}$ and $\overline{\rho_i}$. Additionally, $a_i(\rho)$ are parameter-dependent variables computed on-line, as explained later for the on-line implementation of the LPV controller.

Replacing the LPV matrix (4.3) in (2.13), the polytopic system, by [Apkarian, Gahinet, and Becker 1995], is:

$$\begin{aligned} \dot{x}(t) &= A(\rho)x(t) + B_1 w(t) + B_2 u(t) \\ y(t) &= Cx(t) \end{aligned} \tag{4.4}$$

4.2.2 Reduction of the 2D Polytope

It is obvious that the parameters defined previously, i.e $1/v_x$ and v_x, depend on each other. This may lead to a conservatism using the polytopic approach (this is indeed a drawback of such an approach; see [Robert, Sename, and Simon 2009]., [Corno et al. 2020], [Li et al. 2021]. As a result, the performances of the closed-loop system may be degraded or even the controller might not be implementable, as the result of the optimization may has bad performance or even be unstable.

The modification presented below is to define the LPV controller based on a reduced polytope that expresses at least the possible combinations of the bounds of the parameters (see Fig 4.1(a)).

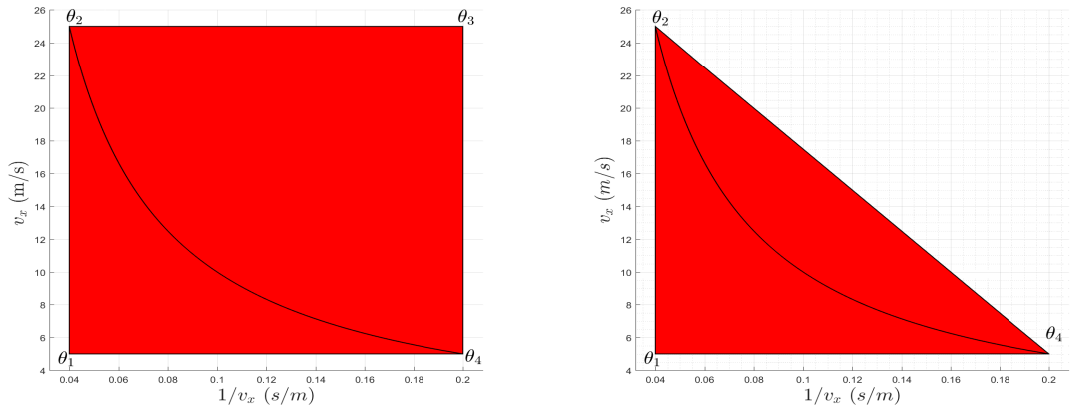

(a) Full 4 vertices polytope

(b) Reduced 3 vertices polytope

Figure 4.1: Full and Reduced Conservatism Polytopes w.r.t the real parameters variations.

The operating domain of speed is considered $v_x \in [5, 25]$ m/s, so the bounds of the parameter vector ρ are the following:

$$\begin{aligned} 5 \leq \rho_1 \leq 25 \\ 0.04 \leq \rho_2 \leq 0.2 \end{aligned} \tag{4.5}$$

The two realistic vertices of the polytope (see Fig. 4.1(a)) are θ_2 and θ_4 but in order to keep the convexity property and solve the equivalent LMIs, the reduced polytope should contain all the intermediate combinations of the parameters; see [Boyd et al. 1994]. For that reason, the third selected vertex for the reduced polytope is θ_1 (Fig. 4.1(b)).

The whole procedure for the reduction of a polytope is detailed in [Robert, Sename, and Simon 2009], where the authors implemented the synthesized controller based on a reduced polytope to a T inverted pendulum.

4.2.3 LPV Polytopic Controller Synthesis & Tuning

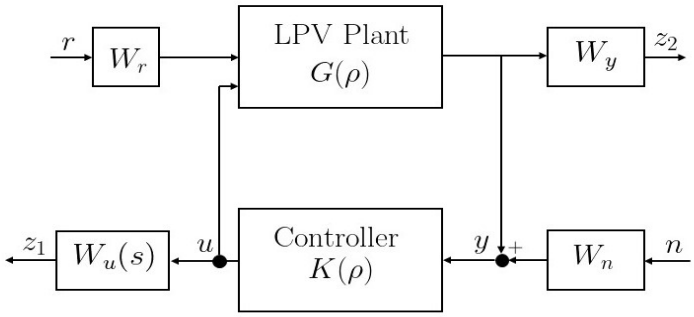

Figure 4.2: Path-following feedback control configuration.

The tuning of the dynamic output feedback LPV/Polytopic controller is achieved by introducing performance/template weighting functions W_y, $W_u(s)$, W_r & W_n [Skogestad and Postlethwaite 2007]. These functions are selected as such:

- The filter $W_u(s)$ is chosen as $W_u(s) = \dfrac{s + w_{bc}/M}{\epsilon s + w_{bc}}$ with $w_{bc} = 1\ rad/s$ to respect the corresponding control objective about the bandwidth of the controller, $M = 2\ (6db)$ to respect the saturation limits and $\epsilon = 0.1\ (10^{-1}\ rad/s)$ that expresses the frequency where the roll-off starts to achieve better noise attenuation.
- The weighting function W_y is chosen as $W_y = 0.5$. It aims at imposing weight on the lateral error at the target point, as a way to achieve the comfortable tracking of the reference trajectory.
- Finally, constant scaling weights are added on the noise signal and the reference, respectively as: $W_n = 0.5$ and $W_r = 0.3$.

The generalized LPV plant (4.6) that describes the control configuration of the weighted control configuration scheme (depicted in Fig. 4.2), is expressed below.

$$\begin{bmatrix} \dot{x}_g(t) \\ y(t) \\ z(t) \end{bmatrix} = \begin{bmatrix} \mathcal{A}(\rho) & \mathcal{B}_1 & \mathcal{B}_2 \\ \mathcal{C} & 0 & 0 \\ \mathcal{C}_z & \mathcal{D}_{z_1} & \mathcal{D}_{z_2} \end{bmatrix} \begin{bmatrix} x_g(t) \\ w(t) \\ u(t) \end{bmatrix} \tag{4.6}$$

where x_g is the augmented state vector that consists of the states of the extended model (2.13) and the states x_z, which express the dynamics of the weighting functions i.e $x_g(t) = \begin{bmatrix} x(t) \\ x_z(t) \end{bmatrix} \in \mathbb{R}^9$, $z(t) = \begin{bmatrix} z_1(t) \\ z_2(t) \end{bmatrix} \in \mathbb{R}^2$ and $w(t) = \begin{bmatrix} r(t) \\ n(t) \end{bmatrix} \in \mathbb{R}^2$.

It has to be remarked that the generalized plant in (4.6) is also in polytopic form made of the vertices $\theta = (\theta_1, \theta_3, \theta_4)$ of the reduced polytope.

Problem Definition: The LPV control synthesis problem consists in finding an LPV controller $K(\rho)$, for the polytopic approach the vertex controllers K_i, by solving off-line the appropriate set of LMIs, so that the closed-loop system represented in Fig. 4.2 is stable and there exists a $\gamma > 0$ s.t.

$$\sup_{||w|| \neq 0} \frac{\|z\|_2}{\|w\|_2} < \gamma, \ \forall \ \theta_i \tag{4.7}$$

4.2.4 Solution & Frequency Response of the LPV Polytopic Controller

The solution of the synthesis of the LPV/Polytopic controller is computed, using Yalmip **[yalmip]** to solve the set of LMIs presented in chapter 3, for an attenuation level $\gamma_{min} = 2.71$. The solution is the set of the vertex LTI controllers in a state space form:

$$\begin{aligned} \dot{x}_c(t) &= A_i x_c(t) + B_i y(t) \\ u(t) &= C_i x_c(t) + D_i y(t) \end{aligned} \tag{4.8}$$

where $x_c(t) \in \mathbb{R}^9$ denotes the state space vector of the controller, $A_i \in \mathbb{R}^{9\times9}$, $B_i \in \mathbb{R}^9$, $C_i \in \mathbb{R}^{1\times9}$, $D_i \in \mathbb{R}^9$ for $i = 1, 2, 3$ are the LTI vertex matrices. $u(t) \in \mathbb{R}$ is the output of each vertex controller.

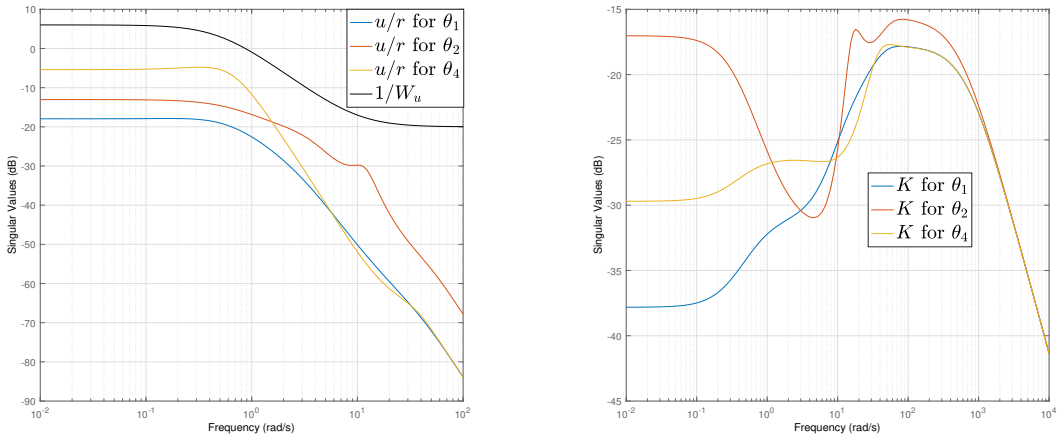

(a) Controller sensitivity function KS over the weighting function $1/W_u$ of the vertex systems.

(b) Frequency response of the controllers K_i.

Figure 4.3: Bode plot of the reduced vertex polytopic system.

Figure 4.3 illustrates the bode plots of the synthesized vertex LTI controllers for the reduced 2D polytope depicted in Fig. 4.1(b). In particular, the controller sensitivity function of the vertex systems is illustrated in figure 4.3(a), showing that for every LTI closed-loop system the performance is satisfied over the selected template function $W_u(s)$.

On the other hand, the magnitude of the computed vertex controllers K_i can be visualized in the bode plot 4.3(b). That plot proves that the remaining non-realistic vertex θ_1 deteriorates the performance of the lateral control system, since the magnitude of the associated vertex controller is the smaller. Thus, the overall bandwidth of the LPV closed-loop system is reduced.

4.2.5 Simulation Results

A simulation scenario that combines an initial lateral error away from the reference trajectory and then, it follows a sharp turn. In that way, a simple scenario is designed to evaluate the controller's tracking capabilities for a constant look-ahead time $T = 1.5\ s$.

Figure 4.4(a) plots the reference trajectory. According to the scenario, the vehicle starts with an initial error of a meter away from the reference path, then it follows a straight line and finally, it tracks a turn of radius $R = 100\ m$.

For speeds $v_x \leq 10\ m/s$ (in Fig. 4.4(b), 4.4(c)) when the vehicle starts from one meter away, the controlled vehicle is able to reach the desired lane without overshoots. As the speed increases, oscillations start to appear as a sign of losing performance for the polytopic controller.

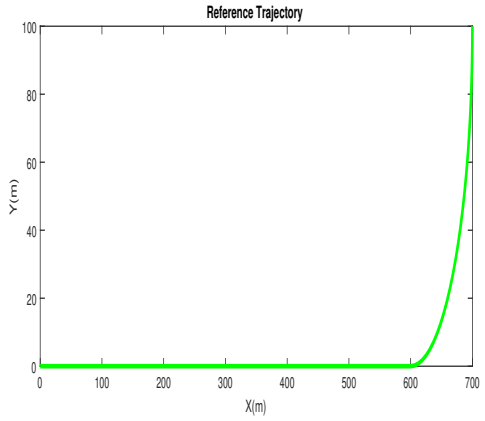

(a) Reference trajectory used for simulation.

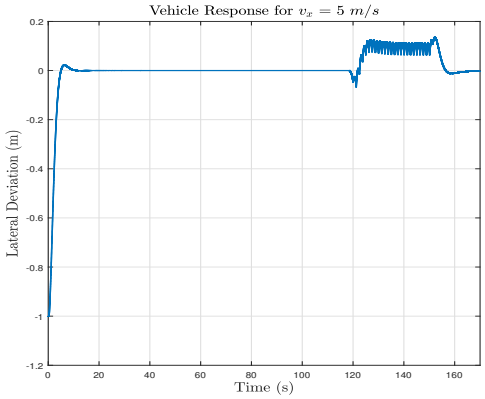

(b) Lateral deviation response for $v_x = 5\ m/s$.

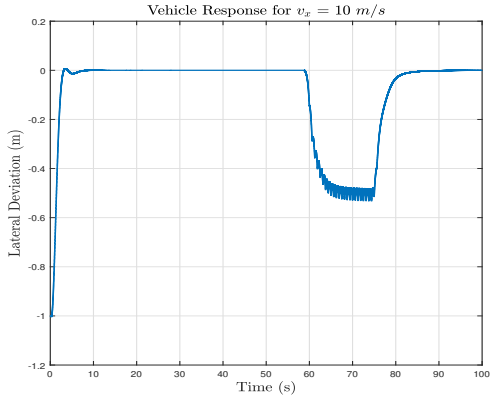

(c) Lateral deviation response for $v_x = 10\ m/s$.

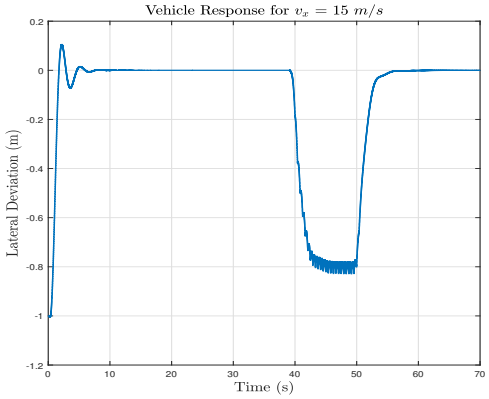

(d) Lateral deviation response for $v_x = 15\ m/s$.

Figure 4.4: Simulation results of the 2D reduced LPV Polytopic Controller

At the part of the turn appearing at the middle of the simulation, the polytopic controller provides good performance (i.e. small lateral errors less than 0.5 m) again for $v_x = 5, 10$ m/s (see Fig. 4.4(b), 4.4(c)). As the speed increases i.e $v_x = 15\ m/s$, as one can see in Fig. 4.4(c), the lateral error at the center of gravity of the car continues to increase during the turn reaching a maximum value of 0.8 m in Fig. 4.4(d).

The increase of the computed lateral error during simulations can be interpreted as a drawback of the choice to consider the look-ahead time T varying, as a way to avoid the enlargement of the polytope's size.

4.2.6 Experimental Results

To further evaluate the proposed LPV/Polytopic controller, the test bed platform is utilized and the proposed control lateral system is deployed to its Lateral Control module.

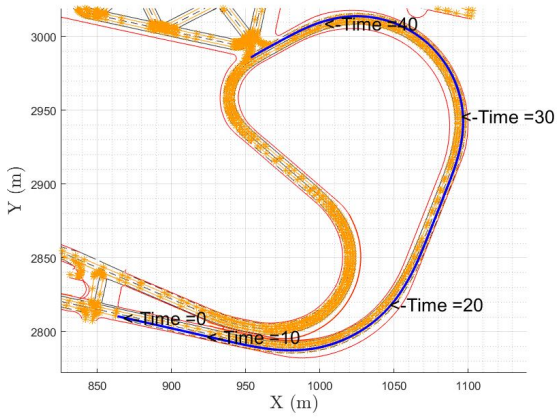

(a) Trajectory segment followed in the test track.

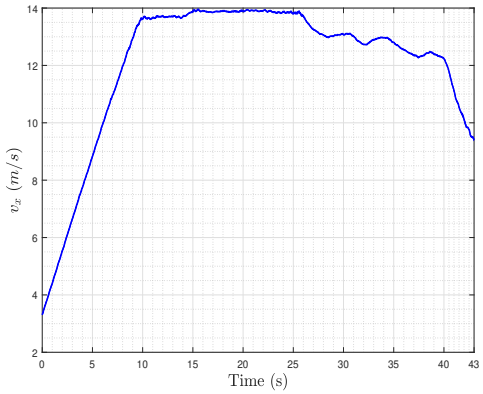

(b) Longitudinal speed profile provided by the NAV.

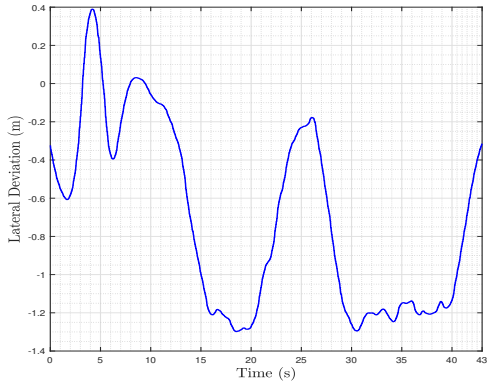

(c) Computed lateral deviation at the center of the gracity of the car.

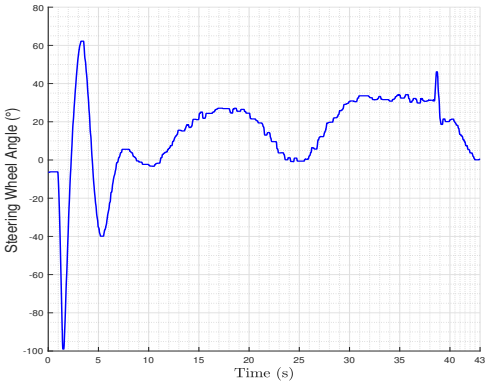

(d) Steering wheel angle.

Figure 4.5: Experimental results collected at the test track.

A segment of a reference trajectory (fig.4.5(a)) of the test track at Satory is utilized, while a varying longitudinal speed profile (figure 4.5(b)) is provided by the NAV. The assessment of the LPV Polytopic controller is achieved by the figures 4.5(d), 4.5(c).

One can see, at the beginning the vehicle starts from an initial lateral offset 0.4 m and it oscillates before converging to the trajectory at 8 s. During the two turns of the reference trajectory, the vehicle is unable to track adequately the path, since the lateral offset is increased even more than 1 m w.r.t the desired trajectory.

The experimental results from the set of figures 4.5 show that the choice of a constant look-ahead time T is a conservative option to design a lateral control system and further examination should be given to the proper choice of the look-ahead time T per speed v_x. In the next sections, further attempts to overcome these limitations in the LPV framework are presented.

4.3 LPV Polytopic Control Design with Varying Look-ahead Time T

The system representation (2.13), can be written in an LPV form, by considering the varying parameters in the plant matrices as bounded and real-time measured. In that sense, the system matrices are fixed functions of the parameter vector $\rho(t)$.

More specifically, it is assumed that the vector ρ varies in a polytope Θ of vertices θ_i.

$$\begin{aligned} \rho(t) &\in \Theta \\ \Theta &= Co\{\theta_1, \theta_2, .., \theta_N\} \end{aligned} \tag{4.9}$$

where Co denotes the convex hull of the finite N vertices θ_i.

The vertices θ_i correspond to the combinations of the extremum values of the parameters ρ_i, i.e $\underline{\rho_i} \leq \rho_i \leq \overline{\rho_i}$. Respectively, the LPV Polytopic model is constructed by assuming that the LPV plant matrices, which contain the parameters ρ_i, vary in a matrix polytope. That polytope is defined as the convex hull of a number of vertex matrices of the same dimention. These vertex matrices are computed for frozen values of parameters equal to the vertices θ_i. Another assumption, it is the affine dependance of the LPV matrices on the parameter vector ρ [Mohammadpour and Scherer 2012], i.e

$$A(\rho) = A_{\rho_0} + \sum_{i=1}^{n} \rho_i A_{\rho_i} \tag{4.10}$$

where A_{ρ_0}, A_{ρ_i} are LTI state matrices and n is the number of parameters.

The varying parameters in this case, are the speed v_x and the look-ahead distance L. These parameters are explicitly included in the system through the system matrix $A(v_x, L)$. However, the affine property cannot be respected since in the matrix A appears also the term $1/v_x$. Hence, that term must be added to the varying parameter vector $\rho(t) = (\rho_1(t),\ \rho_2(t),\ \rho_3(t)) = (v_x(t),\ 1/v_x(t),\ L(t))$ of the LPV Polytopic system.

In this work, the selected look-ahead distance profile per speed is the same as has been presented in [Kapsalis et al. 2020]. More specifically, the operating domain of the varying parameters is the following:

$$\begin{aligned} v_x &\in [5, 25]\ m/s \\ 1/v_x &\in [0.04, 0.2]\ s/m \\ L(v_x) &= a v_x \mathrm{e}^{b v_x} + c v_x \mathrm{e}^{d v_x}\ m \end{aligned} \tag{4.11}$$

where $a = 3.83$, $b = -0.7261$, $c = 1.154$ and $d = -0.01453$.

Then, the LPV matrix $A(\rho)$ can be expressed, according to the vertex property [Apkarian, Gahinet, and Becker 1995], as a convex hull of the vertex matrices created by all the possible combinations of the parameter bounds, as shown below:

$$A(\rho) = \sum_{i=1}^{N} a_{\theta_i}(t) A_i$$
$$\sum_{i=1}^{N} a_{\theta_i}(t) = 1, \; a_{\theta_i}(t) \geq 0 \tag{4.12}$$

where $a_\theta^T(t) = (a_{\theta_1}(t), .., a_{\theta_N}(t))^T$, $N = 2^3$ are the scaling variables and the number of vertices accordingly. The variables $a_\theta(t)$ are computed according to the real-time position of $\rho(t)$ in the 3D polytope Θ and, subsequently w.r.t the vertices $\theta_i \in \mathbb{R}^3$, formulated as such:

$$\rho(t) = \sum_{i=1}^{N} a_{\theta_i}(t) \theta_i \tag{4.13}$$

The resulting LPV Polytopic model, by replacing the LPV matrix from (4.12) to the augmented model (2.13) is the one below:

$$\dot{x}(t) = A(\rho(t))x(t) + B_1 w(t) + B_2 u(t)$$
$$y(t) = C(t)x(t) \tag{4.14}$$

Once again, even selecting the look-ahead distance in a more generic form (eq. (4.11)), it has to be remarked that the look-ahead distance is a varying tuning parameter that is selected by the designer per speed [Kosecka 1996]. Subsequently, it is clear that the parameter L depends from v_x, as the other parameters v_x and $1/v_x$. Thus, it seems imperative the reduction of the polytope Θ.

4.3.1 LPV/Polytopic Model & Reduction of the 3D Polytope

The Polytope that is used to describe the LPV system is first created for the upper and lower bounds of the operating domain of parameters and is illustrated in Fig. 4.6.

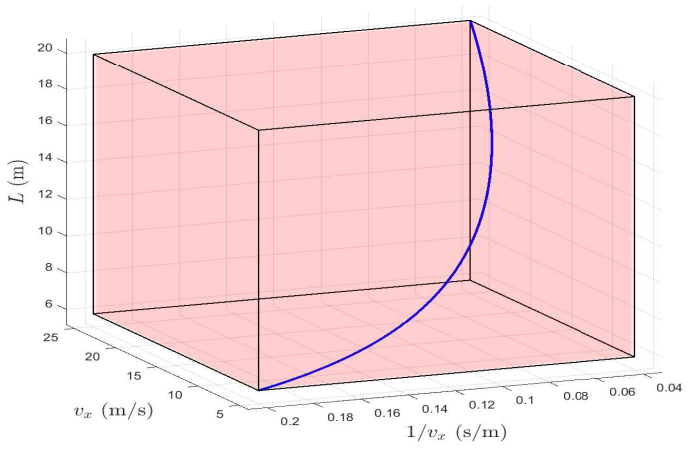

Figure 4.6: The initial over-bounded 8-vertices polytope.

Due to the facts that (i) the parameter vector ρ is augmented to satisfy the affine-dependence and, (ii) all the parameters ρ_i are dependent on each other, the inherent conservatism of the Polytopic approach is enlarged. To treat this limitation of the method and avoid a practical-based solution as selecting the look-ahead time T constant [Kapsalis et al. 2021b] as in the previous section, a 3-dimensional polytopic reduction is proposed.

The reduced parameter polytope has to include the parameter variation as the initial-full 8 vertices (see Fig. 4.6). This statement arises to retain the convexity property, as it is defined for the Polytopic Linear Differential Inclusions [Boyd et al. 1994]. For these reasons, the proposed Alg. 1 is proposed.

As a fist step, the 2-dimensional pairs of parameters variations is illustrated in figure 4.7(a) and in the second step of figure 4.7(b), a new set of vertices is selected for which the merged polytope is convex and compact (Fig. 4.7(c)). In step 3 & Fig.4.7(d), the remaining non-realistic vertices that doesn't affect the inclusion of the 3D parameter trajectory are deleted, i.e θ_4.

In the final step of the algorithm, no-more vertices are deleted, but the coordinates of the remaining vertices are reduced to shrink even more the polytope (see figure 4.7(e)). In that particular case, the vertical coordinate of vertex θ_2, $L_{\theta_2} = 20\ m$, is reduced giving θ_2^*.

It has to be emphasized that θ_3 and θ_5 describe the two realistic cases, and the position of θ_1 is not modified since the inclusion of the parameters trajectory will be affected. Moreover, the vertical coordinate of θ_2^* corresponds to a smaller value of look-ahead distance, $L_{\theta_2^*} = 13\ m$, hence permitting the increased bandwidth around that region of parameters for the closed-loop system. Finally, the remaining vertices of the reduced polytope $\tilde{\Theta}$ are the $\theta^* = (\theta_1, \theta_2^*, \theta_3, \theta_5)$.

Algorithm 1: 3D Polytope Reduction Procedure

Data: $\Theta = Co\{\theta_1, \theta_2, .., \theta_8\}$ from Fig. 4.6.
Result: $\tilde{\Theta} = Co\{\theta_1, \theta_2^*, \theta_3, \theta_5\}$.

1 **Step 1:** Plot the 2D trajectories of the pairs of parameters. Keep the vertices of the triangles that include the 2D parameter variations (Fig. 4.7(a));
2 **Step 2:** Extend the necessary triangles (Fig. 4.7(b)) whose vertices are able to merge to a compact convex set (Fig. 4.7(c));
3 **Step 3:** Reduce the vertices (i.e θ_4 in Fig. 4.7(d)), for which the 3D parameters trajectory is still included;
4 **Step 4:** Shrink the polytope by reducing the vertical coordinate of θ_2 to θ_2^*, till the final geometry includes the parameters trajectory (Fig. 4.7(e));

4.3.2 LPV Polytopic Controller Synthesis

In the H_∞ framework, an LPV Polytopic Controller can be designed off-line, as a solution of a convex optimization. The semi-definite problem subject to a set of Linear Matrix Inequalities

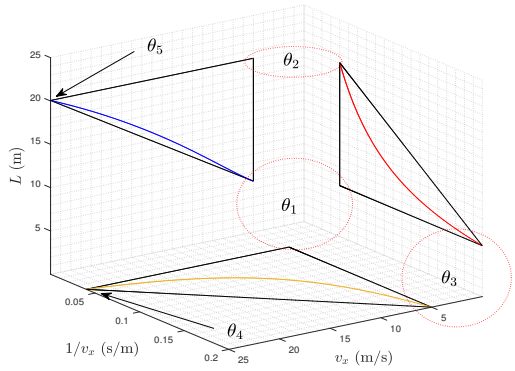

(a) First step of reduction

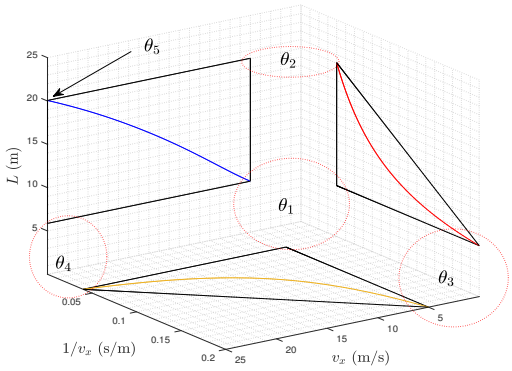

(b) Second step of reduction

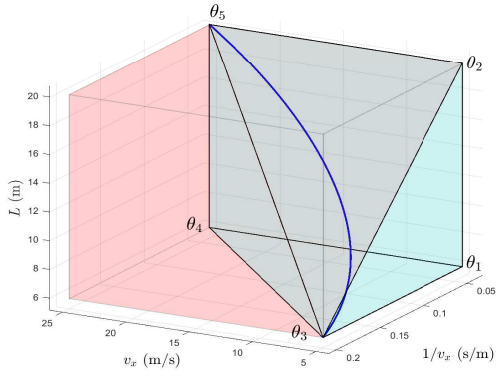

(c) 3D polytope after the second step

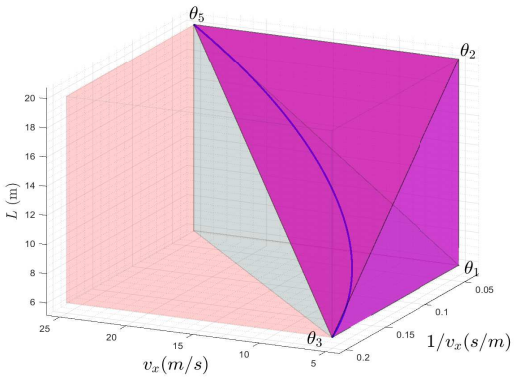

(d) 3D polytope after the third step

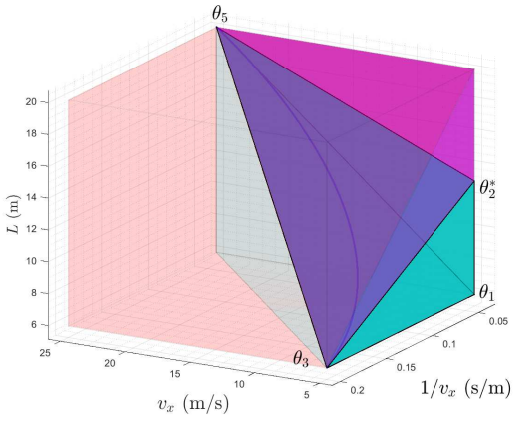

(e) 3D polytope after the fourth step

Figure 4.7: Overall comparison from the initial 8-vertices polytope (pink) to the 4-vertices (green).

(LMI), is formulated at every vertex of the reduced polytope (Fig. 4.7(e)) [Apkarian, Gahinet, and Becker 1995].

The tuning is achieved once again by introducing performance/template weights W_y, $W_u(s)$, W_r & W_n [Skogestad and Postlethwaite 2007]. These functions are selected as in the case of the previous section for the case of constant look-ahead time.

The generalized plant in (4.6) is expressed in polytopic form consisted of the vertices $\theta^* = (\theta_1, \theta_2^*, \theta_3, \theta_5)$ of the reduced polytope.

Problem Definition: The LPV control synthesis problem consists in finding an LPV controller $K(\rho)$ so that the closed-loop system represented in Fig. 4.2 is stable and there exists a $\gamma > 0$ s.t.

$$\sup_{||w|| \neq 0} \frac{\|z\|_2}{\|w\|_2} < \gamma, \ \forall \ \theta^* \tag{4.15}$$

4.3.3 Solution & Frequency response of the LPV Controller

The polytopic approach is here considered to design the vertex controllers $K_i, \ i = 1, 2, 3, 4$, by solving off-line the appropriate set of LMIs (for more details see [Apkarian, Gahinet, and Becker 1995] or [Poussot-Vassal et al. 2011]).

The solution of the synthesis of the LPV/Polytopic controller is computed with an attenuation level $\gamma_{min} = 2.6$. This solution is the set of the vertex LTI controllers in a state space form:

$$\begin{array}{l} \dot{x}_c(t) = A_i x_c(t) + B_i y(t) \\ u(t) = C_i x_c(t) + D_i y(t) \end{array}, i = 1, 2, 3, 4 \tag{4.16}$$

where $x_c(t) \in \mathbb{R}^9$ denotes the state space vector of the controller, $A_i \in \mathbb{R}^{9\times 9}$, $B_i \in \mathbb{R}^9$, $C_i \in \mathbb{R}^{1\times 9}$, $D_i \in \mathbb{R}^9$ are the LTI vertex matrices. $u(t) \in \mathbb{R}$ is the output of each vertex controller.

Fig. 4.8(a) depicts the controller sensitivity function u/r over the closed-loop system for every vertex controller. As it is visualized, the desired performance imposed by the template weighting function $W_u(s)$ is satisfied over the frequency domain for every vertex θ_i^*.

Whereas, in figure 4.8(b), it is depicted the closed-loop behavior for the lateral error at the target point to the yaw-rate reference. Fig. 4.8(c) illustrates the bode plot for the vertex LTI continuous controllers, proving that the smaller magnitudes of vertex controllers is provided by the two non-realistic vertices θ_1 and θ_2^*.

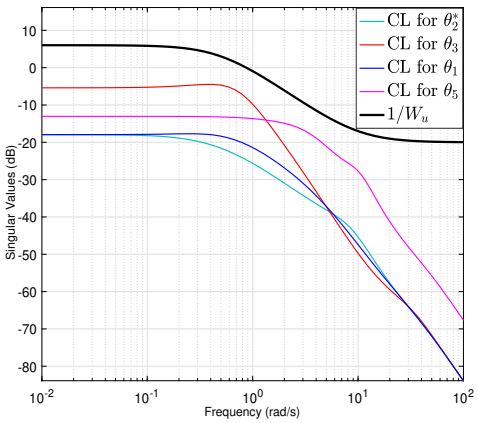

(a) Controller sensitivity function to the weighting function $1/W_u$.

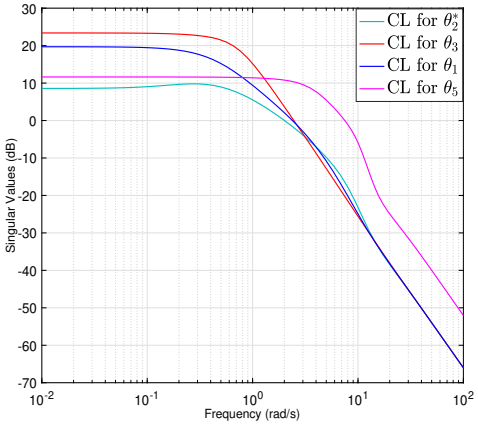

(b) Frequency response y_L/r.

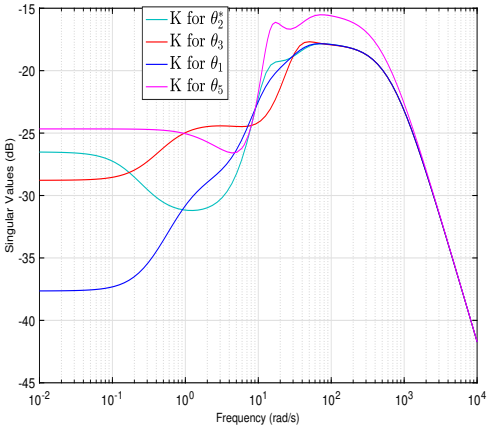

(c) Frequency response of the LTI vertex controllers K_i.

Figure 4.8: Bode Plots of the reduced 4-vertices polytopic closed-loop system.

4.3.4 Real-Time Implementation of the LPV Polytopic Controller

A dynamic output feedback LPV/Polytopic controller is a convex combination of vertex LTI controllers, performed in real-time from the scaling variables a_{θ_i}.

Different formulas exist as a way to compute these interpolation variables. In [Bara et al. 2001] and [Dubuc 2018] binary representations are utilized for the case where the polytope Θ consists of a box, cube or hyper cube when the number of parameters is $n = 2, 3$ or when $n > 3$ respectively. That approach is accurate for the cases where no reduction is applied to the parameters polytope.

The formula that computes the interpolation variables for the i_{th} vertex controller are as follows:

$$a_{\theta_i}(k) = \prod_{j=1}^{N} \frac{\alpha_{ij}\rho_j(k) + \beta_{ij}}{\overline{\rho_j} - \underline{\rho_j}} \tag{4.17}$$

where $\rho_j(k)$ is the real-time measurement of the j parameter and $\overline{\rho_j}$, $\underline{\rho_j}$ are the upper and lower bounds of that vertex respectively. α_{ij} and β_{ij} provide automatically the appropriate sign according to the binary representation that is given to the j vertex.

For a more general case where the polytope is reduced another way can be applied as in the proposition 3.1 of [Martinez, Loukkas, and Meslem 2020]. The interpolation variables are computed as the solution of a linear system that is augmented with the equality $\sum_{i=1}^{N} a_{\theta_i} = 1$.

$$\begin{bmatrix} \theta_1 & \theta_2 & \dots & \theta_N \\ 1 & 1 & \dots & 1 \end{bmatrix} a_\theta = \begin{bmatrix} \rho(k) \\ 1 \end{bmatrix} \tag{4.18}$$

where $\theta_i \in \mathbb{R}^n$ are the coordinates of the associated vertices, n is the dimension of the polytope's space. $i = 1, .., N$ where N is the number of vertices. $a_\theta \in \mathbb{R}^N$, $\rho(k) \in \mathbb{R}^n$ denote the real-time measurements of the time-varying parameter vector.

However, that approach may cause numerical problems especially for the cases where the polytope is tightened and since the inequality $a_{\theta_i} \geq 0$ is absent. Subsequently, a novel on-line implementation procedure is proposed for the LPV/Polytopic controller $K(\rho)$.

4.3.4.1 Off-line Step

First, the discrete-time state space vertex controllers, K_{d_i} are computed as indicated for LTI systems in [Astrom and Wittenmark 1984], for a given sampling time T_s.

The discretized vertex controller K_{d_i} are computed as such:

$$K_{d_i} = \left[\begin{array}{c|c} A_{d_i} & B_{d_i} \\ \hline C_{d_i} & D_{d_i} \end{array}\right] \tag{4.19}$$

and their state space implementation in discrete time is as follows:

$$\begin{aligned} x_c(k+1) &= A_{d_i}x_c(k) + B_{d_i}y(k) \\ u(k) &= C_{d_i}x_c(k) + D_{d_i}y(k) \end{aligned} \tag{4.20}$$

where the discrete LTI matrices A_{d_i}, B_{d_i}, C_{d_i} and D_{d_i} are computed off-line:

$$\begin{aligned} \begin{bmatrix} A_{d_i} & B_{d_i} \\ 0 & 0 \end{bmatrix} &= exp\left(\begin{bmatrix} A_i & B_i \\ 0 & I \end{bmatrix} T_s \right) \\ C_{d_i} &= C_i \ , D_{d_i} = D_i \end{aligned} \tag{4.21}$$

4.3.4.2 On-line Step

The discretized LPV controller is implemented as a convex combination of the vertex controllers K_{d_i} i.e

$$K_d(\rho) = \sum_{i=1}^{4} a_{\theta_i}(k) K_{d_i} \tag{4.22}$$

where the constants $a_\theta(k)$ are the scaling variables, as they specify the contribution of each vertex controller, according to the real-time measurement of the vector $\rho(k)$ [Poussot-Vassal 2008].

In this work, the proposition 3.1 from [Martinez, Loukkas, and Meslem 2020] is extended. Indeed the novel computation of $a_\theta(k)$, is formulated as a real-time constrained LS problem, as presented below:

$$\begin{aligned} \underset{a(k)}{\text{minimize}} \quad & ||\mathcal{M} a_\theta(k) - \rho(k)||_2^2 \\ \text{subject to} \quad & a_{\theta_i}(k) \geq 0 \\ & \sum_{i=1}^{4} a_{\theta_i}(k) = 1 \end{aligned} \tag{4.23}$$

where $\mathcal{M}$ contains the coordinate information of the vertices i.e $\mathcal{M} = \left[\theta_1, \theta_2^*, \theta_3, \theta_5\right] \in \mathbb{R}^{3\times 4}$ and $a_\theta^T(k) = (a_{\theta_1}(k), a_{\theta_2^*}(k), a_{\theta_3}(k), a_{\theta_5}(k))^T \in \mathbb{R}^4$.

4.3.5 Simulation Results

This section presents the simulated results (Fig. 4.9). The synthesized LTI vertex matrices, has been discretized for a sampling time $T_s = 0.01\ s$. The real-time implementation of the constrained LS problem that computes the variables a_{θ_i}, is achieved by the custom-generated QP solver CVXGEN [Mattingley and Boyd 2012].

The dataset that contains the reference trajectory X, Y and its associated speed profile has been collected experimentally from the previous experimental tests explained in [Kapsalis et al. 2020]. The test is a segment of the test track (Fig. 4.9(e)) with two turns, for a varying longitudinal speed profile depicted in figure 4.9(a).

The vehicle at the beginning starts with an initial lateral offset of 0.4 m (figure 4.9(b)) and for that reason the steering, in figure 4.9(c)) is abrupt at the beginning. Apart from that, the steering is smooth enough during the turns while the control system doesn't allow more than 0.2 m of lateral deviations.

It has to be remarked that the solution of the LS, i.e $a_{\theta_i}(k)$ illustrated in Fig. 4.9(d), didn't fail when the velocity of the car at the beginning started outside of the polytope's minimum velocity value. On the contrary, the optimization successfully computed that the

closest vertex is θ_3. As the speed increases, the contribution of each controller varies, as it expected.

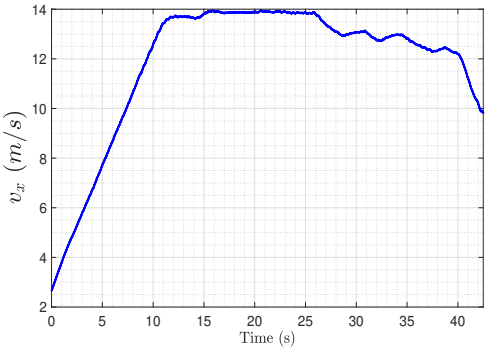

(a) Longitudinal speed profile fed by the NAV

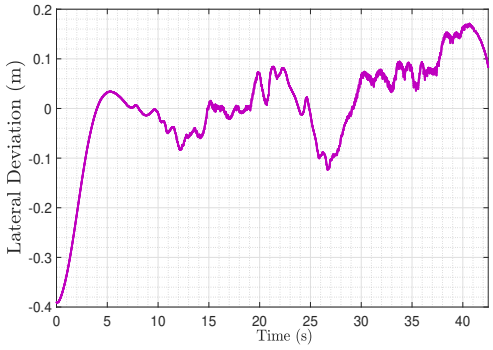

(b) Lateral deviation at the center of gravity

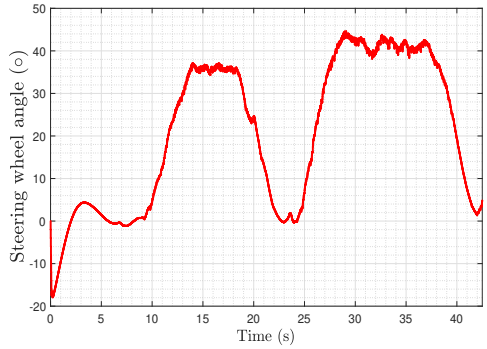

(c) Steering wheel angle command

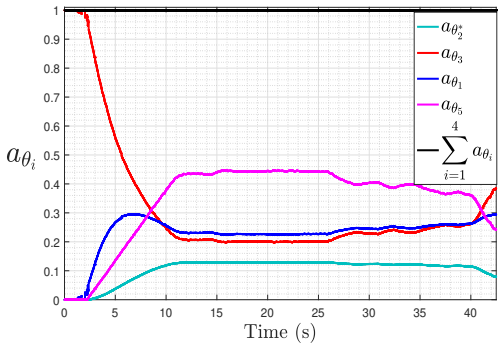

(d) Scaling variables a_{θ_i}

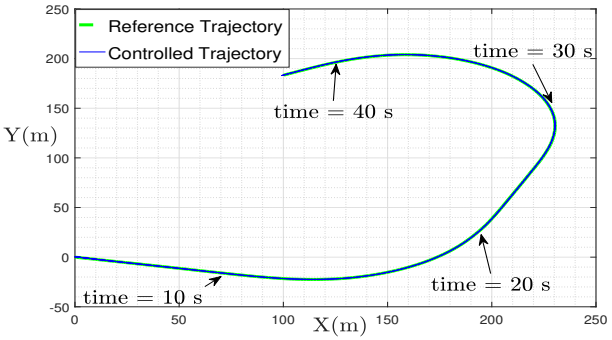

(e) Trajectory followed

Figure 4.9: Simulation results

4.3.6 Experimental Results

In the two following subsections, two different segments of the test track are utilized for

low and high speeds and, their results are illustrated respectively.

4.3.6.1 Path-Tracking at Low Speed Curves

At first, the vehicle is tested at a trajectory segment with two turns (Fig. 4.10(e)) and the measured experimental results are depicted in the set of figures 4.10.

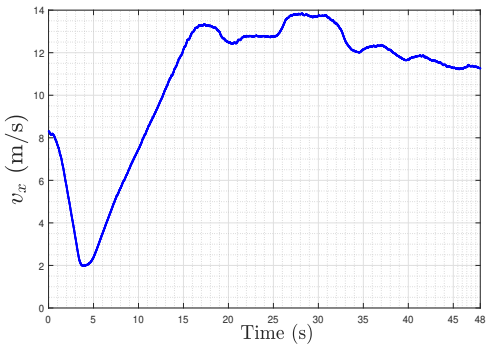

(a) Longitudinal speed profile fed by the NAV

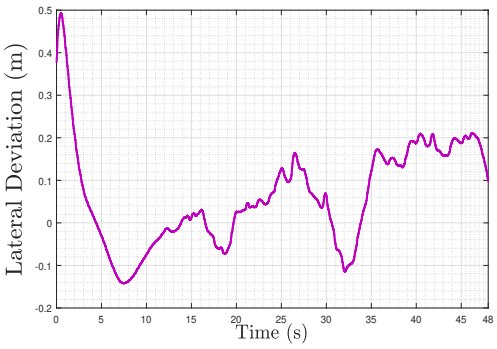

(b) Lateral deviation at the center of gravity

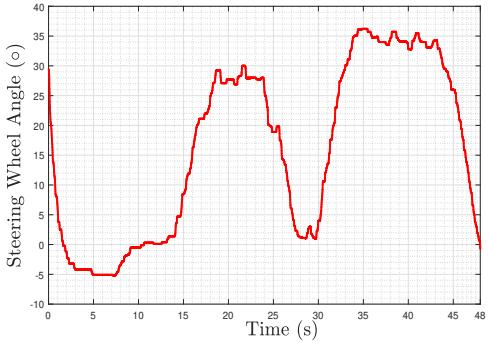

(c) Applied Steering wheel command

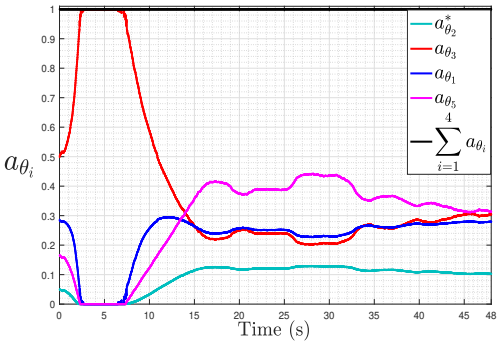

(d) Real-time solution of the LS (4.23), a_{θ_i}

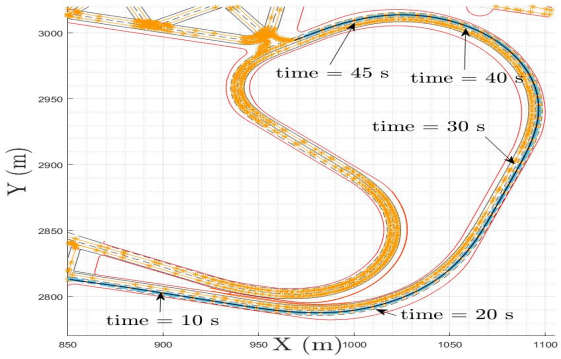

(e) Trajectory followed at the test track.

Figure 4.10: *First case scenario a)*: Experimental results at the test track of Satory.

The vehicle starts in autonomous mode at 8 m/s (Fig. 4.10(a)) with an initial lateral error of 0.4 m (Fig. 4.10(b)) and for that reason an initial abrupt steering is applied (see Fig. 4.10(c)). Then, the vehicle decelerates to 2 m/s and then accelerates again to 13 m/s to enter the first turn and keeps a velocity around $12 - 14$ m/s till then end of the second turn.

The plot of the lateral offset of the car (Fig. 4.10(b)) proves that the proposed controller is able to sustain a good tracking performance since the maximum lateral offset never gets more than 0.2 m. The applied steering command, as it is depicted in figure 4.11(c), shows that the steering is smooth and comfortable enough throughout the ride.

Figure 4.10(d) show that, even though the measured velocity is outside of the parameter variation (when it gets to $2 < 5$ m/s), the proposed optimization achieves to compute the closest vertex controller to treat that case and that is real-time implementable since it respects the computational power for the utilized sampling time.

4.3.6.2 Higher Velocity Curves

In this experimental part, illustrated in the set of figures 4.11, the autonomous mode is activated at 12 m/s and accelerates at a maximum value of 18 m/s at 22 s (Fig. 4.11(a)) to track two smooth curves (Fig. 4.11(e)).

As it can be seen, even though the lateral offset of the vehicle is high at the beginning (Fig. 4.11(b)), the car is able to apply a smooth steering command and track the curves sufficiently comfortable without permitting more than 0.2 m of lateral error at the center of gravity.

The steering, as it is depicted in the figure 4.11(c)) is not sensitive to noise at higher speeds and even though it is increased at 20° during the second curve it was increased in a slow pace.

Moreover, the solutions of the optimization problem, i.e a_{θ_i} are provided in the fig. 4.11(d), where it is illustrated that the scaling variable a_{θ_5} is increased since the closest vertex is θ_5.

These experimental results prove that the proposed 3D reduced LPV/Polytopic controller is an improvement of the 1st section where the look-ahead time T is selected constant.

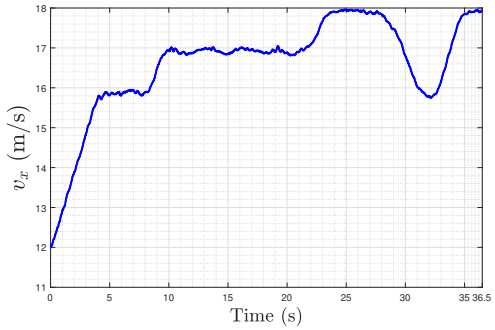

(a) Longitudinal speed profile fed by the NAV

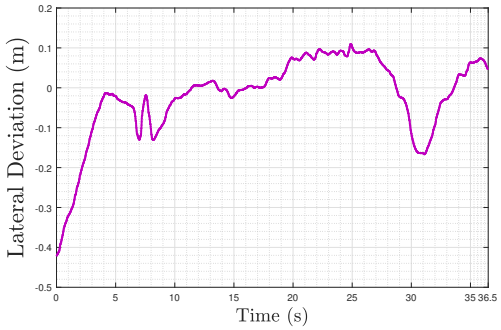

(b) Lateral deviation at the center of gravity

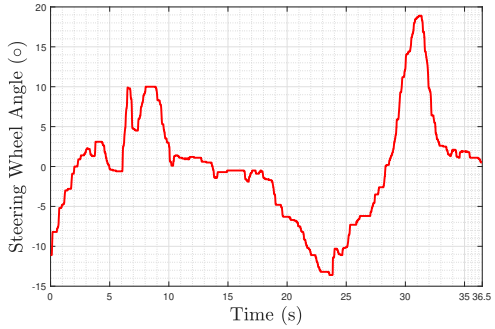

(c) Applied steering wheel command

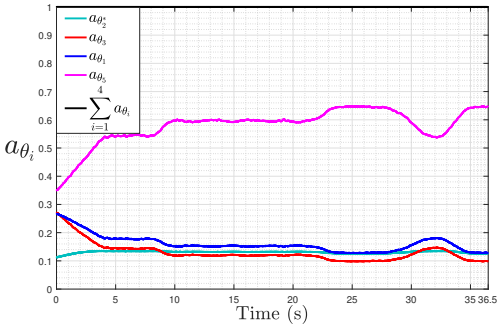

(d) Real-time solution of the LS (4.23), a_{θ_i}

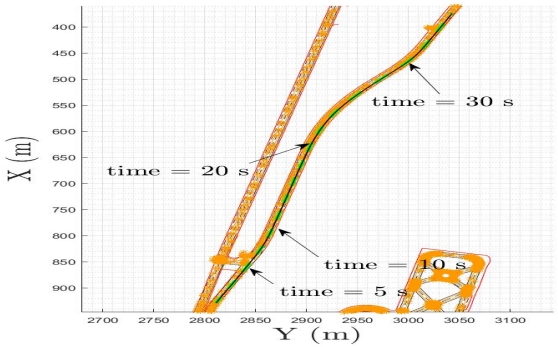

(e) Trajectory followed

Figure 4.11: *Second case scenario b)*: Experimental results at the test track of Satory.

4.4 LPV/Gridding Approach with varying Look-ahead Time T

This section presents the LPV methodology developed in this study to design a dynamic output controller. The LPV approach which is utilized in this chapter is the Set of Gridded Parameter Points. Benefits of the gridded-based approach are theoretically and experimentally demonstrated in the following sections.

4.4.1 LPV Model Formulation

The state space representation described in (2.13) can be rewritten as a dynamical LPV system. Defining the look-ahead time as a function of speed $T(v_x)$, the only parameter remaining is the longitudinal speed i.e $\rho = v_x$.

An intensive simulation study for fixed speeds has been carried out so that to select look-ahead time values so that not to allow big lateral errors. Thus, we select values of the look-ahead time per speed that are the ones that satisfy the control objectives described in section 3.4. Performing an interpolation to fit the data, has allowed to model the look-ahead time in the following exponential form:

$$T(v_x) = a\mathrm{e}^{bv_x} + c\mathrm{e}^{dv_x} \tag{4.24}$$

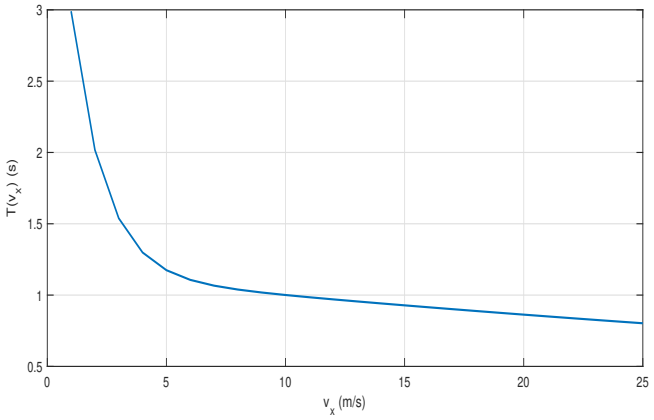

Figure 4.12: Look-ahead time in function of the speed

where $a = 3.83$, $b = -0.7261$, $c = 1.154$ and $d = -0.01453$. Figure 4.12 depicts the look-ahead time in function of the vehicle speed.

From (2.13) it can be seen now that the only matrix or vector that contains the v_x is the matrix A. Thus, the LPV model having as states the vehicle model and the states of the actuator model is written as:

$$\begin{aligned} \dot{x} &= A(\rho)x(t) + B_1 w(t) + B_2 u(t) \\ y(t) &= Cx(t) \end{aligned} \tag{4.25}$$

where $x(t) = \left[\begin{array}{c} x_v(t) \\ \hline x_{act}(t) \end{array}\right] \in \mathbb{R}^8$ is the extended state vector, $A(\rho) = \left[\begin{array}{c|c} A_v(\rho) & B_{v_2}C_{act} \\ \hline 0 & A_{act} \end{array}\right]$, with

$$A_v(\rho) = \begin{bmatrix} -\dfrac{C_f + C_r}{m\rho} & -\rho + \dfrac{C_r L_r - C_f L_f}{m\rho} & 0 & 0 \\ \dfrac{-L_f C_f + L_r C_r}{I_z \rho} & -\dfrac{L_f^2 C_f + L_r^2 C_r}{I_z \rho} & 0 & 0 \\ -1 & -\rho T(\rho) & 0 & \rho \\ 0 & -1 & 0 & 0 \end{bmatrix}, C = \begin{bmatrix} 0 & 0 & 1 & 0 & 0 & 0 & 0 & 0 \end{bmatrix}$$

The other matrices remain unchanged. As it was previously stated, lateral error y_L is the only measurement used in the feedback control.

4.4.2 Control Objectives

Here lies the question of how far or how close should the target point be in order for the vehicle to follow the desired trajectory and simultaneously keep comfort. This work combines the look-ahead time with the weight on the lateral error at the target point for low and high speeds to achieve good performance.

The control objectives conceived to perform optimal lane-tracking are as follows:

- For low speeds ($u_x < 10\ m/s$), fast turning capabilities are required. For that reason, the look-ahead distance is chosen to be small and the weight on the lateral error at the target point to be big.
- For higher speeds ($u_x > 10\ m/s$), the vehicle has not to steer much in order to reach the control point. Thus, the look-ahead distance is chosen to be higher and the weight on the lateral error decreases for higher speeds.
- The steering wheel angle should track the desired trajectory but also sustain comfort as well i.e the bandwidth of the controller should be less than 1 rad/s.
- The look-ahead time has to be the minimum one for lane tracking without causing overshoots and oscillations of the vehicle response.

4.4.3 Control Structure & Synthesis

According to the theory presented in chapter 3, Fig. 4.13 presents how the proposed methodology is formulated in the LPV framework.

In this control scheme is included the LPV plant (4.25), the grid-based controller, the performance output vector z and the weighting functions W_r, W_n, $W_u(s)$ and $W_y(\rho)$. The

signals $n(t)$ and $r(t)$ represent noise signal imposed additively on the measurement y_L and the weighted reference $\dot{\psi}_{ref}$ respectively.

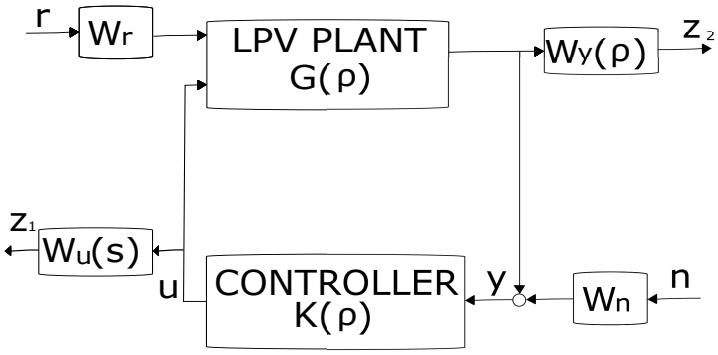

Figure 4.13: LPV Control Scheme

The weighting function $W_y(\rho)$ is chosen as $W_y(\rho) = T(\rho)$. In this way, the proposed methodology is applied by imposing higher weights for low speeds on the lateral error at the target point. Subsequently, as speed increases, the gains of the LPV controller would be reduced and sustain a smoother performance.

The filter $W_u(s)$ is chosen as $W_u(s) = \dfrac{s + \frac{w_{bc}}{M}}{\epsilon s + w_{bc}}$ with $w_{bc} = 0.5\ rad/s$ to respect the corresponding control objective about the bandwidth of the controller ($w_{bc} < 1\ rad/s$), $M = 2$ (6 db) to respect the saturation limits and $\epsilon = 0.1$ ($10^{-1}\ rad/s$) that expresses the frequency where the roll-off starts to achieve better noise attenuation.

Finally, constant weights are added as: $W_n = 0.5$ and $W_r = 0.1$.

Extending the system (4.25) with the the weighting functions, exogenous inputs and controlled outputs, leads to the generalized plant of the system.

$$\begin{bmatrix} \dot{x}(t) \\ \hline z(t) \\ y(t) \end{bmatrix} = \left[\begin{array}{c|cc} A(\rho) & B_1 & B_2 \\ \hline C_1(\rho) & D_{11} & D_{12} \\ C_2 & D_{21} & 0 \end{array}\right] \begin{bmatrix} x(t) \\ \hline w(t) \\ u(t) \end{bmatrix} \tag{4.26}$$

where x is the extended state vector combining the vehicle, actuator and weighting functions state variables, $w(t) = [r(t)\ n(t)]^T$ are the new vector with the exogenous inputs and $z = [z_1\ z_2]^T$ the controlled outputs.

4.4.4 Frequency Domain Analysis

The problem solution has been computed using *LPVtools* toolbox [Hjartarson, Seiler, and Packard 2015]. The generalized plant (5.8) is gridded for frozen values of the parameter $\rho = 5 : 1 : 25\ m/s$ and as parameter variation bounds are imposed $-9 \leq \dot{\rho} \leq 3$ taking into consideration braking and accelerating bounds.

The basis functions f_i and g_i to construct $X(\rho)$ and $Y(\rho)$ are picked as second order polynomial functions judging by simulations, since no concrete methodology exists about their selection.

$$\begin{aligned} X(\rho) &= X_0 + \rho X_1 + \rho^2 X_2 \\ Y(\rho) &= Y_0 + \rho Y_1 + \rho^2 Y_2 \end{aligned} \tag{4.27}$$

Finally, the set of LMIs (3.28) from chapter 3, formed at the grid points of the generalized plant (5.8) are solved for γ and X_i and Y_i. At that point, with $\gamma_{min} = 0.9752$, the reconstruction of LTI state space controllers takes place for each grid point of the speed.

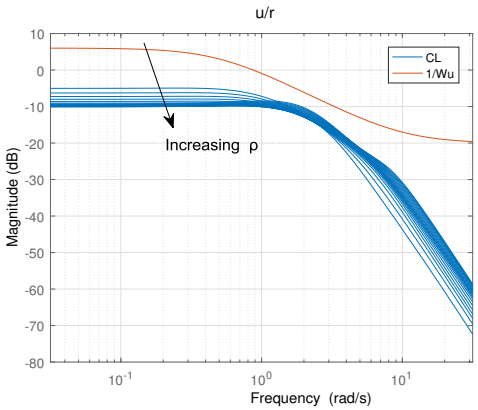

(a) Controller Sensitivity of the closed-loop system.

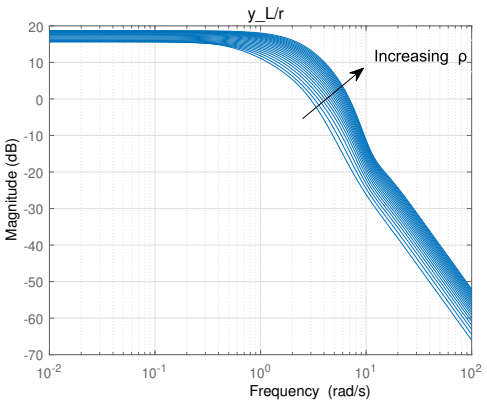

(b) Frequency response y_L/r

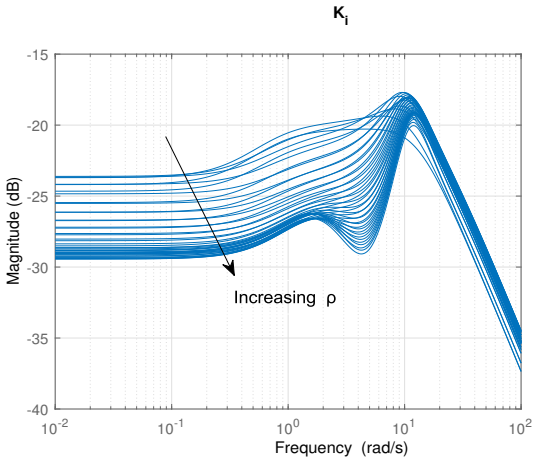

(c) Frequency response of the LTI controllers K_i.

Figure 4.14: Frequency response of the LPV gain-scheduled control system

Figure 4.14(a) presents the frequency response for all speeds from steering wheel angle to the reference yaw rate relatively to the specification imposed by the template weighting function W_u. Fig 4.14(b) shows the bode plot for all speeds from the lateral error at the target

point to the reference yaw rate for the closed-loop system.

It has to be remarked that since $\gamma_{min} < 1$, the control objectives are met. Fig. 4.14(c) shows the frequency response of the LTI controllers corresponding for all gridded points of speed. As speed increases, the output of the controller decreases as is demanded in the control objectives.

4.4.5 Performance assessment using time-domain simulations

The evaluation of the proposed LPV lateral control takes place in the same simulation scenario as in Section 4.2.

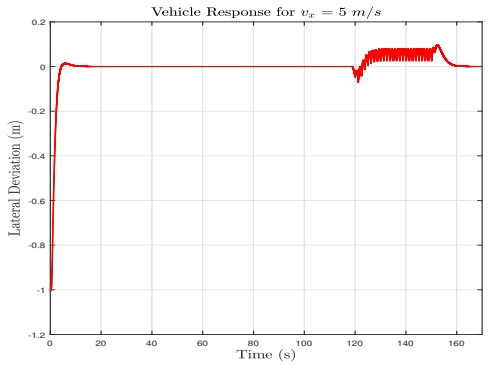

(a) Lateral deviation response for speed test $v_x = 5$ m/s

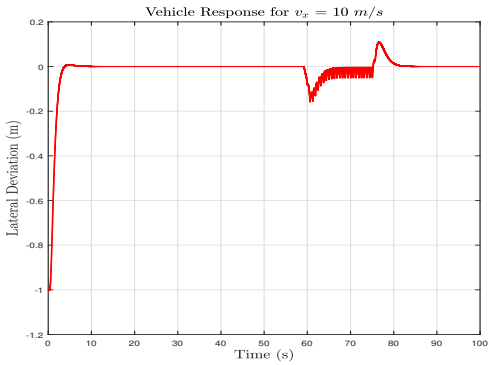

(b) Lateral deviation response for speed test $v_x = 10$ m/s

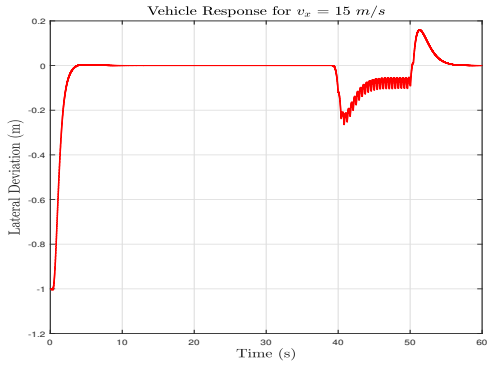

(c) Lateral deviation response for speed test $v_x = 15$ m/s

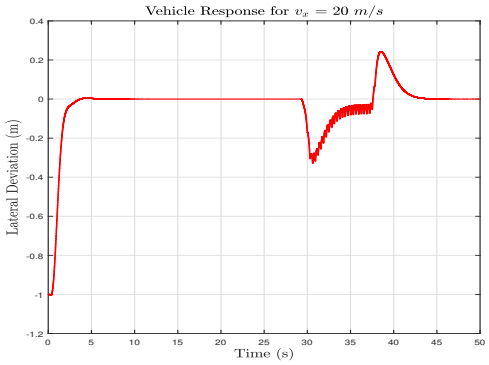

(d) Lateral deviation response for speed test $v_x = 20$ m/s

Figure 4.15: Simulation results for the LPV gain-scheduled controller.

First, Fig. 4.15(a) shows the lateral error at center of gravity of the vehicle for the gridded LPV controller for speed $v_x = 5$ m/s where the look-ahead time is $T = 1.2$ s. Figures 4.15(b), 4.15(c) and 4.15(d) show the lateral error at center of gravity of the vehicle for

speeds $v_x = 10, 15, 20\ m/s$ respectively, where the look-ahead time for the gain-scheduled LPV controller changes according to (4.24).

It is clear that the gain-scheduled controller is capable of handling even such an initial error of 1 m and only for $v_x = 20\ m/s$ small oscillations appear in Fig. 4.15(d). Moreover, for speeds $v_x \leq 15\ m/s$, the lateral error never exceeds 0.2 m (see Fig. 4.15(a), 4.15(b), 4.15(c)), and for $v_x = 20\ m/s$ never gets more than 0.4 m (see Fig. 4.15(d)).

4.4.6 Experimental Results

This subsection presents the experimental results where the proposed LPV/Gridding controller is stressed under two different velocity profiles, while tracking turns of different curvatures.

4.4.6.1 Path-Tracking at Low-Speed Curves

Figure 4.16(a) shows the experimental area, which combines a straight stretch with two turns with variable radius, and the trajectory of the LPV controller which is measured during the test.

Fig. 4.16(b) presents the speed profile during the test which is provided by the navigation system. The autonomous mode is activated when the speed is about 4 m/s. Then, the vehicle accelerates until 14 m/s in a straight stretch, maintaining the same speed up to second 40 where smoothly decelerates up to 9 m/s. It is adapted accordingly to the road curvature, assuring comfort on-board.

To assess the lane-tracking capabilities of the LPV gain-scheduled controller, the lateral offset at the vehicle's center of gravity is examined in Fig. 4.16(c) and the steering wheel angle in degrees computed in Fig. 4.16(d).

The gridded controller handles this continuous change of speed smoothly without having an increase of lateral error Fig. 4.16(c), neither by turning jerkily Fig. 4.16(d). The steering wheel angle is not changing abruptly keeping comfort at all times.

Experimental results validate the interest and efficiency of the proposed LPV gain-scheduling control approach for lateral control of autonomous cars for the case of slow speed tracking curves.

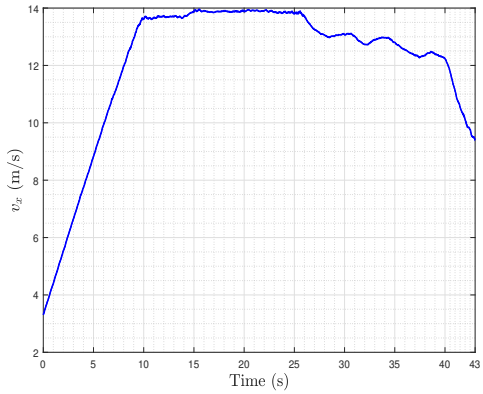

(a) Longitudinal speed profile during test

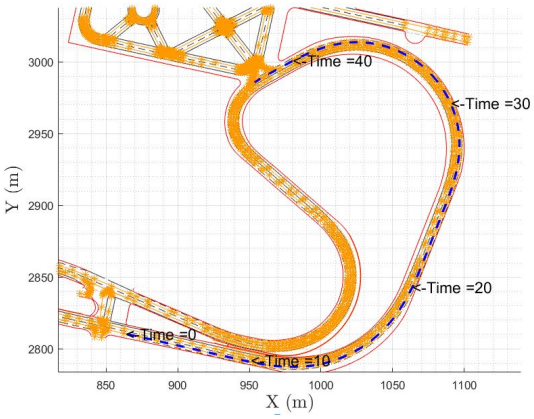

(b) Trajectory followed from the gain-scheduled controller

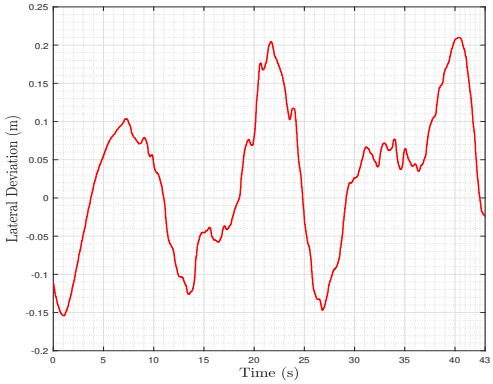

(c) Lateral deviation response of the vehicle

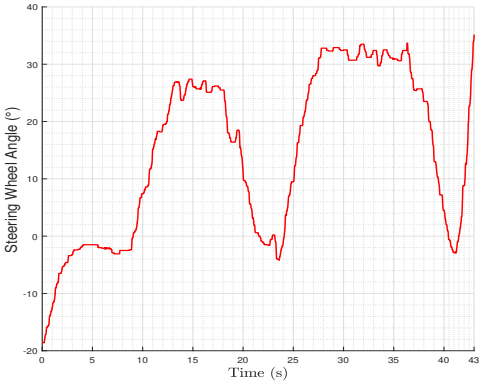

(d) Steering wheel angle response of the vehicle throughout the test.

Figure 4.16: *First case scenario a)*: Experimental results at the test track of Satory.

4.4.6.2 Path-Tracking at High-Speed Curves

Now, the same LPV gain-scheduled controller is tested under higher longitudinal speed profile (Fig. 4.17(b)) for smoother curves, as someone can observe in figure 4.17(a)).

The vehicle starts from standstill and accelerates till 25 m/s where it tracks a low curvature turn and then decelerates till 16 m/s where it tracks a steeper curve. Then, it accelerates again till 20 m/s where it follows a straight stretch.

The LPV gain-scheduled controller is able to handle the high-velocity speed profile without showing jerkily performance (figure 4.17(d)) but at the same time being reactive enough.

In addition, it is clear that the controlled lateral system is not allowing big lateral deviations

even for the steep curve (see Fig. 4.17(c)). The maximum during the first turn is around 0.2 m and during the second one is around 0.4 m, which are considered normal values for the high-velocity speeds.

Thus, the LPV gain-scheduled controller proves that is high performant during faster speeds and at the same time is capable to keep its natural steering behavior.

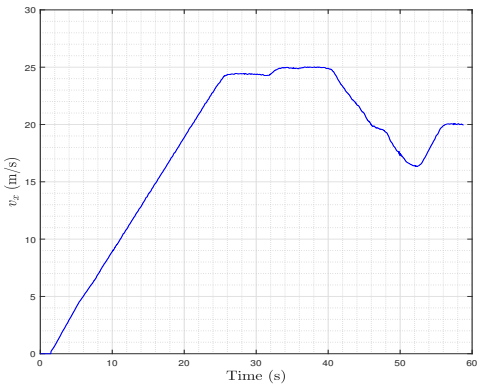

(a) Longitudinal speed profile during test

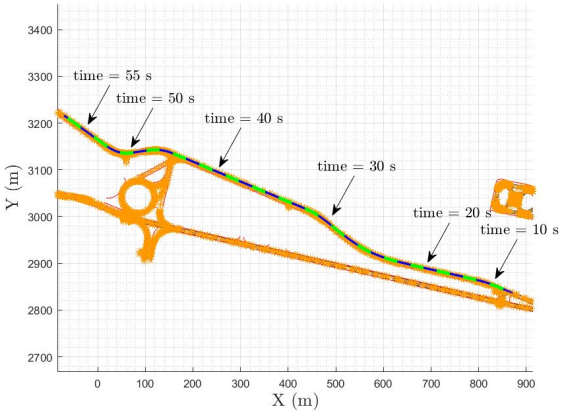

(b) Trajectory followed from the gain-scheduled controller.

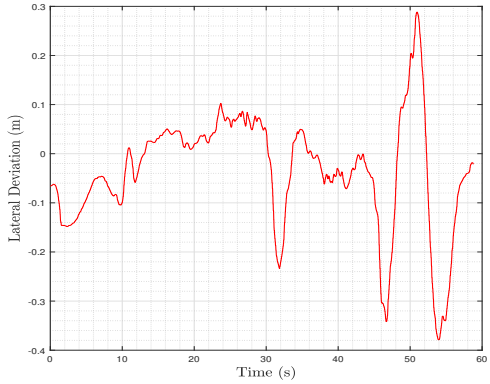

(c) Lateral deviation response of the vehicle

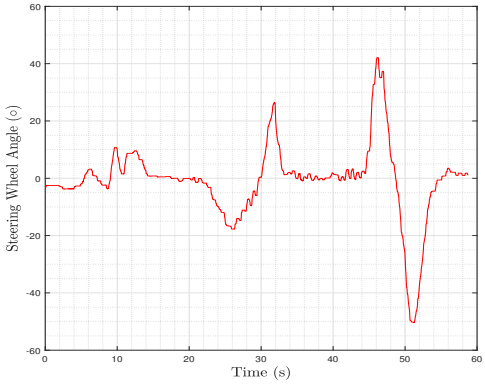

(d) Applied steering wheel angle response

Figure 4.17: *Second case scenario b)*: Experimental results at the test track of Satory.

4.5 Concluding Remarks

This chapter explained how to design a lateral control system fully handled in the LPV framework.

The presented work is associated with three different contributions where the look-ahead

time T is treated differently in the LPV formulation and control design.

1. In the first [Kapsalis et al. 2021b], an exploration, using the Polytopic approach, is conducted for the simple case where the look-ahead time T is selected constant. That choice proves in simulation and experiments that a dynamic steering controller can be designed that minimizes the look-ahead lateral error at the target point. However, it's capabilities are limited, especially when the speed increases.

2. The second LPV/ Polytopic design proves that when the look-ahead time T is selected varying, the limitations shown in the first can be avoided. To achieve the avoidance of these restrictions, an algorithm to reduce the 3-dimensional polytope that includes the parameters trajectory has to be applied. The synthesized LPV/Polytopic controller, with a H_∞ criteria, is implemented on-line by solving a constrained LS problem. The improvement of that control system is validated from the several simulation and experimental results.

3. The third contribution is based on the Gridding approach. The look-ahead time T is again selected varying and according to that approach, the LPV/Gain-scheduled controller is synthesized for a selected range of grid points of the real parameter trajectory. It is also shown that the look-ahead time T can be utilized as a weighting function in the H_∞ framework. The proposed LPV controller shows good performance results for low and high speed tracking curves.

In the next chapter, LPV/Gain-scheduled control strategies will be designed for the Merging of Lateral control scenarios. That means that the designed control architecture will be able to handle at the same time the cases of Lane-Tracking, Lane-Change, their transition and vice-versa.

Chapter 5

LPV/Gain-Scheduled Merging Control

Contents

5.1 Introduction & Contributions

This chapter includes the main contributions to treat the scenario of Lane-Change and how it can be merged with the Lane-Tracking.

The merging of the two scenarios arises as a way to avoid the need of designing several controllers per scenario and, consequently the switching scheme or the further examination of the transition effects between them.

Two different approaches are presented in this chapter.

1. In the first approach, it is presented the LPV gain-scheduled controller and its control configuration that enables a single LPV controller to handle at the same time the lateral control scenarios of lane-change and lane-tracking. That merging of scenarios is achieved by introducing a "high-level" varying parameter that is treated in the LPV/H_∞ framework for the tuning of the controller. The LPV lateral control system is validated in different simulation scenarios and in the test track presented in Chapter 2. The associated paper with the section 5.2 has been:

    - Submitted to the *IEEE Transactions on Intelligent Transportation Systems*.

2. The second approach is conceived based-on the simple question "why putting more effort on the design of the controller and not treat in real-time the reference feeding the controller?". The answer to that question is the design of a Reference Governor. In real-time a modification of the real reference is feeded to the controller and it enables a Lane-Tracking controller to handle the Lane-Change as well. The related contributions has been:

    - Presented at the 24*th IEEE International Conference on Intelligent Transportation Systems*, held in Indianapolis, USA (see [Kapsalis et al. 2021a]).
    - Presented at the *4th IFAC Workshop on Linear Parameter-Varying Systems*, held in Milano, Italy (see [Kapsalis et al. 2021c]).

This chapter is structured as follows. Section 5.2 presents the LPV/Gain-scheduled controller and the results proving the good performance under simulations and experiments scenarios. Section 5.3 details the merging of the two cases of lateral control, i.e lane-tracking and lane-change. By using a yaw-rate Lane-Tracking controller fed with a virtual reference generated by the Reference Governor, the merging is achieved and it can be proven in time-domain simulations. Section 5.4 sums up the chapter and its contributions.

5.2 Merging Lane-Tracking and Lane-Change for Autonomous Vehicles: An LPV Gain-Scheduling approach

5.2.1 Merged Control Objectives & LPV Look-ahead Model formulation

This section introduces the control objectives of the merged control problem and how it can be formulated as the selection of different look-ahead time profiles per speed.

5.2.1.1 Control Objectives

The path-following is achieved through the minimization of the lateral error at the target

point y_L, which is computed every instant to reach a target point located at a look-ahead distance $L = v_x T$ onto the reference trajectory.

Subsequently, the control objectives, handled simultaneously in the LPV framework, are bilateral.

During lane-tracking:

- The look-ahead time T_{tr} has to be as small as possible to have reactive response and at the same time not allow big lateral deviations of the car at the center of gravity for the selected velocity profile, i.e $|y_{cg}| \leq 0.4\ m$.
- The controller has to perform fast tracking of the desired lane while exploiting the full capabilities of the steering actuation system. The bandwidth of the controller should be $\geq 1\ rad/s$.

During lane-change:

- The look-ahead time has to be bigger than the look-ahead time of the above scenario, i.e $T_{ch} \geq T_{tr}$. As closer to the tracking look-ahead time, the faster the convergence to the reference lane.
- The controller's output has to be limited and perform a smooth maneuver towards the adjacent lane. Subsequently, the bandwidth of the controller should be $\leq 1\ rad/s$.

To sum up, the look-ahead time T has to be selected by the designer according to the scenario to be tackled. Similarly, the design of the controller has to be associated with the selected look-ahead time for the corresponding scenario, i.e (lane-tracking/change).

5.2.1.2 Merge of Lane-Tracking/Change

The novel unified control system can be achieved by expressing the look-ahead time T as a convex combination of two different look-ahead time profiles selected for every speed, i.e one for lane-change T_{ch} and one for lane-tracking T_{tr}.

T_{ch} is selected higher than T_{tr} so as to achieve a more smooth performance and reduce the bandwidth of the closed-loop system during the lane-change maneuver. On the contrary T_{tr} is chosen the smallest possible so as to achieve the best tracking of the reference lane without allowing lateral deviations. At the same time the steering must be comfortable enough for the passenger avoiding overshoots or oscillations around the lane [Kapsalis et al. 2020].

The look-ahead time profiles T_{tr} and T_{ch} are expressed in an exponential form (as it has been utilized in [Kapsalis et al. 2020]). To achieve the unified formulation of the smooth transition between the two scenarios, T_{ch} is selected equal to the tracking profile T_{tr} where

a descending linear term $\phi(v_x)$ is added. It is important to get smooth changes of the look-ahead time, and subsequently avoid oscillatory performance, particularly for higher speeds where that may be even more crucial for the overall behavior of the car (see Fig. 5.1).

$$\begin{aligned} T_{tr}(v_x) &= ae^{bv_x} + ce^{-dv_x} \\ \phi(v_x) &= \gamma v_x + \beta \\ T_{ch}(v_x) &= T_{tr}(v_x) + \phi(v_x) \end{aligned} \tag{5.1}$$

with $a = 3.83$, $b = -0.7261$, $c = 1.154$, $d = 0.01453$, $\gamma = -0.05$ and $\beta = 1.25$.

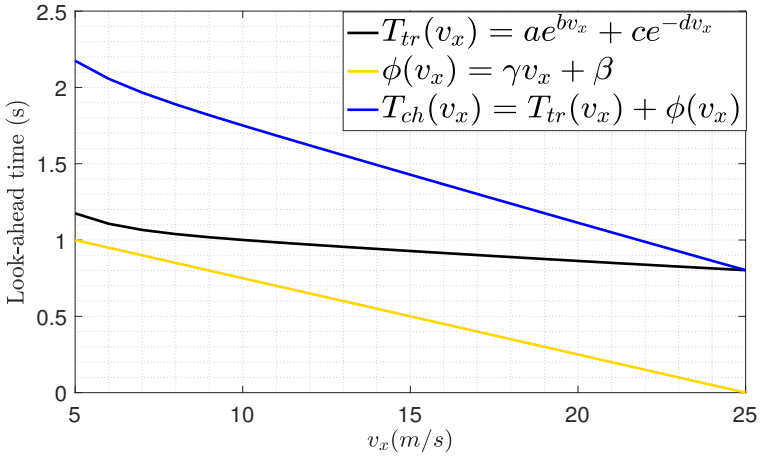

Figure 5.1: The look-ahead time profiles T_{tr} and T_{ch} are depicted as a function of the longitudinal speed, chosen for lane-tracking and lane-change respectively.

The transition from the lane-tracking to the lane-change state, and vice versa, in the path-tracking algorithm is translated as a first step to the convex combination of the two look-ahead time profiles. That is achieved via introducing a new "high level" variable l as an exogenous parameter induced in the model as follows:

$$\begin{aligned} T(v_x, l) &= lT_{ch}(v_x) + (1-l)T_{tr}(v_x) \\ l &\in [0, 1] \end{aligned} \tag{5.2}$$

The equation (5.2) implies that for $l = 0$ the vehicle performs lane-following, while for $l = 1$ it is on a lane-change situation. In the intermediate cases, an interpolation of the two look-ahead time profiles is carried out, according to the on-line computation of l.

This variable is chosen here to be independent of the speed of the car, but depends on the absolute value of the lateral error at the center of gravity of the vehicle, which is considered to be measured at every instant. More specifically, it is considered that for low values of lateral deviation ($|y_{cg}| < 0.4$ meters), the vehicle is in a lane-tracking state, whereas if the lateral offset is high ($|y_{cg}| > 3$ meters) then the vehicle performs a lane-change maneuver.

The equation (5.3) and Fig. 5.2 capture all the above.

$$l(|y_{cg}|) = \begin{cases} l = 0, & \text{if } |y_{cg}| \leq 0.4m \\ l = \frac{|y_{cg}|}{2.6} - \frac{0.4}{2.6}, & \text{if } |y_{cg}| > 0.4m \ \& \ |y_{cg}| \leq 3m \\ l = 1, & \text{if } |y_{cg}| > 3m \end{cases} \tag{5.3}$$

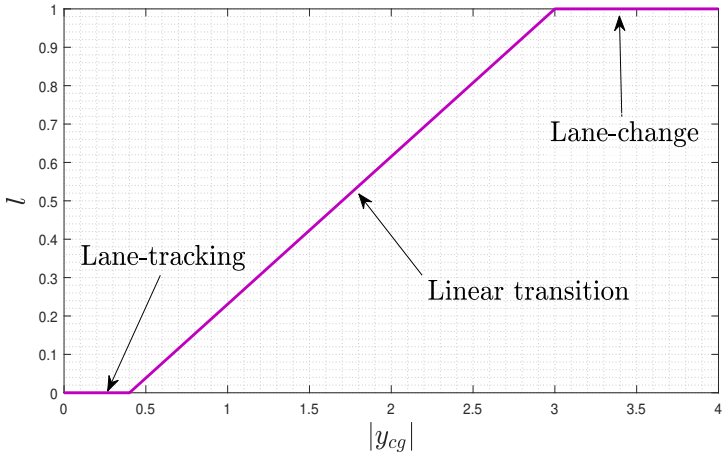

Figure 5.2: Computation of l function of the absolute value of the lateral error at the center of gravity $|y_{cg}|$.

5.2.1.3 LPV/Gridded Model Formulation

The augmented model which expresses the evolution of the lateral model of the vehicle and of the look-ahead errors as well, can be re-written in an LPV form.

The look-ahead distance is decomposed as a product of the speed and the look-ahead time, i.e $L = v_x T(v_x, l)$, and the look-ahead time is selected as in (5.2) as a function of the speed v_x and of the interpolating variable l. Thus, a new LPV model is formulated that consists of the varying parameters v_x and l. Both parameters, which are considered measured and bounded at every instant, are found at the matrix $A_v(\rho)$ only, as follows:

$$A_v(\rho) = \begin{bmatrix} -\frac{C_f+C_r}{m\rho_1} & -\rho_1 + \frac{C_r L_r - C_f L_f}{m\rho_1} & 0 & 0 \\ \frac{-L_f C_f + L_r C_r}{I_z \rho_1} & -\frac{L_f^2 C_f + L_r^2 C_r}{I_z \rho_1} & 0 & 0 \\ -1 & -\rho_1(\rho_2 T_{ch}(\rho_1) - (1-\rho_2) T_{tr}(\rho_1)) & 0 & \rho_1 \\ 0 & -1 & 0 & 0 \end{bmatrix} \tag{5.4}$$

Consequently, the augmented model in (2.13) can be written in an LPV form as a function of the two varying parameters v_x and l as follows:

$$\begin{aligned} \dot{x}(t) &= A(\rho)x(t) + B_1 r(t) + B_2 \delta(t) \\ y(t) &= Cx(t) \end{aligned} \tag{5.5}$$

where, as ρ is defined the varying parameter vector that includes the bounded and rate-bounded varying parameters of the LPV model, as it's given in the set of equations (5.6) below.

The bounds for ρ_1 occur from the known acceleration limits from NAV and for ρ_2 comes from the selected function of l (5.3).

$$\begin{aligned} \rho = [\rho_1 \ \rho_2]^T = [v_x \ l]^T \\ \rho_1 \in [5, 25] m/s, \ \dot{\rho}_1 \in [-9, 3] m/s^2, \\ \rho_2 \in [0, 1], \ \dot{\rho}_2 \in [-1/2.6, 1/2.6] \end{aligned} \tag{5.6}$$

5.2.2 LPV Control Structure & Synthesis

Figure 5.3 depicts the LPV control configuration scheme to impose the aforementioned control objectives in the H_∞ framework.

The signals $r(t)$ and $n(t)$ represent the reference yaw-rate and the noise signal that is additively inserted on the measurement y. The performance outputs $z_1(t)$ and $z_2(t)$ are the variables to be minimized over the reference $r(t)$.

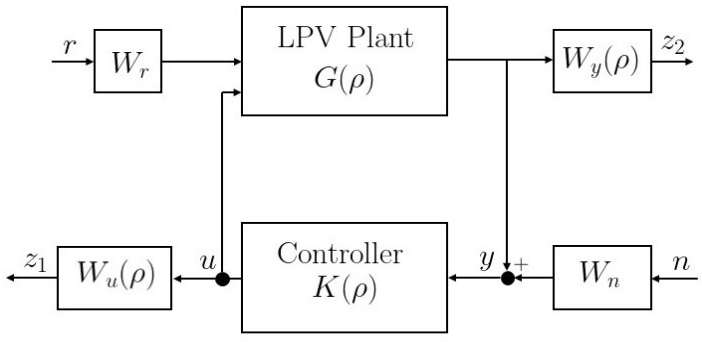

Figure 5.3: LPV Control Scheme

The tuning of the LPV controller $K(\rho)$ is achieved by making use of the varying parameter vector ρ in the weighting functions [Skogestad and Postlethwaite 2007]. In particular, the filters $W_u(s, \rho)$ and $W_y(\rho)$,W_r and W_n are chosen as follows:

- The first-order filter $W_u(\rho)$ is given in a state space form because it is parameter varying.

It's selection is explained below:

$$W_u(\rho) = \frac{z_1}{r}, \quad \begin{matrix} \dot{x}_u = A_u x_u + B_u(\rho) r \\ z_1 = C_u x_u + D_u(\rho) r \end{matrix} \tag{5.7}$$

where the state matrices are: $A_u = -\omega_u/\epsilon_u$, $B_u(\rho) = \dfrac{\omega_u(\epsilon_u - M_u(\rho))}{\epsilon_u}$, $C_u = 1/\epsilon_u$, and $D_u(\rho) = M_u(\rho)/\epsilon_u$. $\omega_u = 10\ rad/s$ and $\epsilon_u = 0.1$ are the bandwidth of the controller for a fast steering control and the roll-off frequency for better noise attenuation, respectively, for the lane-tracking case.

$M_u(\rho) = 2(1 + 249\rho_2)$ is chosen as such to cover both cases and in particular: when (i) $\rho_2 = 0$ (lane-tracking), the actuator's capabilities are fully exploited whereas in (ii) $\rho_2 = 1$ (lane-change), both the demanded bandwidth and the roll-off frequency are significantly decreased and consequently the steering command to perform a smooth and comfortable maneuver.

Fig. 5.4 depicts the frequency specifications for both cases.

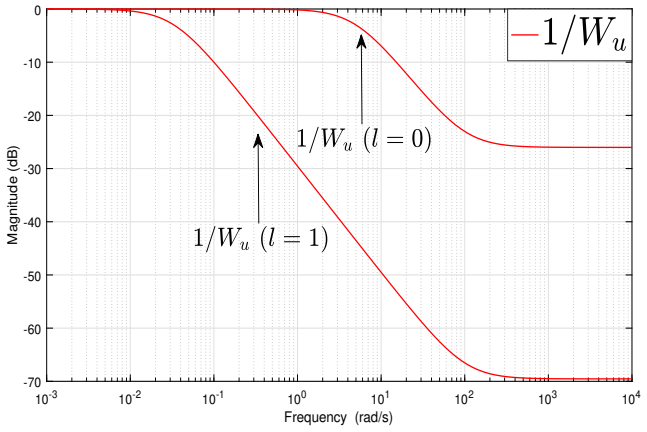

Figure 5.4: Magnitude of the parameter-dependent weighting function $1/W_u(\rho)$ utilized to tune the performance of the LPV controller's effort, for the two cases of lane-tracking ($l = 0$) and lane-change ($l = 1$).

- $W_y(\rho) = T(\rho_1)(1 - 0.5\rho_2)$. When $\rho_2 = 0$ (lane-tracking), then $W_y = T_{tr}(\rho_1)$ as it is already utilized in [Kapsalis et al. 2020]. In the case where $\rho_2 = 1$ (lane-change), the weight on the minimization of the lateral error at the target point is reduced so as to achieve a smoother convergence, especially for higher speeds.

- Finally, constant scaling weights $W_n = 0.5$ and $W_r = 0.1$ are selected on the noise $n(t)$ and the reference yaw-rate $r(t)$ respectively.

The performance variables $z = \begin{bmatrix} z_1 & z_2 \end{bmatrix}^T$, shown in Fig. 5.3, are considered together with the

previous extended model (5.5) to get the generalized LPV plant as shown below:

$$\begin{bmatrix} \dot{x}(t) \\ \hline z(t) \\ y(t) \end{bmatrix} = \left[\begin{array}{c|cc} A(\rho) & B_1 & B_2 \\ \hline C_1(\rho) & D_{11} & D_{12}(\rho) \\ C_2 & D_{21} & 0 \end{array}\right] \begin{bmatrix} x(t) \\ \hline w(t) \\ u(t) \end{bmatrix} \tag{5.8}$$

where $x(t) \in \mathbb{R}^9$ is the extended state vector combining the vehicle, actuator and weighting functions state variables, $w(t) = [r(t)\ n(t)]^T$ is the new vector with the exogenous inputs and $z = [z_1\ z_2]^T$ denote the controlled outputs.

5.2.2.1 Problem solution & Analysis in the Frequency Domain

We have chosen to follow here the set of gridding the parameter space discussed in [Wu 1995; Wu et al. 1996]. This method describes the LPV controller synthesis problem as the solution of a set of LMIs. The LMIs are constructed for the generalized LPV system (5.8), whose solution are the parameter-dependent Lyapunov matrix functions $X(\rho), Y(\rho)$.

Computationally, this problem is solved by selecting user-defined basis functions to interpolate the Lyapunov functions. In this case, the basis functions are chosen as second-order polynomial form, as follows:

$$\begin{aligned} X(\rho) &= X_0 + \rho X_1 + \rho^2 X_2 \\ Y(\rho) &= Y_0 + \rho Y_1 + \rho^2 Y_2 \end{aligned} \tag{5.9}$$

The set of LMIs is finally constructed at the grid points of the varying parameters, which are the bounded velocity of the car and the induced parameter l. More specifically, the LPV system is written in a rectangular grid of specified values of the parameters, as it is shown in Fig. 5.5.

$$\begin{aligned} \rho_1 &= 5 : 1 : 25 m/s \\ \rho_2 &= 0, 1 \end{aligned} \tag{5.10}$$

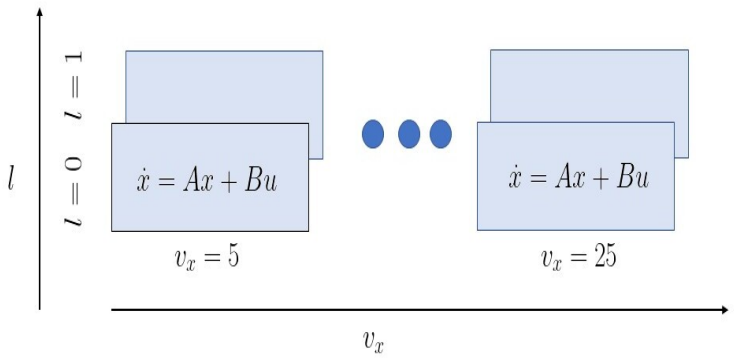

Figure 5.5: LPV model defined on a rectangular grid of the varying parameter vector ρ.

The solution is computed then, by optimizing over the matrices X_s, Y_s $s = 0, 1, 2$. The optimal attenuation index variable is computed $\gamma = 2.3$, using the LPVTools toolbox [Hjartarson, Seiler, and Packard 2015]. Then, the optimal LPV controller is reconstructed as a LTI state space controller for every grid point, using the pair of matrices (X_s, Y_s).

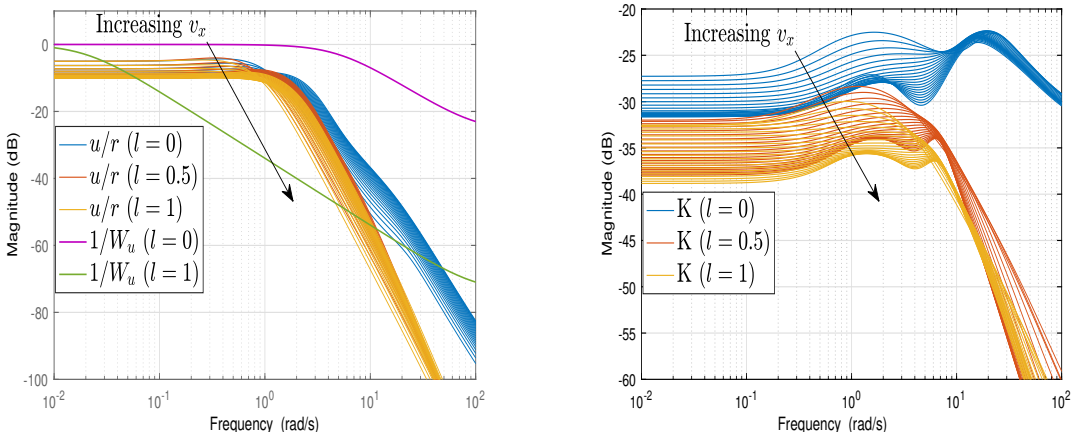

(a) Controller sensitivity u/r of the closed-loop system (b) LPV gain-scheduled state space controller K_i

Figure 5.6: Bode plots depicting the frequency response of the closed-loop system.

Fig. 5.6(a) depict the frequency responses for all speeds from the steering wheel angle command to the reference yaw-rate $r(t)$ with respect to the specification imposed by the template weighting function $W_u(s)$ for the cases of lane-tracking $(l = 0)$, lane-change $(l = 1)$ and the merged case where $(l = 0.5)$, respectively. It has to be remarked that the bandwidth of the control during lane-change case $(l = 1)$ is lower than the one of the merged $(l = 0.5)$, showing that as l is increasing the effort of the LPV controller is more restricted.

Accordingly, Fig. 5.6(b) illustrate the magnitude for every grid value of speed of the synthesized LPV controller for different values of l. One can notice that, as speed increases, the gains of the controller are decreased, especially for the case of lane-change where the steering must be limited. This is proven by the the magnitude of the controller gains, at low frequencies, for the case of lane-change $(l = 1)$ where it never gets higher than -32 dB. As for the tracking $(l = 0)$, it never gets higher than -28 dB.

5.2.3 Implementation of the LPV/Gridded controller

This section presents the two steps that make feasible the implementation of the continuous-time synthesized controller on an embedded platform.

The proposed integrated LPV controller is implemented in a bipartite procedure. Consid-

ering the synthesized in continuous-time gridded state space controllers, defined as $K_{i,j}$,

$$\begin{matrix} \dot{x}_c(t) = A_{i,j}x_c(t) + B_{i,j}y(t) \\ u(t) = C_{i,j}x_c(t) + D_{i,j}y(t) \end{matrix} \ , \ K_{i,j} = \left[\begin{array}{c|c} A_{i,j} & B_{i,j} \\ \hline C_{i,j} & D_{i,j} \end{array}\right] \tag{5.11}$$

where $x_c \in \mathbb{R}^9$ is the controller state vector, $A_{i,j} \in \mathbb{R}^{9\times 9}$, $B_{i,j}\ in\mathbb{R}^9$, $C_{i,j} \in \mathbb{R}^{1\times 9}$, $D_{i,j} \in \mathbb{R}^9$ and $u \in \mathbb{R}$ which is the control command of the controller. $i = 0, 1$ and $j = 1, .., 21$ are the indices denoting the grid points of the parameters from Fig. 5.5. Then:

1. Off-line Step: The discrete-time state space gridded controllers, $Kd_{i,j}$ are computed as follows [Astrom and Wittenmark 1984], for a given sampling time T_s:

$$Kd_{i,j} = \left[\begin{array}{c|c} Ad_{i,j} & Bd_{i,j} \\ \hline Cd_{i,j} & Dd_{i,j} \end{array}\right] \tag{5.12}$$

   So, the discrete-time state space implementation is the one follows:

$$\begin{matrix} x_c(k+1) = Ad_{i,j}x_c(k) + Bd_{i,j}y(k) \\ u(k) = Cd_{i,j}x_c(k) + Dd_{i,j}y(k) \end{matrix} \tag{5.13}$$

   where,

$$\begin{bmatrix} Ad_{i,j} & Bd_{i,j} \\ 0 & 0 \end{bmatrix} = exp\left(\begin{bmatrix} A_{i,j} & B_{i,j} \\ 0 & I \end{bmatrix} T_s \right) \\ Cd_{i,j} = C_{i,j} \ , Dd_{i,j} = D_{i,j} \tag{5.14}$$

2. On-line Step: The discretized controllers are interpolated as such below:

   (a) Using the measured value of the vehicle's velocity between two consecutive grid points $\rho_1 \in [\rho_{1_{j-1}}, \rho_{1_j}]$, a linear interpolation between the LTI discretized controllers $Kd_{i,j-1}, Kd_{i,j}\ \forall i$, takes place as follows:

$$\begin{matrix} Kd_i = \alpha(\rho_1)Kd_{i,j} + (1-\alpha(\rho_1))Kd_{i,j-1} \ , \ i = 0, 1 \\ \alpha(\rho_1) = \dfrac{\rho_1 - \rho_{1_{j-1}}}{\rho_{1_j} - \rho_{1_j}} \end{matrix} \tag{5.15}$$

   where, $\alpha(\rho_1)$ is the scaling factor computed on-line for the measured value of speed that belongs between $\rho_{1_{j-1}}$ and ρ_{1_j}.

   (b) Finally, $l = \rho_2$ is computed as a function of the absolute value of the lateral error at the center of gravity (5.3), so as to distinguish the scenario between lane-change and lane-tracking. Consequently, the applied LPV controller is the one below:

$$K = \rho_2 Kd_0 + (1-\rho_2)Kd_1 \tag{5.16}$$

   where the $Kd_0 = K_{tr}$ and $Kd_1 = K_{ch}$ are the contributions of the LPV controller K, for lane-tracking and lane-change respectively.

5.2.4 Simulation Results

We validate the Merged LPV controller in some first simulations tests, presented in the following parts.

5.2.4.1 Single Lane-change to Lane-tracking

A simulation scenario with a single lane-change is demanded, by starting the vehicle with an initial offset of 4 m away from the desired trajectory.

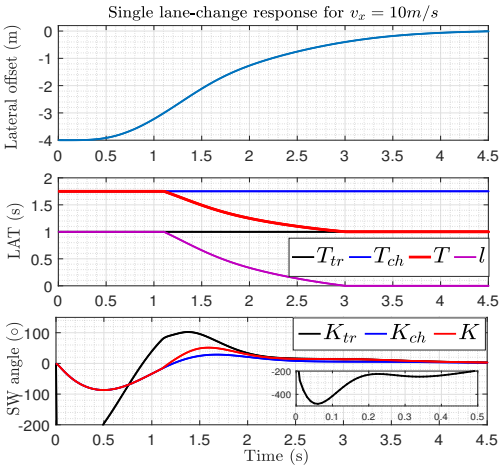

(a) Lane-change response for $v_x = 10\ m/s$.

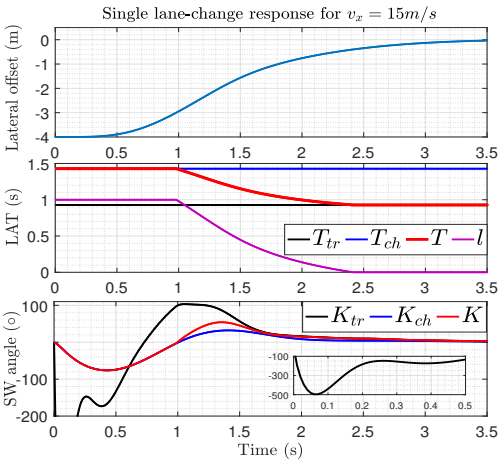

(b) Lane-change response for $v_x = 15\ m/s$.

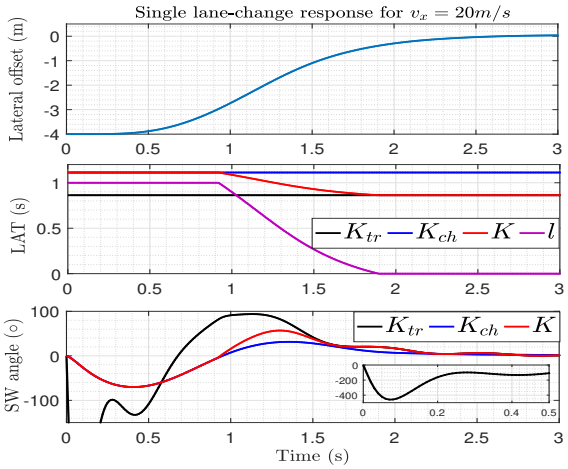

(c) Lane-change response for $v_x = 20\ m/s$.

Figure 5.7: *Simulation case scenario a)*: Single lane-change results of the LPV Controller, for speeds $v_x = 10, 15, 20\ m/s$.

Figures 5.7(a),5.7(b) and 5.7(c) illustrate the performance for several “frozen" speed tests of $v_x = 10, 15, 20\ m/s$ respectively. The first plot of each figure depicts the lateral deviation response of the vehicle, the central the interpolated look-ahead time with respect to the real-time computation of l (according to (5.3)) and the one at the bottom shows the applied steering wheel angle.

At the beginning, the vehicle starts turning by using entirely the part of the LPV controller designed for the lane-change. For this reason, the steering is restrained compared to the tracking part. As the vehicle converges to the lane and $|y_{cg}| < 3\ m$, the lane-tracking part of the controller starts contributing even more. The interpolation of the two parts of the LPV controller, i.e K_{tr}, K_{ch} is achieved in a smooth way, avoiding oscillations and overshoots.

5.2.4.2 Double Lane-changes & Curves

Now, the integrated control system's capabilities are stressed to a more complex and realistic scenario at low and high speeds. That simulation scenario includes the collected trajectory X, Y of the test track in Satory.

The pre-defined path insists of a straight lane and then the trajectory is shifted 5 m to the left twice where the vehicle must perform a double lane-change maneuver as it returns back to the initial lane. Then, the vehicle negotiates three turns of different curvatures, as it is illustrated in Fig. 5.8(a).

Throughout the simulation, the longitudinal velocity profile (Fig. 5.8(b)) is considered varying, as well as during the lane-change cases. The vehicle starts at standstill and accelerates till 23 m/s while performing the first double lane-change and it decelerates during the second one to 8 m/s.

To demonstrate the tracking behavior of the controller, at 50 s, the vehicle accelerates till 20 m/s entering the first two turns. At the last 20 s, the vehicle brakes to 11 m/s and tracks the last sharp curve.

Fig. 5.8(c) details the lateral deviation at the center of gravity throughout the test. At the beginning and the end of the double lane-changes the vehicle's offset is discontinuously increased, since the reference path is placed to an adjacent lane. One can appreciate that the controlled vehicle can successfully perform the maneuvers when the lane-changes are launched, even though the speed of the car is varying.

Figure 5.8(d) supports that statement, as the steering during the maneuver is limited without allowing overshoots as the vehicle converges to the lane, even though the vehicle is far away from the reference trajectory. At the end of the experiment, the vehicle tracked the three turns utilizing the tracking-associated contribution of the LPV controller. It can be seen that the tracking performance is satisfying since no lateral deviations are observed ($|y_{cg}| < 0.5$ m). Finally, in Fig. 5.8(e) it can be observed the smooth transition of the steering framework by interpolating the LPV look-ahead time with respect to the real-time computation of the

induced parameter l.

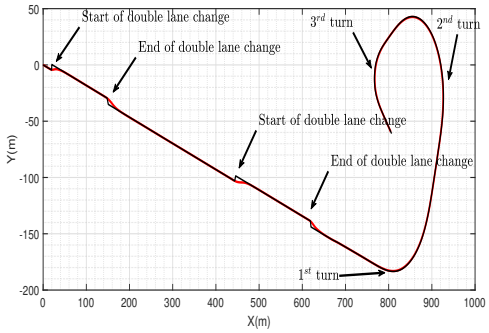

(a) Trajectory Followed

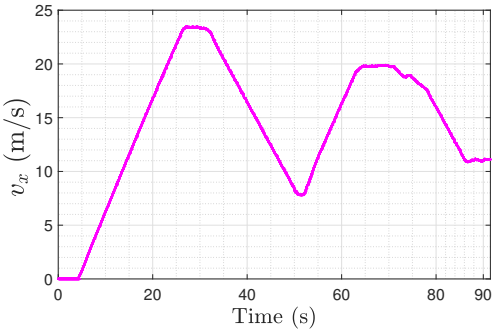

(b) Longitudinal speed profile

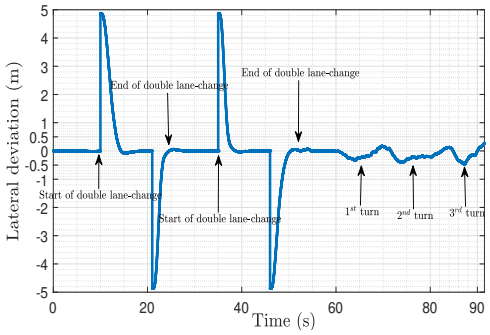

(c) Lateral offset at the center of gravity

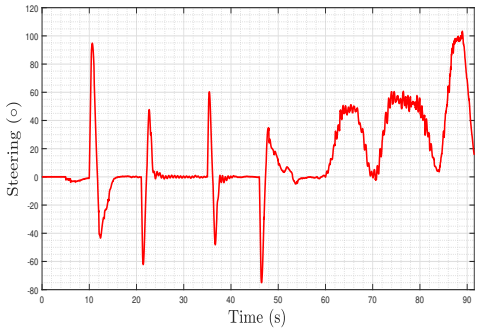

(d) Steering wheel angle response

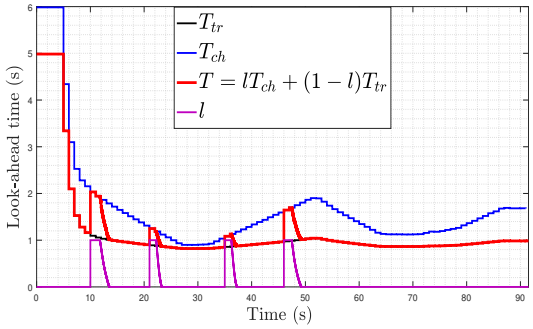

(e) Look-ahead time response

Figure 5.8: *Simulation case scenario b)*: Double lane-change & curve-tracking results of the LPV controller, for a varying speed profile.

5.2.5 Experimental Results

The proposed algorithm was experimentally tested in the facilities of Satory. We remind that the LPV controller is embedded in a MABx that is installed in the trunk of the vehicle

and the running frequency is at 100 H_z. Consequently, the LPV controller is discretized accordingly.

5.2.5.1 Lane-Tracking Evaluation Scenario

This part shows the collected experimental results (set of figures 5.9) where the LPV controller tracks a path (Fig. 5.9(a)) that is composed of three curves for a varying speed profile (Fig. 5.9(b)) that is provided by the NAV system.

The measured lateral offset depicted in figure 5.9(c), never gets more than 0.4 m, thus proving that the controller is performant and does not allow huge lateral errors. Furthermore, the comfort of the passenger is sustained and it can be shown from the steering wheel angle response in figure 5.9(d), since it is smooth without noisy oscillations.

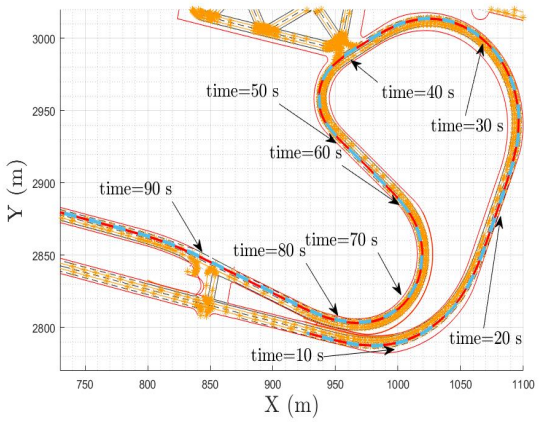

(a) Trajectory followed

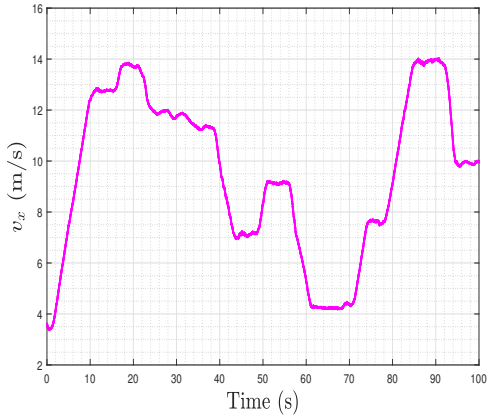

(b) Longitudinal speed profile

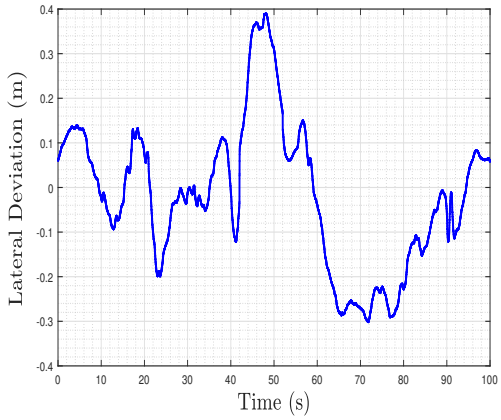

(c) Lateral offset at the center of gravity

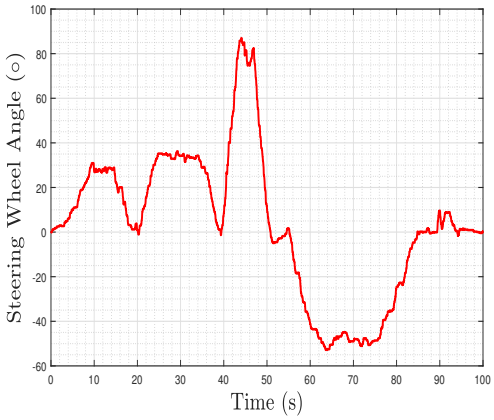

(d) Steering wheel angle response

Figure 5.9: *Experimental case scenario a)*: Curve-tracking results at the test track of Satory.

5.2.5.2 Lane-change Assessment

To assess the merging case, we enforce the vehicle to the extreme case scenario of a recovery lane-change. More specifically, the vehicle is driven to the limits of the road to the opposite direction (Fig. 5.10(a)) and then the LPV controller is switched on in to recover the vehicle, which at this time has already moved away with a high speed and a different heading, to the initial reference lane.

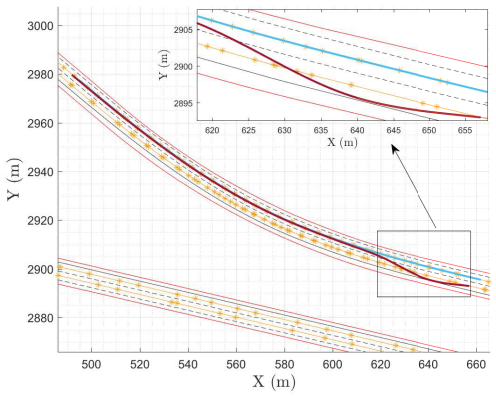

(a) Trajectory Followed

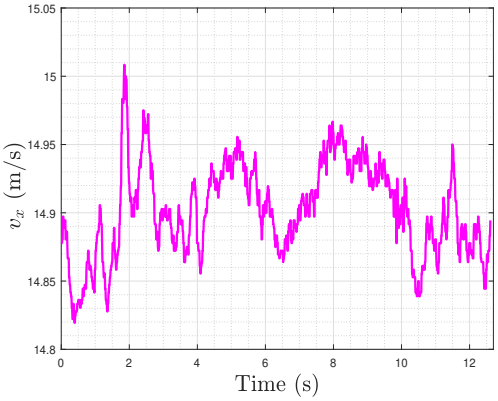

(b) Longitudinal speed profile

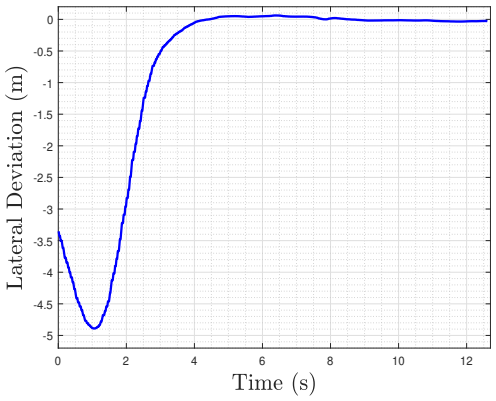

(c) Lateral offset at the center of gravity

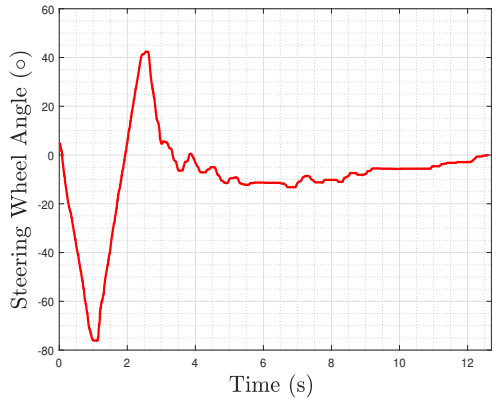

(d) Steering wheel angle response

Figure 5.10: *Experimental case scenario b)*: Fast recovery lane-change results at the test track of Satory.

The set of figures 5.16 illustrate the recovered experimental results. The vehicle's speed (fig. 5.10(b), as it enters a turn at approximately 15 m/s, moves away from the desired path at 3.5 m (fig. 5.10(c) and at that point the proposed LPV controller is applied and enables the vehicle to return safely back to the initial trajectory.

The figure 5.10(d) shows that vehicle utilizes the maximum steering rate of the EPS system

and is able to recover the vehicle to the starting direction without exiting the road width limits. Even though the vehicle moves fast the applied steering command makes a safe and fast maneuver and at the same time proceeds to the tracking of the following curve without presenting any oscillation or degradation of performance.

5.3 A Reference Governor approach for Merged Lateral Control

5.3.1 Introduction & Motivations

This section presents the design of a control system that enables a single lane-tracking controller to handle adequately the case of a lane change as well. In that sense, it can be avoided the need to design a second controller that performs only during the lane-change and even the switching scheme between these two controllers [Mahtout et al. 2018].

For the sake of clarity, Fig. 5.11 is added to illustrate two real yaw-rate references that recovered in experimental tests using the automated Renault Zoe (from Figure 2.1) in autonomous mode.

The vehicle starting in a straight line, for fixed velocity $v_x = 10\ m/s$, (i) in blue it followed a turn (lane tracking) and (ii) in red performed a fast maneuver to reach an adjacent lane more than 3 meters away from the initial position of the vehicle (lane-change).

As it can been seen, the yaw-rate reference during lane-tracking is gradually increasing and, in general, is smooth without abrupt changes. For that reason, the lane-following controllers are designed to be fast, without restricting the steering capabilities of the controller, so as not to allow big lateral deviations from the reference trajectory.

On the other hand, at the beginning of a lane-change the yaw-rate reference is increased discontinuously, function of the required lateral displacement of the car. Then, as the vehicle approaches the desired lane, the yaw-rate reference gradually reduces till zero where the maneuver is performed.

Therefore, to treat the discontinuous phase, usually a lane-change controller has restricted capabilities (compared to a lane-tracking one) so as not to go further the steering rate limitations of the actuator and cause oscillations or even instability [Mahtout et al. 2018].

To address the aforementioned problem, a reference governor is an interesting solution to guarantee performances in both cases while handling the actuator limitations.

5.3.2 Reference Governor Design for the Closed-Loop System

The first part of this section presents the needed background on reference governors for

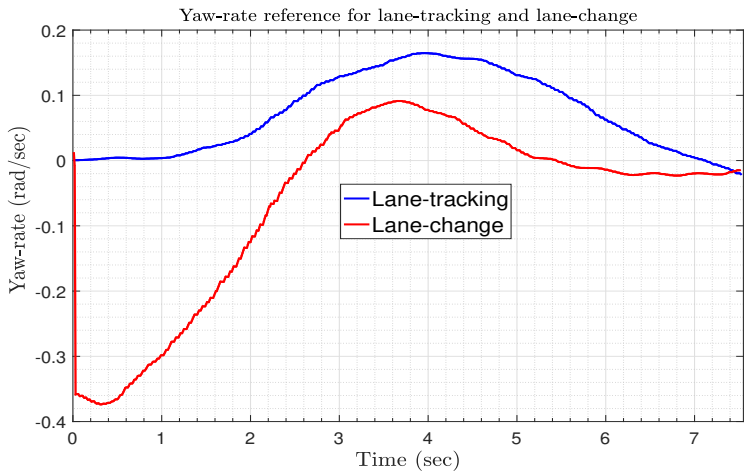

Figure 5.11: Yaw-rate references for the case of tracking a turn (blue) and for a lane-change maneuver (red) recovered in experimental tests while driving in autonomous mode an automated Renault Zoe for $v_x = 10\ m/s$.

this study. Interested readers may study [Garone, Di Cairano, and Kolmanovsky 2017] and [Kolmanovsky, Garone, and Di Cairano 2014] for more details. Then, the design of the proposed reference governor for the lane-keeping system is detailed in order to perform a lane-change maneuver.

5.3.2.1 Brief Background On Reference Governors For Linear Systems

The reference governor is enforced to discrete-time closed-loop systems whose state space dynamics are expressed as:

$$\begin{aligned} x_{cl}(k+1) &= Ax_{cl}(k) + Bv(k) \\ y_{cl}(k) &= Cx_{cl}(k) + Dv(k) \in Y \end{aligned} \tag{5.17}$$

where $x_{cl} \in R^n$ is the state space vector, $v \in R^m$ is the virtual reference, $y_{cl} \in R^p$ is the output vector and $Y \subseteq R^p$ is the constraint output admissible set.

The scheme in Fig. 5.12 depicts the general structure of the reference governor. An initial reference $r \in R^q$ is fed to the reference governor and assuming full information of the state or its estimation $\hat{x}_{cl}$, reference governor alters it to the virtual reference v. The alteration is made in order to satisfy closed-loop constraints, keeping v close to r.

The fulfillment of the constraints is achieved by

$$(v, \hat{x}_{cl}) \in O_\infty \tag{5.18}$$

where $O_\infty \subseteq R^m \times R^n$. The set O_∞ is the maximal output admissible set which contains the set of all states $\hat{x}_{cl}$ and constant references v for which constraints are satisfied for present

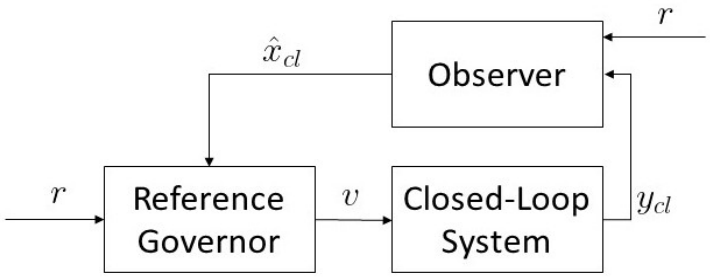

Figure 5.12: Full control scheme including the reference governor

and future time k, i.e

$$O_\infty = \{(v, \hat{x}_{cl}) : y_{cl}(k) \in Y, \forall k \in Z_+\} \tag{5.19}$$

where the output $y(k)$ at every time instant k can be computed as follows:

$$y_{cl}(k) = CA^k\hat{x}_{cl} + C(I - A^k)(I - A)^{-1}Bv + Dv \tag{5.20}$$

To ensure robustness and steady state constraints enforcement, O_∞ is tightened as:

$$\begin{gathered} \tilde{O}_\infty = O_\infty \cap O^\epsilon, \text{with} \\ O^\epsilon = \{v : \bar{y}_{v,cl} \in (1 - \epsilon)Y\}, 1 \gg \epsilon > 0 \end{gathered} \tag{5.21}$$

where the steady state output response $\bar{y}_v$ is expressed as such:

$$\bar{y}_{v,cl} = C(I - A)^{-1}Bv + Dv \tag{5.22}$$

If A is Schur and the pair (C, A) is observable, it is proven in [Gilbert and Tan 1991] that $\tilde{O}_\infty$ is finitely determined, i.e there exists a finite time index k^* such that:

$$\tilde{O}_\infty = \{(v, \hat{x}_{cl}) : y_{cl}(k) \in Y, k = 0, .., k^*\} \cap O^\epsilon \tag{5.23}$$

In the simplest case, where the constraint set Y is expressed in a polytopic form, i.e as a set of linear inequalities as explained below:

$$Y = \{y : Hy_{cl}(k) \preceq h, \forall k \in Z_+\}, h > 0 \tag{5.24}$$

then, the computation of the $\tilde{O}_\infty$ is easy. More precisely, given a $1 \gg \epsilon > 0$ and sufficiently large k^*,

$$\tilde{O}_\infty = \left\{(v, \hat{x}_{cl}) : \begin{bmatrix} HD & HC \\ HCB + HD & HCA \\ \vdots & \vdots \\ HC(I - A^{k^*})(I - A)^{-1}B + HD & HCA^{k^*} \\ HC(I - A)^{-1}B + HD & 0 \end{bmatrix} \begin{bmatrix} v \\ \hat{x}_{cl} \end{bmatrix} \preceq \begin{bmatrix} h \\ h \\ \vdots \\ h \\ (1 - \epsilon)h \end{bmatrix} \right\} \tag{5.25}$$

Finally, a minimal representation of $\tilde{O}_\infty$ is obtained when redundant or almost redundant inequality constraints are eliminated. The reduced inequalities of (5.25) that express the maximal admissible set are written as:

$$\tilde{O}_\infty = \{(v, \hat{x}_{cl}) : \mathcal{H}_v v + \mathcal{H}_x \hat{x}_{cl} \preceq \mathcal{L}\} \tag{5.26}$$

where $\mathcal{H}_v$, $\mathcal{H}_x$ and $\mathcal{L}$ are the matrices that correspond to the reduced inequalities.

According to the dynamic reference governor, at every instant k, a line search along the segment $v(k-1)$ and $r(k)$ is performed in the convex set $\tilde{O}_\infty$ so as to compute the virtual reference solving the following optimization problem:

$$\begin{aligned} \underset{K\in[0,1]}{\text{maximize}} \quad & K \\ \text{subject to} \quad & v(k) = v(k-1) + K(r(k) - v(k-1)) \\ & \mathcal{H}_v v(k) + \mathcal{H}_x \hat{x}_{cl}(k) \preceq \mathcal{L} \end{aligned} \tag{5.27}$$

5.3.2.2 Reference Governor Design for Lane-Change Maneuvers

The following subsection describes the design of the reference governor for lateral control. The aim of the reference governor is, given a lane-tracking controller, 1) to generate a smooth virtual reference that permits the lane-change maneuver and 2) respects the maximum steering actuation capabilities.

The first step of the design of the reference governor is the selection of the model used for prediction, which in this paper is chosen as the closed-loop system between the vehicle model G and the dynamic output feedback controller C (it will be explained later), eq.(2.6) and (5.34) respectively.

This model is discretized at the sampling time $T_s = 0.01\ s$, for which the automated vehicle accepts steering command. The discrete state space model is expressed below:

$$\begin{aligned} x_{cl}(k+1) &= A_d x_{cl}(k) + B_d r(k) \\ y_{cl}(k+1) &= C_d x_{cl}(k) + D_d r(k) \in Y \end{aligned} \tag{5.28}$$

where $x_{cl} = \left[\frac{x}{x_c}\right] \in \mathbb{R}^{10}$, since $x_c \in \mathbb{R}^8$ as it will be explained in the next section and x_{cl} is the closed-loop state space vector (without the states of the actuator so as to reduce the size of the optimization), $y_{cl} = \delta$ is the steering wheel angle enforced to stay in the constraint admissible set Y, $A_d \in \mathbb{R}^{10\times 10}$, $B_d \in \mathbb{R}^{10}$, $C_d = [0 \mid C_c] \in \mathbb{R}^{1\times 10}$, $D_d = 0$ are the closed-loop system space matrices.

To implement the global control scheme depicted in Fig. 5.12, an LTI observer has been designed so as to provide full knowledge over the state x_{cl} at every instant for the system (5.28). Moreover, the constraint admissible set is constructed to include boundaries of the

steering angle.

$$-\delta_{max} \leq y_{cl}(k) \leq \delta_{max} \tag{5.29}$$

where δ_{max} is the maximum admissible steering angle in rad. Y can be written in a polytopic form below:

$$Y = \{y_{cl} : Hy_{cl}(k) \leq h, \forall k \in Z_+\}, h > 0 \tag{5.30}$$

where $H = \begin{bmatrix} -1 & 0 \\ 0 & 1 \end{bmatrix}$, $h = \begin{bmatrix} \delta_{max} \\ \delta_{max} \end{bmatrix}$, $\delta_{max} = \frac{\pi}{180\kappa}\delta^{\circ}_{max} > 0$, δ°_{max} is the selected maximum value in degrees and the gain κ is the gear ratio of the steering actuation system.

The objective of rendering smooth the virtual yaw-rate reference, feasible for the lane-tracking controller, is chosen as an extra constraint which limits the slew rate of the virtual reference as follows:

$$|v(k) - v(k-1)| \leq \Delta_v \tag{5.31}$$

where Δ_v is the selected slew rate of the virtual reference.

That constraint is included in the optimization problem (5.27). This leads to the proposed maximization from which the virtual reference v is found on-line as such:

$$\begin{aligned} \underset{K\in[0,1]}{\text{maximize}} \quad & K \\ \text{subject to} \quad & v(k) = v(k-1) + K(r(k) - v(k-1)) \\ & \mathcal{H}_v v(k) + \mathcal{H}_x \hat{x}_{cl}(k) \preceq \mathcal{L} \\ & |v(k) - v(k-1)| \leq \Delta_v \end{aligned} \tag{5.32}$$

The set $\tilde{O}_\infty$ has been computed off-line, for $\epsilon = 10^{-6}$, $k^* = 7$ for the two different cases where $\delta^{\circ}_{max} = 50^{\circ}$, 100°, and its minimal representation matrices $\mathcal{H}_v$, $\mathcal{H}_x$ and $\mathcal{L}$ are obtained using Multi-Parametric Toolbox [Herceg et al. 2013]. The slew rate of the virtual reference Δ_v is selected as 0.01 to enable a smooth lane-change maneuver when the H_∞ lane-tracking controller is present.

The embedded solver used for the maximization problem (5.32), that computes v on-line, is CVXGEN [Mattingley and Boyd 2012]. It is worth to mention that the resulted optimization problem is fast enough for a real-time implementation.

5.3.3 H_∞ Yaw-rate Lateral Controller Structure & Synthesis

The control algorithm is based on tracking a yaw-rate reference $r(t)$, which is computed in order to reach a target point located on a look-ahead distance onto the reference trajectory [Tan and Huang 2014]. The lane-following system has to perform fast tracking capabilities and provide comfort as well.

The chosen control design method is the H_∞ approach where the requirements are specified using weighting functions [Skogestad and Postlethwaite 2007]. In the case of the lane-tracking

controller, the above objectives are defined using the weighting functions $W_u(s)$ and $W_e(s)$ according to the control scheme shown in Fig. 5.13. The first-order filters $W_u(s)$ and $W_e(s)$

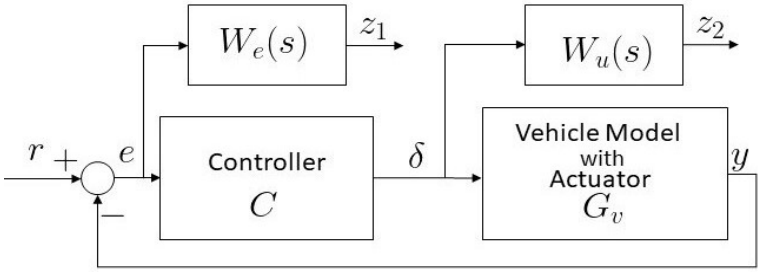

Figure 5.13: Lateral control design via yaw-rate tracking.

are chosen as:

- $W_u(s) = \dfrac{s + \omega_u/M_u}{\epsilon_u s + \omega_u}$, where $\omega_u = 10\ rad/s$ is the bandwidth of the controller and have a smooth steering wheel angle change. $M_u = 2\ (6db)$ is chosen in order to satisfy the saturation limits of the actuator and $\epsilon_u = 0.1$ which is the roll-off frequency for better noise attenuation.

- $W_e(s) = \dfrac{s + \omega_e/M_e}{\epsilon_e s + \omega_e}$, where $\omega_e = 3\ rad/s$ is the bandwidth for fast tracking of the reference. $M_e = 2\ (6db)$ is chosen to ensure robustness and $\epsilon_e = 0.001$ which corresponds to the steady state tracking error.

The tuning of the dynamic output controller is achieved by minimizing off-line the performance variables $z = \begin{bmatrix} z_1 \\ z_2 \end{bmatrix}$ with respect to the reference r for a performance index $\gamma > 0$, i.e

$$\sup_{||r||\neq 0} \frac{||z||_2}{||r||_2} < \gamma \tag{5.33}$$

The design of the nominal H_∞ controller is carried out assuming a constant longitudinal speed $v_x = 10\ m/s$. Solving the appropriate linear matrix inequalities [Gahinet and Apkarian 1994] leads to the optimal attenuation level $\gamma = 0.9053$. Since $\gamma < 1$, the closed-loop met the required objectives for the nominal case where $v_x = 10\ m/s$ (see Fig. 5.14).

A first robustness analysis is presented in Fig. 5.14, where are shown the frequency responses of the performance variables z to the reference r (so the S and KS sensitivity functions) relatively to the specifications $1/W_e$, $1/W_u$ imposed, considering an uncertain velocity i.e $v_x \in [5, 15]\ m/s$. This emphasizes the robust performance of the closed-loop system w.r.t speed uncertainties.

Note that the dynamic output controller can be expressed in a state space form, which has as input the yaw-rate error $e(t) = r(t) - y(t)$ and as an output the steering wheel angle $\delta(t)$.

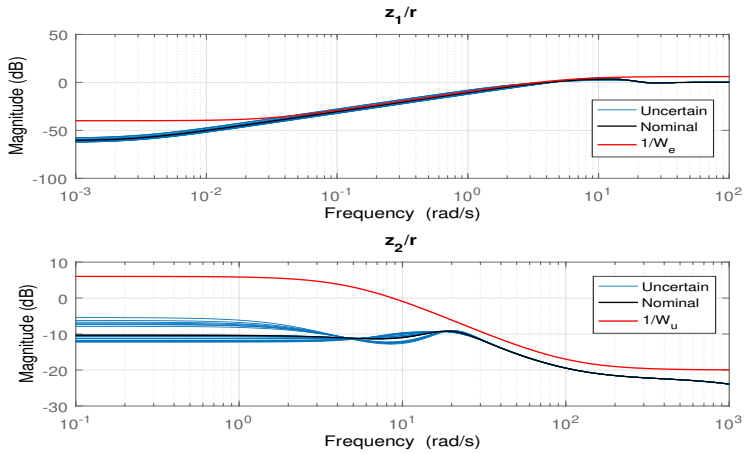

Figure 5.14: Frequency responses z_1/r and z_2/r of the closed-loop system.

$$\begin{array}{c} \dot{x}_c(t) = A_c x_c(t) + B_c e(t) \\ \delta(t) = C_c x_c(t) + D_c e(t) \end{array} \quad , \quad C = \left[\begin{array}{c|c} A_c & B_c \\ \hline C_c & D_c \end{array}\right] \tag{5.34}$$

where, $x_c(t) \in \mathbb{R}^8$ is the state vector of the controller, $A_c \in \mathbb{R}^{8\times 8}$, $B_c \in \mathbb{R}^8$ and $C_c \in \mathbb{R}^{1\times 8}$ are the controller's state space matrices.

5.3.4 Robust stability and performance analysis using μ-analysis

In this section, a more complete robustness analysis is carried out considering several parameter uncertainties.

First let us recall that a control system is robust if it is insensitive to differences between the actual real system and the model used to design the controller. This is formulated through the well know concepts below (see [Skogestad and Postlethwaite 2007]):

- **Robust Stability (RS)**. The system is stable for all perturbed plants about the nominal model up to the worst-case model uncertainty.

- **Robust Performance (RP)**. The system satisfies the performance specifications for all perturbed plants about the nominal model up to the worst-case model uncertainty.

Now, for a deeper analysis, the μ-analysis methodology is considered to conclude on the robustness of the proposed H_∞ controller w.r.t parameter uncertainties (see [Skogestad and Postlethwaite 2007]). We here consider that the parameters of the bicycle model are uncertain

as given below

$$\begin{array}{rcll} \overline{C_f} & = & C_f(1+p_{C_f}\delta_{C_f}), & p_{C_f}=15\%, \quad \delta_{C_f}\in[-1,1] \\ \overline{C_r} & = & C_r(1+p_{C_r}\delta_{C_r}), & p_{C_r}=15\%, \quad \delta_{C_r}\in[-1,1] \\ \overline{m} & = & m(1+p_m\delta_m), & p_m=10\%, \quad \delta_m\in[-1,1] \\ \overline{I_z} & = & I_z(1+p_{I_z}\delta_{I_z}), & p_{I_z}=10\%, \quad \delta_{I_z}\in[-1,1] \end{array}$$

As we consider structured uncertainties, a μ-analysis is used to study RS and RP. The method consists in applying the μ-small gain theorem for structured uncertainties, so to build the so-called $N-\Delta$ form representing the uncertain closed-loop system. In this framework, N is written as $N(s)=\begin{bmatrix} N_{11}(s) & N_{12}(s) \\ N_{21}(s) & N_{22}(s) \end{bmatrix}$, and the closed-loop transfer matrix is:

$$T_{ew}(s)=N_{22}(s)+N_{21}(s)\Delta(s)(I-N_{11}(s))^{-1}N_{12}(s) \tag{5.35}$$

First the structured singular value is defined as:

$$\mu_{\underline{\Delta}}(M)^{-1}:=\min\{\overline{\sigma}(\Delta):\Delta\in\underline{\Delta},\ \det(I-\Delta M)\neq 0\}. \tag{5.36}$$

Assuming nominal stability, RS and RP analysis for structured uncertainties are therefore such that:

$$\text{RS} \quad \Leftrightarrow \quad \mu_{\underline{\Delta}}(N_{11})<1,\ \forall\omega \tag{5.37}$$

$$\text{RP} \quad \Leftrightarrow \quad \mu_{\underline{\Delta}}(N)<1,\ \forall\omega \tag{5.38}$$

Finally, let us remark that the structured singular value cannot be explicitly determined, so that the method consists in calculating an upper bound and a lower bound, as closed as possible to μ.

Now as shown below the maximal bounds of the μ for RS and RP are less than one, then the H_∞ controller keeps stability and performance for the considered uncertainties.

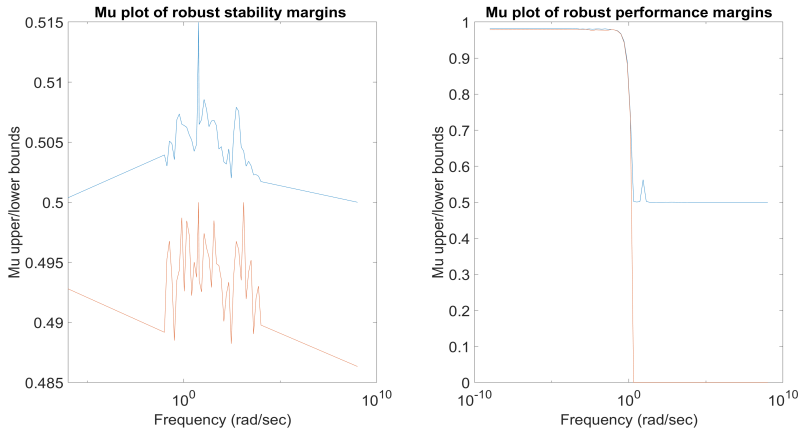

Figure 5.15: μ-bounds of the Robust stability and Robust Performance analysis

5.3.5 Simulation Results

We consider as a case scenario where the vehicle starts more than 3 meters away from the reference lane and simulate closer to the collected experimental data.

In that way, the lane-keeping system equipped with the reference governor can prove that performs a lane-change maneuver. The longitudinal speed is fixed at $v_x = 10\ m/s$.

Fig. 5.16(a) illustrates the lateral deviation during the lane-change scenario. When the reference governor is used, a smooth convergence is achieved to the reference lane with maximum overshoot of $0.1m$.

When the steering wheel angle bound is $100°$, the convergence is faster than $50°$. On the contrary, when the reference governor is absent the lane-tracking controller shows jerky performance since it oscillated before converging to the desired lane.

Fig. 5.16(b) depicts the steering wheel angles during the maneuver for all cases. When the reference governor is added to the loop, the controller's output is smooth without violating the imposed constraint for $\delta_{max} = 50°$.

As for case where $\delta_{max} = 100°$, the steering wheel angle does not reach it since is not needed to turn that much to perform the maneuver. Whereas, for the case of the lateral controller, the steering is jerky especially at the beginning where is discontinuous.

Figures 5.16(c), 5.16(d) and 5.16(e) show the yaw-rate responses for the cases where the reference governor is out of the loop and when $\delta_{max} = 50°, 100°$ respectively.

In Fig. 5.16(c), the reference governor is absent and the yaw-rate of the vehicle overshoots during the tracking of the reference which is discontinuous at the beginning.

On the other hand, the virtual reference shown in figures 5.16(d) and 5.16(e) is gentler compared to the desired one and for that reason the steering wheel angle is increasing in an admissible rate.

In addition, in Fig. 5.16(d), the virtual reference saturates automatically to a certain value in order to avoid the violation of the steering wheel constraint.

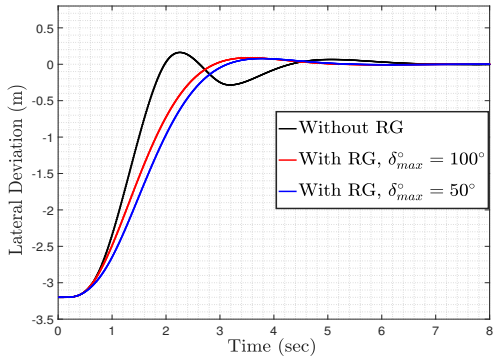

(a) Lateral deviation when $\delta^{\circ}_{max} = 50$ (blue), $\delta^{\circ}_{max} = 100$ (red) and the reference governor is absent (black).

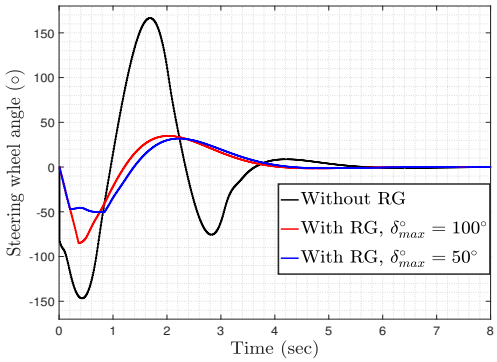

(b) Steering wheel angle when $\delta^{\circ}_{max} = 50$ (blue), $\delta^{\circ}_{max} = 100$ (red) and the reference governor is absent (black).

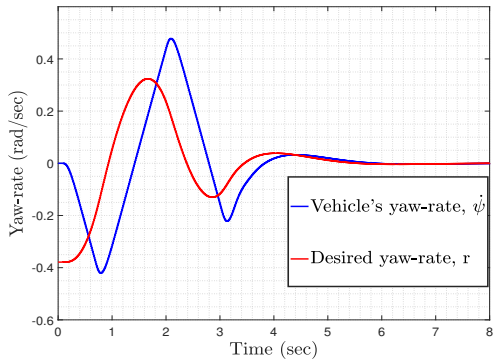

(c) Yaw-rate references when the reference governor is absent. Vehicle's yaw rate is in blue and the desired yaw-rate in red.

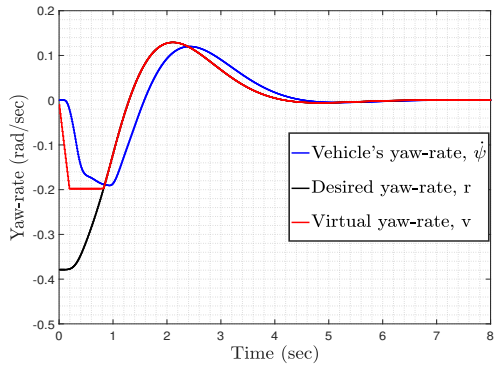

(d) Yaw-rate references when the reference governor is utilized and $\delta^{\circ}_{max} = 50$. Vehicle's yaw rate is in blue, the desired yaw-rate in black and the virtual in red.

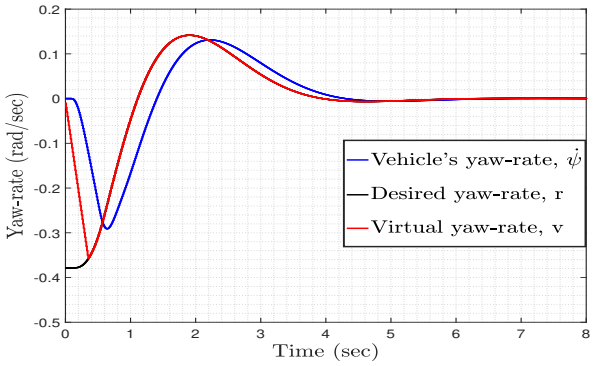

(e) Yaw-rate references when the reference governor is utilized and $\delta^{\circ}_{max} = 100$. Vehicle's yaw rate is in blue, the desired yaw-rate in black and the virtual in red.

Figure 5.16: *Simulation case scenario*: Lane-change results using a lane-tracking controller.

5.3.6 Extension of the RG approach to LPV closed-loop systems

In this section, we remark that the proposed approach can be directly extended to the case where the closed-loop system is written in an LPV form. For instance the longitudinal velocity of the vehicle model can be considered varying and measured at every instant. Thus, two different approaches can be applied to govern the LPV closed-loop system.

1. Express the discrete LPV system to an LPV Polytopic form. Then, according to [Casavola, Mosca, and Angeli 2000], the maximal output admissible set is augmented such that all the LTI vertex closed-loop systems are included in the closed-loop constraints.

   Subsequently, the maximal output admissible set is computed as such below:

   $$\tilde{O}_\infty = \bigcap_{i=1}^{N} \tilde{O}_\infty^i \tag{5.39}$$

   where N are the number of the vertices of the polytope that includes the closed-loop system. Then, as in the previous section, the redundant linear inequalities are eliminated so as to reduce the size $\tilde{O}_\infty$ and thus, the optimization problem to be solved online.

2. In [Kapsalis et al. 2021c], we formulate the discrete-time LPV closed loop system, equipped with a $\mathcal{LFT}/\mathcal{H}_\infty$ controller, and express it in a LFT form. Thus, in real-time and taking at every instant the measured value of the varying parameter, the closed-loop matrices $A_{cl}(\rho), B_{cl}(\rho), C_{cl}(\rho), D_{cl}(\rho)$, can be updated accordingly [Apkarian and Gahinet 1995].

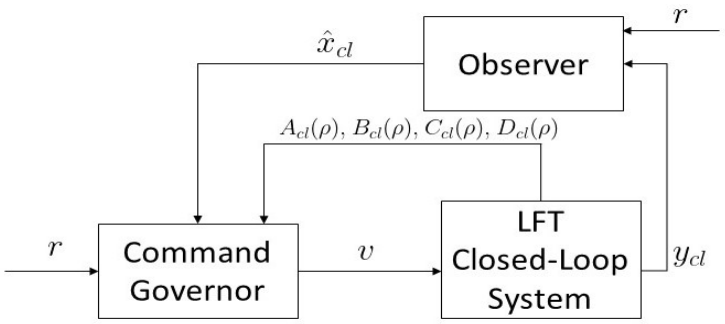

Figure 5.17: Control scheme of the LPV/LFT closed-loop system including the Command Governor.

As state and virtual reference constraints are chosen to limit the maximum steering angle, ensure that the virtual reference $v(k)$ does not overshoot the reference $r(k)$ and

is smooth enough respectively.

$$\begin{aligned} |\delta(k)| \leq \delta_{max}, \text{ or } \ |E(\rho)x_{cl}(k)| \leq D \\ |v(k)| \leq r(k) \\ |v(k) - v(k-1)| \leq D_v \end{aligned} \tag{5.40}$$

All the above constraints and model formulation lead to the quadratic programming problem (5.41) called Command Governor, where constraint fulfillment and tracking performance is evaluated throughout a prediction horizon N. The global control scheme for the governed closed-loop system is illustrated in Fig. 5.17.

$$\begin{aligned} \underset{v(k)}{\text{minimize}} \quad & J = |v(k) - r(k)|^2 + \sum_{i=1}^{N} (\dot{\psi}(k+i) - r(k))^2 \\ \text{subject to} \quad & x_{cl}(k+1+i) = A_{cl}(\rho)x_{cl}(k+i) + B_{cl}(\rho)v(k), \\ & E(\rho)x_{cl}(k+i) \leq D, \\ & |v(k)| \leq r(k), \\ & |v(k) - v(k-1)| \leq \mathcal{D}_v, \\ & \forall i = 1, .., N \end{aligned} \tag{5.41}$$

5.4 Concluding Remarks

This chapter has emphasized and focused on two main contributions of this thesis in the merging of lateral control scenarios.

In the first one, a high-level exogenous parameter is introduced, which is utilized in the LPV model formulation of the two scenarios and their transition and also in the tuning of the LPV/Gain-scheduled controller via the parameter-dependent weighting functions. Various simulation and experimental results show that the proposed controller is capable to handle the Lane-Tracking to Lane-Change and vice-versa.

In the second approach, the merging of the two scenarios is treated via modifying the desired yaw-rate reference on-line for the case where the vehicle's steering is controller by a yaw-rate Lane-Tracking controller. According to that approach, a Reference Governor is designed that computes a virtual yaw-rate reference, as a solution of a real-time convex optimization. That virtual reference feeds the controller so that to reduce the bandwidth of the closed-loop system in real-time and perform a lane-change maneuver. The proposed methodology is validated in time-domain simulations.

The next chapter will present the main conclusions of this thesis and will give some future perspectives as a continuum of this work.

Chapter 6

Conclusion and Perspectives

Contents

This chapter is twofold. At first, it aims at presenting a general summary of the included chapters and highlight the novelties and the main contributions derived from this thesis. Finally, it concludes by proposing future works and perspectives to improve the presented architecture or on relevant domain of applications.

6.1 Summary

This thesis is concerned with the study, analysis and the design of a lateral control system through the utilization of advanced robust control theory and more specifically LPV theory. The defined goals are to design an automatic steering control system for an automated vehicle that can operate successfully for a range of velocities, while lateral control scenarios (i.e lane-tracking/change) can be performed. This work is presented in six chapters.

- The first chapter introduces the lateral control problem this thesis aims at tackling and the underlying objectives to be met. Then, the associated contributions that led to conference, journal and patent publications are presented. Finally, a general structure of the following chapters is given to the reader.
- Chapter two provides the important definitions so that the reader is capable to understand how an LPV dynamic feedback controller can be designed. Thus, notions as LMIs and LPV systems are introduced and the necessary theorems for the control synthesis. Moreover, in the same chapter is given a brief overview of the existing bibliography about the lateral control system design.

- The third chapter reports the main components that cooperate in the vehicle's architecture to enable an automated passenger vehicle (Renault Zoe) used in this thesis to drive in autonomous mode. In addition, it details the gradual modeling of the lateral dynamics of the vehicle, that includes the states in the vehicle's frame, the look-ahead error dynamics and the LTI identified model of the EPS system. Then, the generic LPV model is formulated according to the induced time-varying parameters, and that model is used in the next chapters for control synthesis.

- Chapter four details the study, analysis and design of LPV dynamic output feedback lane-tracking controllers for a varying speed profile utilizing two different approaches, the Polytopic and the Gridding ones according to the presented theory from chapter two. The LPV controllers take into account the speed which is an inherent varying parameter of the model and the look-ahead distance in front of the vehicle that is a tuning parameter. Thus, novel LPV control strategies with H_∞ performance guarantees are designed while these parameters feed in real-time the control systems for the lane-tracking scenario. The proposed approaches are validated in various simulation results and in a real test track where the automated test-bed platform is utilized.

- The fifth chapter is divided into two main sections where in both the main aim is to tackle the merging of the lane-tracking and switching of lanes. The first is a continuum of the third section of chapter four. In particular, a high-level parameter is introduced to model the linear transition between the lane-tracking and lane-change. Subsequently, an LPV controller is designed for the merging of both scenarios. The encouraging results are validated in several simulations and collected experimental results in a test track where the control code is embedded to the automated Renault Zoe. The second approach to tackle the merging of the two scenarios is based-on solving a real-time convex optimization, called Reference Governor. The solution of that problem is a virtual reference that feeds a yaw-rate lane-tracking controller for which closed-loop steering constraints are satisfied and enabling thus, the lane-change maneuver by a lane-tracking controller. The overall performance is validated in simulation results.

6.2 Main Contributions

The main contributions of this thesis are based-on applying LPV theory for lateral control applications. They mainly concern:

6.2.1 LPV Model Formulation

- The development of a novel augmented LPV generic model that includes the linearized dynamics of the vehicle, the look-ahead error dynamics and the identified steering model of the actuator. The time-varying parameters are the longitudinal speed and the look-ahead distance. The interest of that model lies on the fact that an LPV controller

can be designed in combination with LPV control theory, and thus the overall lateral architecture can be treated in the LPV framework.

6.2.2 LPV Path-Following Control

- The design and the implementation procedure of a 3D LPV/ Polytopic controller that can handle the successful lane-keeping of an autonomous vehicle. We also propose an algorithm to reduce the size of the over-bounded polytope that describes the parameter space. Thus, we propose and implement successfully the reduced-polytope-based LPV controller via solving a real-time constrained LS problem, so that to compute the contribution of each LTI vertex controller according to the real-time measured values of the parameter vector.

- The LPV configuration of a gain-scheduled control that adapts its performance according to the measurements of the speed and the look-ahead distance. The main difference w.r.t the previous contribution is that the grid points of the parameters are taken into account in the LPV control synthesis and they are not considered as max and min bounds as in the polytopic approach. Thus, a different and more precise synthesis is proposed.

6.2.3 LPV Merging Lane-Tracking/Change Control

- The merging of the two different lateral control scenarios, i.e lane-tracking and change, is formulated in the LPV framework by introducing a new high-level varying parameter that model the transition from one scenario to another and vice versa. This parameter is utilized in the H_∞ weighting functions to tune the performance of the LPV controller and in real-time feeds the controller, according to the scenario that has to be handled.

- A second approach to handle the merging of the two cases of lateral control is proposed by treating the merging outside of the controller. That means, that a virtual yaw-rate reference feeds a lane-tracking controller that enables it to perform both lane-tracking and change maneuvers. That virtual reference is the solution of a real-time convex optimization problem, that satisfies performance criteria and closed-loop state constraints by taking into account the dynamics of the yaw-rate tracking controller.

6.3 Future works

This sections gives some ideas for some future works and extensions to the current contributions detailed in the chapters of this thesis. According to every chapter and to other domains of applications, the following can be done:

About chapter two, below it is proposed to:

- Construct a new LTI identified model for the ESP of the vehicle. Apply different Padé approximations of the time-delay term and compare the overall performance of the controller vehicle.
- Construct a new lateral LPV model by including an LPV actuator model that is derived from an LPV identification algorithm for a varying longitudinal speed of the vehicle.
- Investigate the case where the lateral forces applied in the bicycle model are not linearized. Thus, the lateral forces can be expressed as a function of time-varying and measured parameters. These parameters are the side-slip angles and can be estimated in real-time and feed an LPV controller. Furthermore, these varying parameters can be utilized in the H_∞ weighting functions so as to tune an LPV controller that is capable to treat the non-linear case of the vehicle dynamics.

Further extensions are proposed for the contributions presented in chapter four.

- Propose a new algorithm for the reduction of the size of a polytope that describes the parameter space, when the size of the parameter vector is greater than three.
- Develop a weighted real-time constrained LS problem to improve the performance of the LPV/Polytopic controller by limiting the contribution of the conservative vertex controllers.
- Design a high-level planner that is based-on the constrained LS process. This can be achieved by introducing some performance criteria, expressed as quadratic functions for tracking performance and comfort for the passenger.
- Formulate the look-ahead distance as the solution of a real-time convex optimization problem according to the scenario (lane-tracking/change) or the traffic agents near the vehicle so that to regulate in real-time the velocity of the vehicle.

According to chapter five, the following suggestions are given:

- Introduce a new high-level parameter that aims at improving the lane-tracking performance for the case where higher curves have to be tracked or where the lateral error is increased.
- Experimental validation of the proposed Reference Governor scheme for fixed speed and for the case where the longitudinal speed is varying.
- Develop a Reference Governor scheme where it enables a fast (again lane-tracking controller) to perform an obstacle avoidance maneuver. The avoidance of the obstacle can be formulated as a real-time yaw-rate constraint via simple geometrical calculations.
- Propose a non-linear Reference Governor scheme that in the optimization problem the real-time modification of the longitudinal speed is achieved as well. Thus, the speed can be regulated according to the lateral closed-loop control dynamics. In this way, tracking and speed regulation can be assessed at the same time.

Apart from extending the presented work to the lateral control applications, we suggest to:

- Integrate the longitudinal & lateral control in the LPV framework. Thus, the longitudinal speed is a state and will have to be considered as a quasi-LPV parameter. That parameter in real-time will feed an LPV controller to adapt the speed regulation and the tracking performance according to the scenario.
- Develop an LPV control scheme for the cases of Adaptive Cruise Control or even Cooperative Cruise Control. These applications are strongly-dependent from the perception and thus from the sensors. Thus, we propose that a future work will be to design a control system that adapts its performance according to the sensors quality.

Bibliography

Ackermann, J, T Bünte, and D Odenthal (1999). "Advantages of active steering for vehicle dynamics control." In: (cit. on p. 31).

Alcalá, Eugenio, Vicenç Puig, and Joseba Quevedo (2020). "LPV-MP planning for autonomous racing vehicles considering obstacles." In: *Robotics and Autonomous Systems* 124, p. 103392 (cit. on p. 33).

Alcalá, Eugenio et al. (2020). "Autonomous racing using linear parameter varying-model predictive control (LPV-MPC)." In: *Control Engineering Practice* 95, p. 104270 (cit. on p. 33).

Apkarian, Pierre and Richard J Adams (2000). "Advanced gain-scheduling techniques for uncertain systems." In: *Advances in linear matrix inequality methods in control*. SIAM, pp. 209–228 (cit. on p. 24).

Apkarian, Pierre and Pascal Gahinet (1995). "A convex characterization of gain-scheduled h/sub/spl infin//controllers." In: *IEEE Transactions on Automatic Control* 40.5, pp. 853–864 (cit. on p. 92).

Apkarian, Pierre, Pascal Gahinet, and Greg Becker (1995). "Self-scheduled H_∞ control of linear parameter-varying systems: a design example." In: *Automatica* 31.9, pp. 1251–1261 (cit. on pp. 20, 24, 27, 38, 45, 49).

Astrom, Karl J and Bjorn Wittenmark (1984). *Computer controlled systems: theory and design*. Prentice Hall Professional Technical Reference (cit. on pp. 51, 76).

Atoui, Hussam et al. (2021). "LPV-Based Autonomous Vehicle Lateral Controllers: A Comparative Analysis." In: *IEEE Transactions on Intelligent Transportation Systems* (cit. on p. 34).

Bara, G Iulia et al. (2001). "Parameter-dependent state observer design for affine LPV systems." In: *International journal of control* 74.16, pp. 1601–1611 (cit. on p. 50).

Barker, Jeffrey M and Gary J Balas (2000). "Comparing linear parameter-varying gain-scheduled control techniques for active flutter suppression." In: *Journal of Guidance, Control, and Dynamics* 23.5, pp. 948–955 (cit. on p. 33).

Beal, Craig Earl and J Christian Gerdes (2012). "Model predictive control for vehicle stabilization at the limits of handling." In: *IEEE Transactions on Control Systems Technology* 21.4, pp. 1258–1269 (cit. on p. 32).

Becker, Greg and Andy Packard (1994). "Robust performance of linear parametrically varying systems using parametrically-dependent linear feedback." In: *Systems & Control Letters* 23.3, pp. 205–215 (cit. on p. 25).

Beltrán, Jorge et al. (2020). "Towards autonomous driving: a multi-modal 360 perception proposal." In: *2020 IEEE 23rd International Conference on Intelligent Transportation Systems (ITSC)*. IEEE, pp. 1–6 (cit. on p. 10).

Boyd, Stephen and Lieven Vandenberghe (2004). *Convex optimization*. Cambridge university press (cit. on p. 20).

Boyd, Stephen et al. (1994). *Linear matrix inequalities in system and control theory*. Vol. 15. SIAM (cit. on pp. 20, 23, 39, 47).

Broggi, Alberto et al. (1999). "The ARGO autonomous vehicle's vision and control systems." In: *International Journal of Intelligent Control and Systems* 3.4, pp. 409–441 (cit. on p. 32).

Casavola, Alessandro, Edoardo Mosca, and David Angeli (2000). "Robust command governors for constrained linear systems." In: *IEEE transactions on Automatic Control* 45.11, pp. 2071–2077 (cit. on p. 92).

Corno, Matteo et al. (2020). "An LPV Approach to Autonomous Vehicle Path Tracking in the Presence of Steering Actuation Nonlinearities." In: *IEEE Trans. Control Syst. Technol.* Pp. 1–9 (cit. on pp. 33, 38).

Coulter, R Craig (1992). *Implementation of the pure pursuit path tracking algorithm.* Tech. rep. Carnegie-Mellon UNIV Pittsburgh PA Robotics INST (cit. on p. 17).

Doumiati, Moustapha et al. (2013). "Integrated vehicle dynamics control via coordination of active front steering and rear braking." In: *European Journal of Control* 19.2, pp. 121–143 (cit. on p. 31).

Dubuc, Donatien (2018). "Observation and diagnosis for trucks." PhD thesis. Université Grenoble Alpes (cit. on pp. 20, 50).

Dugard, Luc and Erik I Verriest (1998). *Stability and control of time-delay systems.* Vol. 228. Springer (cit. on p. 15).

Falcone, Paolo et al. (2007). "Predictive active steering control for autonomous vehicle systems." In: *IEEE Transactions on control systems technology* 15.3, pp. 566–580 (cit. on pp. 32, 36).

Fényes, Dániel, Balázs Németh, and Péter Gáspár (2020). "LPV based data-driven modeling and control design for autonomous vehicles." In: *2020 European Control Conference (ECC).* IEEE, pp. 1371–1376 (cit. on p. 33).

Fényes, Dániel et al. (2021). "Observer design with performance guarantees for vehicle control purposes via the integration of learning-based and LPV approaches." In: *2021 IEEE Intelligent Vehicles Symposium Workshops (IV Workshops).* IEEE, pp. 122–127 (cit. on p. 33).

Funke, Joseph et al. (2016). "Collision avoidance and stabilization for autonomous vehicles in emergency scenarios." In: *IEEE Transactions on Control Systems Technology* 25.4, pp. 1204–1216 (cit. on p. 32).

Gahinet, Pascal and Pierre Apkarian (1994). "A Linear Matrix Inequality approach to H_∞ control." In: *International journal of robust and nonlinear control* 4.4, pp. 421–448 (cit. on p. 87).

Garone, Emanuele, Stefano Di Cairano, and Ilya Kolmanovsky (2017). "Reference and command governors for systems with constraints: A survey on theory and applications." In: *Automatica* 75, pp. 306–328 (cit. on p. 83).

Gáspár, Péter et al. (2016). "Robust control design for active driver assistance systems." In: *Springer, DOI* 10, pp. 978–3 (cit. on p. 33).

Gilbert, Elmer G and K Tin Tan (1991). "Linear systems with state and control constraints: The theory and application of maximal output admissible sets." In: *IEEE Transactions on Automatic control* 36.9, pp. 1008–1020 (cit. on p. 84).

González, David et al. (2015). "A review of motion planning techniques for automated vehicles." In: *IEEE Transactions on Intelligent Transportation Systems* 17.4, pp. 1135–1145 (cit. on p. 31).

Guechi, E-H et al. (2012). "Output feedback controller design of a unicycle-type mobile robot with delayed measurements." In: *IET control theory & applications* 6.5, pp. 726–733 (cit. on p. 32).

Guechi, El-Hadi et al. (2009). "Tracking-error model-based PDC control for mobile robots with acceleration limits." In: *2009 IEEE International Conference on Fuzzy Systems*. IEEE, pp. 197–202 (cit. on p. 32).

Guo, Hongyan et al. (2017). "Nonlinear model predictive lateral stability control of active chassis for intelligent vehicles and its FPGA implementation." In: *IEEE Transactions on Systems, Man, and Cybernetics: Systems* 49.1, pp. 2–13 (cit. on p. 31).

Herceg, M. et al. (2013). "Multi-Parametric Toolbox 3.0." In: *Proc. of the European Control Conference*. `http://control.ee.ethz.ch/~mpt`. Zürich, Switzerland, pp. 502–510 (cit. on p. 86).

Hingwe, Pushkar et al. (2002). "Linear parameter varying controller for automated lane guidance: experimental study on tractor-trailers." In: *IEEE Transactions on control systems technology* 10.6, pp. 793–806 (cit. on p. 33).

Hjartarson, Arnar, Peter Seiler, and Andrew Packard (2015). "LPVTools: A toolbox for modeling, analysis, and synthesis of parameter varying control systems." In: *IFAC-PapersOnLine* 48.26, pp. 139–145 (cit. on pp. 31, 59, 75).

Hoffmann, Christian and Herbert Werner (2014). "A survey of linear parameter-varying control applications validated by experiments or high-fidelity simulations." In: *IEEE Transactions on Control Systems Technology* 23.2, pp. 416–433 (cit. on p. 33).

Jochem, Todd and Dean Pomerleau (1996). "Life in the fast lane: The evolution of an adaptive vehicle control system." In: *AI magazine* 17.2, pp. 11–11 (cit. on p. 32).

Kang, Chang Mook, Seung-Hi Lee, and Chung Choo Chung (2018). "Linear parameter varying design for lateral control using kinematics of vehicle motion." In: *2018 Annual American Control Conference (ACC)*. IEEE, pp. 3239–3244 (cit. on p. 33).

Kapsalis, Dimitrios et al. (2020). "Gain-scheduled steering control for autonomous vehicles." In: *IET Control Theory and Applications* (cit. on pp. 36, 45, 52, 69, 73).

Kapsalis, Dimitrios et al. (2021a). "A Reference Governor approach for Lateral Control of Autonomous Vehicles." In: *2021 IEEE International Intelligent Transportation Systems Conference (ITSC)*. IEEE, pp. 580–585 (cit. on p. 68).

Kapsalis, Dimitrios et al. (2021b). "Design and experimental validation of an lpv pure pursuit automatic steering controller." In: *IFAC-PapersOnLine* 54.2, pp. 63–68 (cit. on pp. 36, 47, 65).

Kapsalis, Dimitrios et al. (2021c). "LPV/LFT Control Design Equipped with a Command Governor for Different Steering Scenarios." In: *IFAC-PapersOnLine* 54.8, pp. 142–147 (cit. on pp. 68, 92).

Kolmanovsky, Ilya, Emanuele Garone, and Stefano Di Cairano (2014). "Reference and command governors: A tutorial on their theory and automotive applications." In: *2014 American Control Conference*. IEEE, pp. 226–241 (cit. on p. 83).

Kosecka, Jana (1996). "Vision-based lateral control of vehicles: Look-ahead and delay issues." In: (cit. on p. 46).

Li, Panshuo et al. (2021). "Polytopic LPV approaches for intelligent automotive systems: State of the art and future challenges." In: *Mechanical Systems and Signal Processing* 161, p. 107931 (cit. on pp. 33, 36, 38).

Mahtout, Imane (2020). "Youla-Kucera based multi-objective controllers: Application to autonomous vehicles." PhD thesis. Université Paris sciences et lettres (cit. on p. 15).

Mahtout, Imane et al. (2018). "Youla-kucera based lateral controller for autonomous vehicle." In: *2018 21st International Conference on Intelligent Transportation Systems (ITSC)*. IEEE, pp. 3281–3286 (cit. on p. 82).

Martinez, John J, Nassim Loukkas, and Nacim Meslem (2020). "H-infinity set-membership observer design for discrete-time LPV systems." In: *International journal of control* 93.10, pp. 2314–2325 (cit. on pp. 51, 52).

Mattingley, Jacob and Stephen Boyd (2012). "CVXGEN: A code generator for embedded convex optimization." In: *Optimization and Engineering* 13.1, pp. 1–27 (cit. on pp. 52, 86).

Milanés, Vicente et al. (2021). "The Tornado Project: An Automated Driving Demonstration in Peri-Urban and Rural Areas." In: *IEEE Intelligent Transportation Systems Magazine* (cit. on pp. 9, 32).

Mohammadpour, Javad and Carsten W Scherer (2012). *Control of linear parameter varying systems with applications*. Springer Science & Business Media (cit. on pp. 26, 33, 37, 45).

Nguyen, Anh-Tu, Chouki Sentouh, and Jean-Christophe Popieul (2018). "Fuzzy steering control for autonomous vehicles under actuator saturation: Design and experiments." In: *Journal of the Franklin Institute* 355.18, pp. 9374–9395 (cit. on p. 32).

Onieva, Enrique et al. (2011). "Automatic lateral control for unmanned vehicles via genetic algorithms." In: *Applied Soft Computing* 11.1, pp. 1303–1309 (cit. on p. 32).

Pérez, Joshué, Vicente Milanés, and Enrique Onieva (2011). "Cascade architecture for lateral control in autonomous vehicles." In: *IEEE Transactions on Intelligent Transportation Systems* 12.1, pp. 73–82 (cit. on p. 32).

Poussot-Vassal, Charles (2008). "Commande robuste LPV multivariable de chassis automobile." PhD thesis. Grenoble INPG (cit. on pp. 20, 52).

Poussot-Vassal, Charles et al. (2011). "Attitude and handling improvements through gain-scheduled suspensions and brakes control." In: *Control Engineering Practice* 19.3, pp. 252–263 (cit. on p. 49).

Rajamani, Rajesh (2011). *Vehicle dynamics and control*. Springer Science & Business Media (cit. on pp. 12, 36).

Robert, David (2007). "Contribution à l'interaction commande/ordonnancement." PhD thesis. Institut National Polytechnique de Grenoble-INPG (cit. on p. 20).

Robert, David, Olivier Sename, and Daniel Simon (2009). "An H_∞ LPV Design for Sampling Varying Controllers: Experimentation With a T-Inverted Pendulum." In: *IEEE Trans. Control Syst. Technol.* 18.3, pp. 741–749 (cit. on pp. 38, 39).

Scherer, Carsten, Pascal Gahinet, and Mahmoud Chilali (1997). "Multiobjective output-feedback control via LMI optimization." In: *IEEE Transactions on automatic control* 42.7, pp. 896–911 (cit. on pp. 20, 27).

Scherer, Carsten and Siep Weiland. "Linear matrix inequalities in control." In: () (cit. on p. 20).

Sename, Olivier, Luc Dugard, Peter Gáspár, et al. (2019). "H_∞/LPV controller design for an active anti-roll bar system of heavy vehicles using parameter dependent weighting functions." In: *Heliyon* 5.6, e01827 (cit. on p. 33).

Sename, Olivier, Peter Gaspar, and József Bokor (2013). *Robust control and linear parameter varying approaches: application to vehicle dynamics*. Vol. 437. Springer (cit. on p. 33).

Shladover, Steven E (1995). "Review of the state of development of advanced vehicle control systems (AVCS)." In: *Vehicle System Dynamics* 24.6-7, pp. 551–595 (cit. on p. 31).

Skogestad, Sigurd and Ian Postlethwaite (2007). *Multivariable feedback control: analysis and design*. Vol. 2. Wiley New York (cit. on pp. 40, 49, 72, 86, 88).

Tan, Han-Shue and Jihua Huang (2014). "Design of a high-performance automatic steering controller for bus revenue service based on how drivers steer." In: *IEEE Transactions on Robotics* 30.5, pp. 1137–1147 (cit. on pp. 32, 36, 86).

Taylor, Camillo J et al. (1999). "A comparative study of vision-based lateral control strategies for autonomous highway driving." In: *The International Journal of Robotics Research* 18.5, pp. 442–453 (cit. on p. 13).

Thrun, Sebastian et al. (2006). "Stanley: The robot that won the DARPA Grand Challenge." In: *Journal of field Robotics* 23.9, pp. 661–692 (cit. on p. 32).

Wu, Fen (1995). "Control of linear parameter varying systems." In: (cit. on pp. 28, 74).

Wu, Fen et al. (1996). "Induced L2-norm control for LPV systems with bounded parameter variation rates." In: *International Journal of Robust and Nonlinear Control* 6.9-10, pp. 983–998 (cit. on pp. 20, 28, 29, 74).

Xu, Philippe et al. (2018). "System architecture of a driverless electric car in the grand cooperative driving challenge." In: *IEEE Intelligent Transportation Systems Magazine* 10.1, pp. 47–59 (cit. on p. 32).

Xu, Shaobing, Huei Peng, and Yifan Tang (2020). "Preview path tracking control with delay compensation for autonomous vehicles." In: *IEEE Transactions on Intelligent Transportation Systems* 22.5, pp. 2979–2989 (cit. on p. 32).

Yamamoto, Kazusa (2017). "Control of electromechanical systems, application on electric power steering systems." PhD thesis. Grenoble Alpes (cit. on p. 20).

Ziegler, Julius et al. (2014). "Making bertha drive—an autonomous journey on a historic route." In: *IEEE Intelligent transportation systems magazine* 6.2, pp. 8–20 (cit. on p. 32).

Résumé — Cette thèse traite du problème de la conception de contrôleurs à base de LPV (Linear Parameter Varying) et de Gain-scheduling pour le système de contrôle latéral, nécessaire pour qu'un véhicule de passagers puisse se diriger automatiquement en mode autonome. L'objectif principal de cette thèse est de proposer un système de direction automatique qui assure la sécurité du passager et maintient le confort tout en effectuant des manœuvres rapides selon la trajectoire de référence. Les architectures de système de contrôle latéral proposées sont basées sur les approches a) Polytopique et b) Gridded de l'espace des paramètres pour concevoir de tels contrôleurs dynamiques à rétroaction de sortie LPV. Par la suite, une étude est menée pour concevoir un contrôleur permettant d'éviter les problèmes de conservatisme de la méthode, d'assurer des garanties de performance H-infini tout en tenant compte de la dynamique de suivi des erreurs. Les principaux scénarios de contrôle latéral que ce travail vise à aborder sont le suivi de voie et le changement de voie. Dans un premier temps, nous traitons uniquement le problème du maintien dans la voie pour une vitesse longitudinale variable, puis la transition entre ces scénarios. Dans le cadre du LPV, cette transition est modélisée pour adapter en temps réel les performances du contrôleur en fonction du scénario traité. La même application est également formulée comme un problème d'optimisation en temps réel, appelé Gouverneur de référence, qui alimente une référence virtuelle pour laquelle le contrôleur à gain régulé peut gérer à la fois les manœuvres de suivi et de changement de voie et les contraintes d'état en boucle fermée sont respectées. Les architectures de contrôle proposées sont d'abord validées sur des simulateurs haute-fidélité pour plusieurs scénarios. De plus, le code de contrôle embarqué est déployé sur un logiciel de Renault Zoe électrique automatisé et testé sur une piste d'essai réelle pour des virages à basse vitesse et des courbes à haute vitesse. Ainsi, les méthodes suggérées sont validées par une analyse des résultats expérimentaux collectés et prouvent ainsi leurs performances encourageantes.

Mots clés : Contrôle latéral, contrôle robuste, contrôle LPV, véhicules autonomes, systèmes de transport intelligents.

Abstract — This thesis deals with the problem of designing Linear Parameter Varying (LPV)-based Gain-scheduling controllers for the lateral control system, needed for a passenger vehicle to steer automatically in autonomous mode. The main objective of this thesis is to suggest an automatic steering system that provides safety for the passenger and sustain comfort while performing fast maneuvers according to the reference trajectory. The proposed lateral control system architectures are based-on the a) Polytopic and b) the Gridded parameter space approaches to design such LPV dynamic output feedback controllers. Subsequently, a study is conducted to design a controller to avoid method's conservatism issues, assure H-infinity performance guarantees while taking into account the error tracking dynamics. The

main scenarios of lateral control this work aims at tackling, are the lane-tracking and the switching of lanes. At first is treated solely the lane-keeping problem for varying longitudinal speed and then, the transition between these scenarios. In the LPV framework, this transition is modeled to adapt the controller's performance in real-time according to the treated scenario. The same application is also formulated as a real-time optimization problem, called Reference Governor, that feeds a virtual reference for which the gain-scheduled controller can handle both tracking and switching lanes maneuvers and closed-loop state constraints are respected. The proposed control architectures are validated at first on high-fidelity simulators for several scenarios. Moreover, the embedded control code is deployed on an automated electric Renault Zoe's software and tested in a real test track for low-speed turns and high-velocity curves. Thus, the suggested methods are validated through an analysis of the collected experimental results and proving in that way the encouraging performance.

Keywords: Lateral control, robust control, LPV control, autonomous vehicles, intelligent transportation systems.